Electrostatic Self-Assembly of Linear and Nonlinear Optical Thin Films

by

Kristie Lenahan Cooper

Dissertation submitted to the Faculty of
Virginia Polytechnic Institute and State University
In partial fulfillment of the requirements for the degree of

DOCTOR OF PHILOSOPHY
in
Electrical Engineering

APPROVED:

Richard O. Claus, Chairman
Ioannis M. Besieris
Ronald S. Gordon
Ira Jacobs
Anbo Wang

April 20, 1999
Blacksburg, Virginia

Keywords: electrostatic self-assembly (ESA), optical thin films, linear optical filtering, nonlinear optics (NLO), $\chi^{(2)}$ effect, dielectric stack filter

Electrostatic Self-Assembly of Linear and Nonlinear Optical Thin Films

by
Kristie Lenahan Cooper
Dr. Richard O. Claus, Chairman
Electrical Engineering

ABSTRACT

This dissertation demonstrates the feasibility of using novel electrostatic self-assembly (ESA) methods to fabricate linear and nonlinear optical thin films and components. The ESA process involves the layer-by-layer alternate adsorption of anionic and cationic complexes from aqueous solutions. Selection of the molecules in each layer, their orientation at the molecular level, and the order in which the layers are assembled determine the film's bulk optical, electronic, magnetic, thermal, mechanical and other properties. In this work, the capability of nanoscale control over film optical properties allowed the fabrication of complicated refractive index profiles required for linear optical interference filters. The inherent ordered nature of ESA films yielded extremely stable noncentrosymmetric thin films for second-order nonlinear optical applications. The ESA technique offers numerous advantages over conventional thin film fabrication methods and offers great potential in commercial applications such as reflectance and AR filters, EO waveguides and modulators and other optoelectronic devices.

The structure of each monolayer in ESA films is dependent on the processing parameters, producing subsequent variations in bulk film properties both intentionally and incidentally. As this method is still in its infancy, variations in ESA processing methods, including process automation, are considered first in this document. These results allowed carefully controlled refractive index experiments and the synthesis of both step and graded index structures, several microns thick. Dielectric stack, Rugate, and antireflection optical interference filters were designed, synthesized and demonstrated. $\chi^{(2)}$ films of both commercially available polymer dyes and novel polymers designed specifically for the ESA process were demonstrated using second harmonic generation. UV/vis spectroscopy, ellipsometry and atomic force microscopy analysis are presented.

for my father, Michael John Lenahan, who has worked hard all his life to give me mine.

Acknowledgements

First and foremost, I would like to express my sincere gratitude to my advisor and mentor, Dr. Rick Claus for his thoughtful guidance, seemingly limitless enthusiasm, and steadfast encouragement and support. Working with him has been the most rewarding experience of my professional life. At the Fiber & Electro-Optics Research Center, he provides an environment that challenges his students to expand the boundaries of what they are capable of accomplishing by unknowingly setting high standards through his own work. I would also like to thank all my committee members, Dr. Ioannis Besieris, Dr. Ron Gordon, Dr. Ira Jacobs and Dr. Anbo Wang, for their valuable suggestions and insights into this research.

I am indebted to our thin film fabrication experts, Shannon Lenahan, Tod Distler, Al Cooper, and Adam Duncan for their fine work and irrepressible sense of humor. Numerous other people at FEORC have assisted me in this research through helpful comments and technical discussions, including Francisco Arregui, Paul Duncan, Yanjing Liu, Tingying Zeng and Wei Zhao. I appreciate their expertise and their company. No list of acknowledgements would be complete without Linda Jones. For her nonstop cheerful attitude always accompanied by astonishing efficiency, the endless piles of paperwork, all the last-minute FEDEX runs, the singing in the hallway, and the sanity check when needed, I extend my deepest appreciation.

Many thanks to Ann for reminding us all that the river is calling and there is a life outside of this work. I am ever grateful to Linda Coffman Skornia for her boundless enthusiasm for my life and my work, and her enduring conviction that I would succeed, despite any obstacle. Finally, I would like to thank my husband, Al, who has endured with less than my full regard for far too long, and has supported and encouraged me from the first experiments to the final days and nights of writing.

The platinum nanoparticles were kindly provided by Dr. Yanjing Liu. I would like to thank Dr. J.R. Heflin and his students for their work on the SHG measurements of these films. This work was supported in part by ARO Grant DAAG55-92-1-0101, AFOSR contract F49620-97-C-0047, and Air Force contract F33615-98-C5421.

Table of Contents

List of Tables and Figures

Chapter 1

Chapter 2

Chapter 3

Chapter 4

Chapter 5

CHAPTER 1

Introduction

Fabrication of organic thin films by spontaneous molecular assembly is a powerful tool in creating carefully controlled supermolecular structures for optical and numerous other applications. The bulk properties of these novel materials can be controlled by both the molecular structure and the organization of the molecules. Organic thin films with carefully designed structures and properties have attracted a great deal of interest in recent years [1-4] due to their potential in a number of different fields, including sensors, surface coatings, optoelectronics and nonlinear optics. These applications require, in general, well-ordered films consisting of molecules with specific properties, carefully aligned with respect to each other and the substrate. In addition to application specific requirements, such films must exhibit stability to a variety of stresses, including thermal, chemical, and solvent exposure, implying that the interaction between the molecules in the film must be more favorable than the competing interaction.

Self-assembled organic thin films combine the advantages of molecular engineering by versatile organic synthesis with spontaneous molecular self-assembly, which produces stable structures at a thermodynamic minimum. The creation of such stable and carefully ordered films requires a multidisciplinary approach, encompassing such fields as organic synthesis, physical chemistry, materials science and electrical engineering for film preparation, modification, and characterization. Organic materials permit greater variability in composition and structure than their inorganic counterparts; organic synthesis techniques allow the formation of molecules with properties specifically tailored for each application by assembling molecules with defined composition and shape by the creation of sequential covalent bonds [5]. The careful organization of these molecules into thin film structures can be achieved spontaneously, without external intervention, by molecular self-assembly. The driving forces for such thermodynamically favorable processes are the chemistry of the intermolecular interactions, e.g. ionic, hydrogen, van der Waals, and covalent bonds [4-6]. The "rules of organization" are determined by molecular structure and the conditions under which the deposition occurs. Self-assembly performs some of the most difficult nanofabrication steps, those which require atomic

and molecular-level manipulation [7]. Its advantages mimic those of systems found in nature. ' Since the molecules adjust themselves to the thermodynamic minimum, defects are limited and self-healing. The resulting structures are stabilized by contacts between complementary units, e.g. anionic and cationic molecular segments, and are therefore intrinsically resistant to impurity incorporation because incorrect units are rejected [5]. Individual layers within the structure may contain different molecules of application-appropriate functionality, allowing the incorporation of multiple functions within a single structure.

Self-assembled materials such as Langmuir-Blodgett films [3,8] and covalently self-assembled monolayers [3, 9] have been thoroughly investigated in the past and are discussed below in Section 1.1. Recently, Decher and co-workers extended the pioneering work of Iler *et al.*[10] to a new method of organizing thin films using layer-by-layer adsorption of polyelectrolytes [11-13]. Alternate adsorption of polyanionic and polycationic molecules on oppositely charged surfaces is accomplished by immersion in aqueous polyelectrolyte solutions. This technique is distinguished by several advantages, including the ease of fabrication, the availability of numerous water-soluble polyions, and the capability for thick, multilayer synthesis.

This electrostatic self-assembly (ESA) process can be adapted to incorporate a wide variety of molecules, including nonlinear optical chromophores, conducting polymers, biological macromolecules, magnetic materials, dielectrics, and metallic or metallic oxide nanoparticles. This makes ESA thin films an excellent choice for use in applications covering a wide range of fields, including optics, electronics, biosensing and surface modification. The composition of each layer can be controlled by the incorporation of appropriately chosen molecules [14] and the structure of each layer can be manipulated by adjusting the deposition parameters [12,15-17].

This dissertation work extends that of previous researchers by several parallel efforts concerning potential optical applications of ESA films, namely

- Characterization and control of the refractive index of ESA films,
- Fabrication of multilayer films several microns thick with nanoscale control of the refractive index profiles,
- Synthesis of optical interference filters by ESA,
- Incorporation of novel NLO polymers and demonstration of the resulting nonlinear optical behavior using second harmonic generation, and
- Consideration of process automation, which will be required for transition of ESA to commercial manufacturing.

This chapter is organized as follows. Other organic thin film fabrication methods and their advantages and shortcomings are reviewed in Section 1.1. Section 1.2 introduces the ESA process and outlines its development and application up to the present. The motivation for this dissertation research is explained in Section 1.3, An outline of the material covered in the remaining four chapters is presented in Section 1.4.

1.1 Organic thin film self-assembly methods

This section presents a brief review of other organic self-assembly methods, namely Langmuir-Blodgett films and covalent self-assembly, which have been utilized in recent years, in order to give some perspective on the contributions and uniqueness of this work.

1.1.1 Langmuir-Blodgett films

The Langmuir-Blodgett technique, consisting of the transfer of successive organized monolayers from an air-water interface to a solid substrate, was the first of the molecular-level synthesis techniques. The effects of an oriented monolayer at a liquid-gas interface have been observed since ancient times in the form of the calming effect of oil on waves. Langmuir first confirmed that a film of amphiphilic molecules on a water surface is one molecule thick and oriented with the hydrophilic headgroup down and the hydrophobic tail extending up from the surface [18]. As early as 1920 he was able to transfer a monolayer from the water surface to a solid substrate, with much experimental work being performed by Katharine Blodgett. Multilayer assemblies of such monolayers on solid substrates, now referred to as Langmuir-Blodgett, or L-B, films, were not formally reported until 1935 [19] and not until the 1960s did the field develop steadily.

L-B deposition is carried out as follows. A Langmuir film, or oriented monolayer, is formed on a water surface by mechanically forcing the molecules together, maintaining constant surface pressure for close packing of the molecules without film collapse. A substrate is lowered through the monolayer and then withdrawn, depositing a monolayer on the substrate surface. Repeated immersion and withdrawal may build up as many as 100 layers. The resulting film will have either a hydrophobic or hydrophilic surface depending on which motion was last in the deposition. A more detailed description of the process may be found in Ref. 8.

Although these films have the advantages of a high degree of order and room temperature and pressure processing, a number of limitations exist. Little flexibility exists in choosing molecules of different structures and functions since L-B films are restricted to amphiphilic molecules [6, 20]. Also, substrates are limited to planar materials of only a few square centimeters [12]. Even accepting these limitations, it is still very difficult to form films several hundred Ångstroms thick of good optical quality [2]; microdomains and structure irregularities produce scattering [4]. In addition, the resulting films are not stable to thermal or chemical treatment [2,6]. L-B films are, in general, metastable structures that are easily disrupted [4].

1.1.2 Covalent self-assembly

Self-assembled monolayers (SAMs) are formed by a reaction between active surface sites (on the substrate or a previously formed monolayer) and corresponding functional groups of molecules in solution. There are three principal types of SAMs: alkanethiols on noble metals [21], organosilane on oxides [4] and fatty acids on metals or metal oxides [22]. SAMs are generally formed by dipping the substrate into a solution containing the molecule to be assembled.

Monolayer formation may take several seconds to several hours depending on the molecular species, substrate and solvent conditions. To construct a multilayer, the monolayer surface must then be modified to provide a functional group for the adsorption of the subsequent layer. This requires a high reaction yield to maintain functional group surface density. It is questionable whether each layer generates enough functionalities so the subsequent layer will be of good quality [4]. Surface defects must be repaired by cross-linking or they will grow exponentially. In addition, each layer may require several chemical activation steps; the synthesis of multilayer films can be very time consuming [12].

1.2 Electrostatic self-assembly process

1.2.1 Process description

Figure 1-1 shows the basic concept behind the ESA process, which can be used equally well for the fabrication of coatings on structural materials or functional electronic and optoelectronic devices on planar substrates. On the left, the substrate surface has been thoroughly cleaned and negatively charged through chemical processing. The charged substrate is dipped into an aqueous solution containing polycations, which are attracted to the anionic substrate surface and assemble themselves into a molecular monolayer. The molecular order of such individual monolayers is nearly perfect, in much the same way that electrical charge on a free conducting surface distributes itself uniformly over the surface in order to minimize total system energy. Upon removal from the "positive" solution, the surface of the substrate is flushed with ultrapure water to remove any loose particles that may be held on the surface by weak van der Waals forces and are not part of the ionically bonded monolayer. A polyanionic monolayer is deposited in the same manner, and subsequent layers are added in

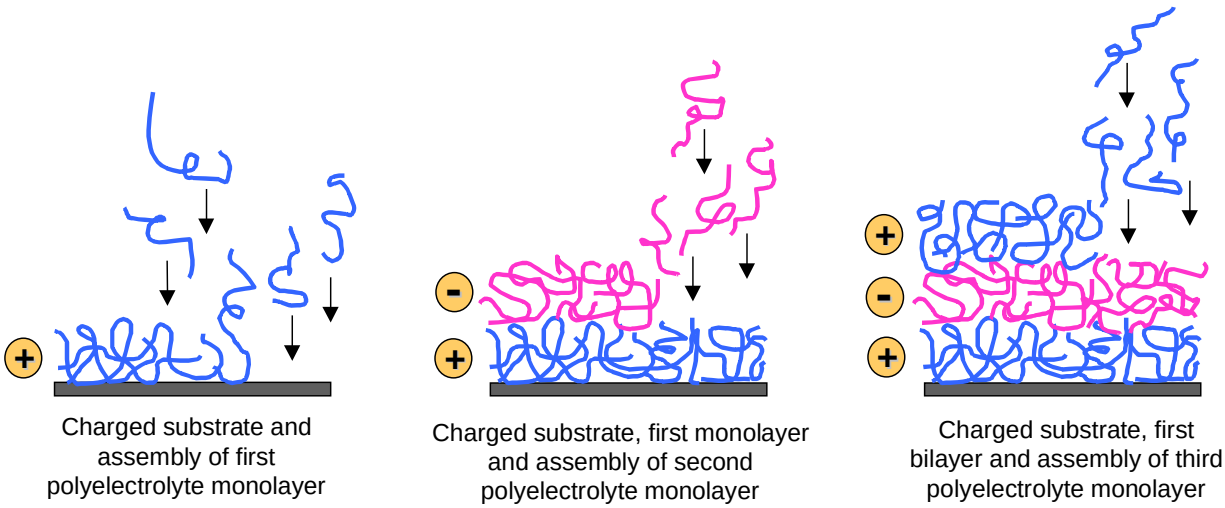

Figure 1-1. Basic ESA schematic for buildup of multilayer assemblies by consecutive adsorption of anionic and cationic polyelectrolytes.

bilayer pairs by alternating between the polyanion and polycation solutions, producing a multilayer thin-film structure as shown. Although Figure 1-1 suggests that each of the successive layers is a long polymer-like molecular chain, individual nanoparticles may be incorporated into any or all of the monolayers, allowing wide design opportunities for thin films with specific or multifunctional properties.

ESA processing of optical thin films for linear and nonlinear applications has the following major advantages over traditional methods.

- **Excellent nanoscale molecular level uniformity** permits the fabrication of high quality films and devices with extremely low scattering losses.
- **Self-assembly** without the need for additional processing.
- **Long-term stability** - The molecules arrange themselves to achieve a thermodynamic minimum; the structural ordering of the self-assembled film will not decay over time.
- **Excellent long-term environmental robustness** is achieved by excellent molecular order that limits defects, and can be enhanced through the incorporation of pliable high performance polymers (such as polyimides and polyamides).
- **Synthesis at room temperature and pressure** - Avoiding high temperature processes allows multilayer coatings to be created on nearly any solid substrate, including plastics, semiconductors, organic films, ceramics or metals, without degrading or destroying the substrate. NLO thin film synthesis requires neither the high temperature, difficult crystallization methods of inorganic crystals nor the elevated temperature and high electric field processing of poled polymers.
- **Low-cost manufacturing** - ESA thin-film fabrication simply consists of dipping or spraying a charged substrate with an aqueous polyelectrolyte solution, rinsing it, then dipping or spraying it with a second polyelectrolyte solution of opposite charge, and so on, until a desired thickness is obtained. Capital equipment costs for basic fabrication are thus extremely low (the cost of large liquid containers and sprayers), and the process may be upscaled in size and volume and easily automated.
- **Capability for high quality, thick, multilayer fabrication** is allowed due to the uniformity of each layer and the avoidance of geometrical defects caused by conventional covalent bonding-based self-assembled monolayer (SAM) approaches. Unlike other self-assembly methods that allow deposition of only a few layers, the synthesis of more than 2000 ESA bilayers has been demonstrated as part of this work. Multilayer structures allow the incorporation of multiple functions into a single film.
- **Broad range of layer functionality** - Since the ESA technique involves the use of alternating anionic and cationic layers, materials that provide enhanced secondary properties can be easily incorporated, allowing control of the optical, electronic, magnetic, thermal and mechanical properties. For example, the use of high performance polymers as the alternate layer can give excellent thermal stability, mechanical properties and processability.
- **Compatibility with conventional photolithographic processes** - Multiple layers self-assembled by ionic bonding may be patterned using standard methods to create integrated devices.

- **Environmentally friendly** - ESA is a water-based process, involving no volatile organic compounds, and consuming negligible power.
- **Independent of substrate size or topology** - In contrast to Langmuir-Blodgett films, substrates of any size or shape may be coated uniformly on all surfaces.
- **No covalent bonds need to be formed** - In contrast to chemisorption techniques [9], 100% reaction yield is not required to maintain uniform multilayer film growth.

1.2.2 Previous ESA work

The development of ESA thin films provides significant advantages over the production of organic thin films by alternate methods. For example, ESA films exhibit long-term stability of in contrast to poled polymers [23], can provide thicker films (upwards of 10 microns) than the Langmuir-Blodgett technique, and can be fabricated much more rapidly than covalent self-assembly [24] methods. ESA processing has thus been the focus of a wealth of research in the last decade.

The concept of alternate adsorption of oppositely charged polyions began with Iler's [10] demonstration of sequential deposition of negative silica colloids and positive alumina fibrils in 1966. The potential of this novel process was largely ignored until the early 1990s, when Decher and coworkers at Gutenberg University in Mainz, Germany, demonstrated optically transparent multilayer films of four different polyelectrolytes [11]. Uniform growth was verified using UV/vis spectroscopy and small angle X-ray scattering (SAXS) and it was observed that aperiodic assemblies were possible, with no substrate size limitation, both significant advantages over the L-B method. Subsequent research has moved in two equally important directions: a) the understanding of the process itself and variables that control the resulting film structures and b) the incorporation of a wider range of molecules for an expanding number of potential applications.

Decher's group has appeared to focus on investigations of process and structure. Using what has become a somewhat standard test film, anionic polystyrensulfonate sodium salt (PSS) and cationic polyallylamine hydrochloride (PAH), 0.5Å-level control of each bilayer thickness was demonstrated by increasing the dipping solution salt concentration [12]. The increased numbers of counterions resulted in a "loopy," or coiled conformation of the polymers, rather than a flat conformation, by screening the electrostatic forces between ionic groups on the polyelectrolyte chains, forming monolayers much thicker than the cross-section of the polymers involved. At very high salt concentrations, however, the film does not grow because of the extremely rough film surfaces produced by these "loopy" structures [15].

The content of ESA films may include three components: polyelectrolytes, counterions (e.g. NaCl) and water [17]. The thermal behavior of ESA films was found to be dependent on this water content by observing changes in the film thickness with variations in temperature. Decreased thickness at elevated temperatures is due to a loss of water, as verified using FTIR and SAXS [13]. Cooling back to room temperature restores a certain amount, but water lost in this manner is only completely recovered after remaining in ambient conditions for extended periods of time, up to two weeks [15].

Consistent film growth requires that the film surface charge density and roughness return to the same values after each adsorption cycle (anion and cation layer pair). As discussed in more detail in Chapter 2, this requires some minimum immersion time for the molecules to move to the film surface and arrange themselves in a monolayer. The first study on the effects of dipping time variations [15] indicated that at immersion times less than this minimum, the surface charge may be reversed, but the surface roughness was increased, producing smaller layer thicknesses. For the poly(vinyl sulfate) potassium salt (PVS) / PAH system investigated, this process was not diffusion limited, but most likely dependent on molecular conformation changes on the film surface. Recently, dipping times as short as 20 seconds have been demonstrated and the limiting factors (diffusion vs. conformation) found to be species dependent [25].

It has been confirmed that ESA films are deposited in individual molecular layers and that the chain-chain interdigitation length is less than the layer thicknesses [17,26]. This investigation of the internal film structure also revealed that the initial film layers are thinner than those in the remainder of the film [15,17,27]. The equilibrium layer thickness is reached only after several adsorption cycles. More recently, the molecular mechanisms responsible for this effect were more closely considered [16]. The polymer layer binding was found to be due to the formation of ion pairs, whose binding energy is relatively weak. The polymer sticks not because the bonding is strong, but because there are a large number of binding sites. In addition, the amount of material adsorbed in each layer is not limited by the number of these ionic binding sites as only about half are actually utilized. It is the electrostatic barrier which produces the self-limited monolayer thickness. It is evident therefore that the highly charged substrate surface could greatly affect the layer thicknesses close to the substrate, resulting in thinner layers until sufficient distance from the substrate is established. Since the binding is not site-limited, surface defects and roughness do not affect film assembly because there are plenty of other sites to bind to.

As understanding of the process grew, it became possible to incorporate an expanding variety of molecules into ESA films. Due to the water-based chemistry of ESA, this work initially focused on biological molecules, beginning with DNA [28], an obvious choice due to the similarity of its long chain structure to the molecules previously assembled. Deposition of large, spherical virus particles was then demonstrated [29]. Such particles were found to partially penetrate the previously assembled layers, producing monolayers that were thinner than the diameter of the particles with extremely rough surfaces. This surface roughness was smoothed by the deposition of the following polymer layers, which filled in the gaps between the particles. The assembly of globular proteins exhibited similar results [30,31]. In this case, the spatial ordering of the molecules is critical for biosensing and enzymatic reaction applications. Decher and coworkers established the first ESA of biological macromolecules in their active state [32], again made possible by the water-based process. Recently, the electrode-driven aerobic oxidation of styrene was demonstrated using ESA films of redox proteins assembled on gold electrodes [33].

Other groups have focused on electronic and optical applications of ESA films. Rubner's group at MIT produced band-gap modulated thin film architectures by assembling electroactive and conductive polyions [27,34]. Subsequent ESA work in that group has focused on poly(p-phenylene vinylene) (PPV)-based LEDs [35-38]. Using a similar process, but replacing the polyanions with 2-D lamellar sheets, MINIM (metal-insulator-nanocluster-insulator-metal)

capacitors, which allow the observation of single electron effects, have been fabricated [39]. TiO_2/polymer nanocomposite ESA films have been demonstrated [40]; potential applications include catalysts, sensors, nanofiltration, semiconductor devices and packaging materials. Ultrathin magnetic ESA films of Fe_3O_4 and polyimide offer possibilities for information storage and magnetic imaging [41]. More recently, ESA has been used to deposit functional coatings on optical fibers to form nanointerferometric cavities for use in humidity sensing at the Fiber & Electro-Optic Research Center here at Virginia Tech [42].

It is therefore evident that the ESA process can be adapted to incorporate a wide variety of molecules, including nonlinear optical materials, conducting polymers, biological macromolecules, magnetic materials, and metallic and oxide nanoparticles. The composition of each layer can be controlled by the incorporation of appropriately chosen molecules and the structure of each layer can be controlled by adjusting the deposition parameters, allowing nanoscale control over film properties. The versatility of this technique offers potential in a wide range of fields, including optics, electronics, biosensing, filtration and surface modification.

1.3 Motivation and objectives for this work

New thin-film materials and devices having a wide range of optical, electronic, mechanical and other capabilities are required for applications in communication systems, information storage, display systems, sensors, and other fields. The potential to incorporate multiple properties into the films at the molecular level is attractive due to secondary property requirements and the desire for fast and inexpensive production. Conventional thin film methods fall short of meeting all these objectives. For example, spin coating, while inexpensive, lacks control of exact thickness and molecular-level structure. Vapor deposition techniques produce thermal stresses, which reduce film integrity in micron-thick films. The limitations of other self-assembly methods such as L-B films and covalent self-assembly are discussed above. As delineated in Section 1.2, ESA offers a number of advantages over these methods. Due to the multicomponent, layer-by-layer nature of ESA, not only two, but a variety of polyions can be used as long as proper polyanion/polycation alternation is maintained, allowing the incorporation of a wide variety of molecules to provide multiple functions and properties. Its application has already been demonstrated in work related to LEDs, magnetics, hard coatings and biosensors.

The major objective of this dissertation is to demonstrate the feasibility of novel, low-cost ESA processing for the manufacture of linear and nonlinear optical thin film components. This includes the following.

- Investigation of ESA processing parameters and capabilities, including consideration of process automation,
- Review of optical filtering methods and functions,
- Synthesis of prototype thin films, filters and coatings, with optical properties designed at the molecular level,
- Demonstration of multimicron films with controlled refractive index profiles, both continuous and discontinuous, and

- Demonstration of molecular orientation in ESA films, resulting in second-order nonlinear optical effects.

It will become obvious that there is a great amount work remaining to be done in this area. One may potentially build a lifelong career studying this process and the resulting films for various applications. Suggested investigations that will build on this work are described in Chapter 5.

1.4 Outline of dissertation

This dissertation is organized as follows - **Chapter 2** presents a discussion of ESA processing and film characterization methods. The origin of materials used and the experimental methods for fabrication and characterization are given. Process variables that control resulting film properties, both intentionally and incidentally, are investigated. This is followed by a study of the effect of environmental conditions on ESA film characteristics. Finally, a description of initial process automation efforts, which will be required for transition of ESA to a manufacturing environment, is presented.

The application of ESA technology to linear optical interference filters is discussed in **Chapter 3**. Basic ABAB layered ESA films of multiple material combinations were fabricated and characterized. Using this information, two methods of controlling refractive index in ESA films were demonstrated, multilayer patterning and aqueous mixtures. High and low index films were chosen from the basis of ESA optical materials established, and dielectric stack reflectance filters were fabricated, demonstrating the capability of step-index profile synthesis. This was expanded to continuous index profile, or rugate-type, filters. Finally, ESA antireflection (AR) filters for visible and IR wavelengths were fabricated.

While Chapter 3 concerned the linear optical applications of ESA films, **Chapter 4** evaluates noncentrosymmetric films fabricated using ESA technique and second order nonlinear optical results. Initial studies utilized commercially available NLO polymer dyes. The nature of the ESA process inherently yields polar ordering of the molecules, suggesting that similar films may be fabricated from other commercially available molecules, as well as from molecules specifically designed to yield an enhanced macroscale net dipole moment. Consequently, the second half of Chapter 4 concerns the ESA processing of novel NLO polymers synthesized at Virginia Tech and the resulting enhanced $\chi^{(2)}$ results.

Chapter 5 concludes this dissertation with a summary of the significance and primary contributions of this investigation. In addition, recommendations for future research in this area are made.

1.5 References

1. Special issue on organic thin films, *Adv. Mater.* **3**, (1990).
2. H. Fuchs, H. Ohst and W. Prass, "Ultrathin Organic Films: Molecular Architectures for Advanced Optical, Electronic and Bio-Related Systems," *Adv. Mater.* **3**, no.1, 10 (1991).

3. A. Ulman, *An Introduction to Ultrathin Organic Films, From Langmuir-Blodgett to Self-Assembly*, Academic Press: New York (1991).
4. D. Li and O. Ramos Jr., "Molecular Self-Assemblies as Advanced Materials," in *Photonic Polymer Systems - Fundamentals, Methods and Applications*, ed. D.L. Wise et al., Marcel Dekker, New York (1998).
5. G.M. Whitesides, J.P. Mathias, C.T. Seto, "Molecular Self-Assembly and Nanochemistry: A Chemical Strategy for the Synthesis of Nanostructures," *Science* **254**, 1312 (1991).
6. D.L. Allara, "Critical issues in applications of self-assembled monolayers," *Biosensors and Bioelectronics* **10**, 771 (1995).
7. G.M. Whitesides, "Self-assembly and Nanotechnology," *Proc. SPIE* **2716** (1996).
8. G. Roberts, *Langmuir-Blodgett Films*, Plenum Press: New York (1990).
9. J. Gun, G. Sagiv, "On the formation and structure of self-assembling monolayers. 3. Time of formation, solvent retention, and release," *J. Colloid Interface Sci.* **112**, 457 (1986).
10. R.K. Iler, *J. Colloid Interface Sci.* **21**, 569 (1966).
11. G. Decher, J.D. Hong and J. Schmitt, "Buildup of ultrathin multilayer films by a self-assembly process: II. Consecutively alternating adsorption of anionic and cationic polyelectrolytes on charged surfaces," *Thin Solid Films* **210/211**, 831 (1992).
12. G. Decher and J. Schmitt, "Fine-Tuning of the film thickness of ultrathin multilayer films composed of consecutively alternating layers of anionic and cationic polyelectrolytes," *Progr. Colloid Polym. Sci.* **89**, 160 (1992).
13. J.D. Hong, K. Lowack, J. Schmitt and G. Decher, "Layer-by-layer deposited multilayer assemblies of polyelectrolytes and proteins: from ultrathin films to protein arrays," *Progr. Colloid Polym. Sci.* **93**, 98 (1993).
14. G. Decher, Y. Lvov and J. Schmitt, "Proof of multilayer structural organization in slef-assembled polycation-polyanion molecular films," *Thin Solid Films* **244**, 772 (1994).
15. Y. Lvov, G. Decher and H. Möhwald, "Assembly, Structural Characterization, and Thermal Behavior of Layer-by-Layer Deposited Ultrathin Films of Poly(vinyl sulfate) and Poly (allylamine)," *Langmuir* **9**, 481 (1993).
16. K. Lowack and C.A. Helm "Molecular Mechanisms Controlling the Self-Assembly Process of Polyelectrolyte Multilayers," *Macromolecules* **31**, 823 (1998).
17. J. Schmitt et al., "Internal Structure of Layer-by-Layer Adsorbed Polyelectrolyte Films: A Neutron and X-ray Reflectivity Study," *Macromolecules* **26**, 7058 (1993).
18. I. Langmuir, *J. Am. Chem. Soc.* **39**, 1848 (1917).
19. K.B. Blodgett, *J. Am. Chem. Soc.* **57**, 1007 (1935).
20. J.A. Zasadinski et al., "Langmuir-Blodgett Films," *Science* **263**, 1726, March 25, 1994.
21. J.P. Folkers, P.E. Laibinis and G.M. Whitesides, "Self-assembled monolayers of alkanethiols on gold: Comparisons of monlayers containing mixtures of short-chain and long-chain constituents with CH_3 and CH_2OH terminal groups," *Langmuir* **8**, 1330 (1992).
22. J.M. Tour et al., "Self-assembled monolayers and multilayers of conjugated thiols, alpha, omega-dithiols, and thioacetyl-containing adsorbates: Understanding attachments between potential molecular wires and gold surfaces," *J. Am. Chem. Soc.* **117**, 9529 (1995).
23. K.D. Singer, S.J. Lalama, and J.E. Sohn, Appl. Phys. Lett. **49**, 248 (1986).
24. W. Lin et al., *Agnew Chem. Int. Ed. Engl.* **23**, 1497 (1995).
25. Y. Lvov et al., "High speed multilayer film assembly by alternate adsorption of silica nanoparticles and linear polycations, *Chem. Commun.* **1998**.

26. J.J. Ramsden, Y.M. Lvov, G. Decher, "Determination of optical constants of molecular films assembled via alternate polyion adsorption," *Thin Solid Films* **254**, 246 (1995).
27. M. Ferreira, J.H. Cheung and M.F. Rubner, "Molecular self-assembly of conjugated polyions: a new process for fabricating multilayer thin film heterostructures," *Thin Solid Films* **244**, 806 (1994).
28. Y. Lvov, G. Decher and G. Sukhorukov, "Assembly of Thin Films by Means of Successive Deposition of Alternate Layers of DNA and Poly(allyamine)," *Macromolecules* **26**, 5396 (1993).
29. Y. Lvov, et al., "Successive Deposition of Alternate Layers of Polyelectrolytes and a Charged Virus," *Langmuir* **10**, 4232 (1994).
30. Y. Lvov, K. Ariga, I. Ichinose and T Kunitake, " Assembly of Multicomponent Protein Films by Means of Electrostatic Layer-by-Layer Adsorption," *J. Am. Chem. Soc.* **117**, 6117 (1995).
31. Y. Lvov, K. Ariga and T. Kunitake, "Layer-by-layer Assembly of Alternate Protein/Polyion Ultrathin Films," *Chem. Lett.* **1994**, 2323.
32. G.B. Sukhorukov, H. M☂hwald, G. Decher and Y. Lvov, "Assembly of polyelectrolyte films by consecutively altenrating adsorption of polynucleotides and polycations," *Thin Solid Films* **284/285**, 220 (1996).
33. Y. Lvov et al., "Direct Electrochemistry of Myoglobin and Cytochrome $P450_{cam}$ in Alternate Layer-by-Layer Films with DNA and Other Polyions," *J. Am. Chem. Soc.* **120**, 4073 (1998).
34. J.H. Cheung, A.F. Fou and M.F. Rubner, "Molecular self-assembly of conducting polymers," *Thin Solid Films* **244**, 985 (1994).
35. A.C. Fou et al., "Fabrication and properties of light emitting diodes based on self-assembled multilayers of poly (p-phenylene vinylene)," *J. Appl. Phys.* **79**, 7501 (1996).
36. O. Onitsuka et al., "Enhancement of light emitting diodes based on self-assembled heterostructures of poly (p-phenylene vinylene)," *J. Appl. Phys.* **80**, 4067 (1996).
37. H. Mattoussi, "Electroluminescence from heterostructures of poly (phenylene vinylene) and inorganic CdSe nanocrystals," *J. Appl. Phys.* **83**, 7965 (1998).
38. J.W. Baur et al., "Thin-film light emitting devices based on sequentially adsorbed multilayers of water-soluble poly (p-phenylene vinylene)," *Adv. Mater.* **10**, 1452 (1998).
39. D.L. Feldheim, K.C. Grabar, M.J. Natan and T.E. Mallouk, "Electron transfer in Self-Assembled Polyelectrolyte/Metal Nanoparticle Heterostructures," *J. Am. Chem. Soc.* **118**, 7640 (1996).
40. Y. Liu, A. Wang and R. Claus, "Molecular Self-Assembly of TiO_2/Polymer Nanocomposite Films," *J. Phys. Chem. B* **101**, 1385 (1997).
41. Y. Liu, A. Wang and R. Claus, "Layer-by-layer electrostatic self-assembly of nanoscale Fe_3O_4 particles and polyimide precursor on silicon and silica surfaces," *Appl. Phys. Lett.* **71**, October 1997.
42. F.J. Arregui et al., Optical Fiber Humidity Sensor Formed by the Ionic Self-Assembly Monolayer Process," *Proc. SPIE* **3670**, Newport Beach, CA, March 1999.

CHAPTER 2

ESA Processing and Film Characterization Methods

As discussed in Chapter 1, the ESA process offers significant advantages over conventional thin film fabrication methods, making it an excellent choice for the synthesis of both linear and nonlinear optical filters, coatings and devices. The molecular-level uniformity achieved in each monolayer permits thin-film scaling to thousands of bilayers and precise grading of properties. Extremely homogeneous mixtures of inorganic nanoparticles, polymers, and other molecules can be incorporated into each monolayer, allowing nanoscale control over film optical, electronic, magnetic, mechanical and multifunctional properties. Film characteristics are dependent on the composition of each monolayer, the process parameters used to deposit the monolayers, and the order in which the layers are assembled. The ionic bonding of molecules inherently self-limits each monolayer thickness, producing stable thin films on substrate surfaces of arbitrary shape and size. Much like the behavior of electrons on conductive surfaces, the polyelectrolyte molecules arrange themselves uniformly across the charged substrate surface. This chapter discusses the ESA processes used for this dissertation work and resulting film properties.

The chapter is organized as follows. The first section explains the materials and methods used in film fabrication and characterization. Section 2.2 demonstrates the capability of ESA processing to coat substrates of a wide variety of materials, shapes and sizes. Variations in the process that can control the resulting film characteristics are discussed in Section 2.3. These variables should be considered both as methods in designing films and as conditions to consider to produce controlled experiments. Section 2.4 investigates the environmental stability of the polymer films in this study and process automation efforts are discussed in Section 2.5. The chapter summary is found in Section 2.6.

2.1 Experimental processes

As shown in Figure 2-1 (p. 16), the key to a successful buildup of multilayer thin film assemblies in such a layer-by-layer fashion is the inversion and subsequent reconstruction of substrate surface properties. In order to obtain a linear increase in the total film thickness with an increase in the number of adsorption cycles, the appropriate deposition conditions must be determined. In the case of polyelectrolyte films, the surface charge must be reversed after every other adsorption step, and this is achieved by alternating the deposition of polyanions and polycations from their respective aqueous solutions. For each molecule incorporated into the film, a particular combination of pH and concentration must be determined to produce both uniform growth and a homogeneous film. Uniform film buildup was confirmed using UV/vis spectroscopy and ellipsometry techniques. Linear increases in thickness and absorption indicate consistent monolayer assembly with each dipping step.

Further examples of dipping parameters with related film characteristics include salt concentration, dipping time, and drying procedures. Monolayer thicknesses may be increased by the addition of NaCl to the solutions. This also must be balanced with homogeneity; if the concentration is too high, agglomerates will form, producing a cloudy film with a high level of scattering. As fabrication procedures are optimized, the dipping time will be reduced to the minimum possible value for high-speed fabrication. As described above, after the adsorption of each monolayer, the films are carefully rinsed with ultrapure water. The film may then be immersed in the subsequent solution wet, or dried in a stream of nitrogen gas. This will affect the structure of the monolayer interfaces and the thickness of the film. For non-optimized films, at minimum the correct pH/concentration combination and sufficient dipping time must be established before self-assembly can occur. Multilayer films may then be synthesized on a wide variety of substrates, as demonstrated in the following section.

2.1.1 Materials

Numerous materials were required for this research, as both film components and substrates. Their details are summarized in Tables 2-1 and 2-2. All materials were used without further purification.

The ultrapure water used for all experiments and cleaning procedures was obtained from a Barnstead Nanopure III system, with a resistivity greater than 17 MΩ·cm.

2.1.2 Substrate modification procedures

In this study, glass, quartz, single-crystal silicon and ITO-coated glass with hydrophilic surfaces were used as substrates for ESA film deposition. The first three substrate types were cleaned with a "piranha solution," a 30:70 mixture of 30% hydrogen peroxide (H_2O_2) and concentrated sulfuric acid (H_2SO_4) at room temperature for 1 hour, followed by extensive rinsing with ultrapure water, and dried in an oven at 50°C for several hours. A substrate modified in this way is negatively charged.

Table 2-1. Materials used as film components.

MOLECULE	DETAILS	OBTAINED FROM
PDDA	Poly diallyldimethyl ammonium chloride 20 wt.% in H_2O M_w 400,000-500,000	Aldrich
PAH	Poly allylamine hydrochloride M_n 50,000-65,000	Aldrich
PSS	Poly(sodium 4-styrenesulfonate) M_w ca. 70,000	Aldrich
Poly S-119	M_w 100,000-160,000 Poly(vinylamine) backbone Azo chromophore Color: orange Poly S-119 is a trademark of Dynapol, Palo Alto, CA	Sigma
Poly R-478	Poly(vinylamine) sulfonate backbone Anthrapyridone chromophore Color: violet Poly R-478 is a trademark of Dynapol, Palo Alto, CA	Sigma
Direct Red 75	Molecular Formula: $C_{33}H_{26}N_8O_{15}S_4$ Molecular Weight: 990.8 UV wavelength max. (nm): 522 Dye content ~30%	Aldrich
Direct Yellow 50	Molecular Formula: $C_{35}H_{28}N_6O_{13}S_4$ Molecular Weight: 956.83 UV wavelength max. (nm): 390 Dye content ~40%	Aldrich
Alcian Blue 8GX, certified	Molecular Formula: $C_{56}H_{68}Cl_4CuN_{16}S_4$ Molecular Weight: 1298.88 UV wavelength max. (nm): 615 Dye content ~50%	Aldrich
ZrO_2 nanocluster	F. W. 23.22 20 wt.% in H_2O; colloidal dispersion	Alfa Aesar
PCBS	Poly{1-[4-(3-carboxy-4-hydroxyphenylazo)-benzenesulfonamido]-1,2-ethanediyl, sodium salt}	Aldrich
Polydye1 - Polydye9	Novel NLO polymer dyes synthesized at the Fiber & Electro-Optics Research Center of Virginia Tech	Virginia Tech

Table 2-2. Substrate materials.

MATERIAL	OBTAINED FROM
Quartz	Chemglass, Inc.
Single crystal silicon	EL-CAT, Inc.
Glass microscope slides	Fisher Scientific
Indium tin oxide (ITO) -coated glass	Applied Films, Inc.

ITO coated glass substrates were first cleaned by ultrasonically agitating them twice in ethanol. They were then immersed in a 1:1 mixture of ethanol:H_2SO_4 at room temperature for 1 hour and rinsed extensively in ultrapure water.

2.1.3 Multilayer dip processing procedures

Solutions of the commercially available polyions were made by dissolving the polymers in acidic solutions. Typical pH value of these solutions was 4.5. The Polydye solutions required both acidic and basic solutions, as discussed in Chapter 4.

As the hydrophilic substrates possessed negatively charged surfaces, film synthesis began by immersing the substrate in the polycationic solution (PAH, PDDA, ZrO_2, Alcian Blue) at room temperature to adsorb a monolayer of the polycation molecule, resulting in a positive film surface charge. After rinsing in ultrapure water, the substrate was dipped in the polyanionic solution to adsorb a monolayer of polyanion molecule, restoring the negative surface charge. The substrate was rinsed again with ultrapure water to remove any loose molecules not ionically bonded to the surface. By repeating these dipping procedures, multilayer films were self-assembled, as shown schematically in Figures 2-1 and 2-2. The substrate surfaces were washed a minimum of three times between each adsorption step.

A typical adsorption time for the polymer dyes and PAH/PDDA or PSS systems times was 1 minute. ZrO_2 nanoparticle/polymer composite systems were dipped using a 3 minute immersion time. An investigation on the effect of dipping time is discussed below.

After each adsorption and rinsing step pair, the films were either dried in a stream of nitrogen, or dipped in the subsequent solution still wet. The effects of these drying procedures on film structure were studied using ellipsometry and UV/vis spectroscopy, as discussed in Section 2.3.

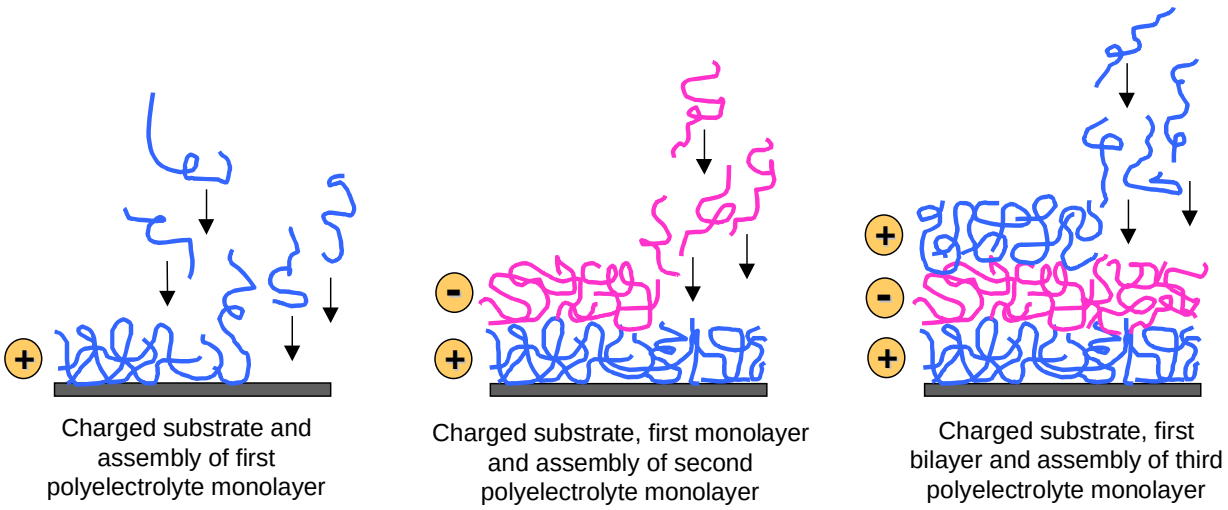

Figure 2-1. Basic ESA schematic for the buildup of multilayer assemblies by consecutive adsorption of anionic and cationic polyelectrolytes (This figure, first shown in Chapter 1, is repeated here for convenience).

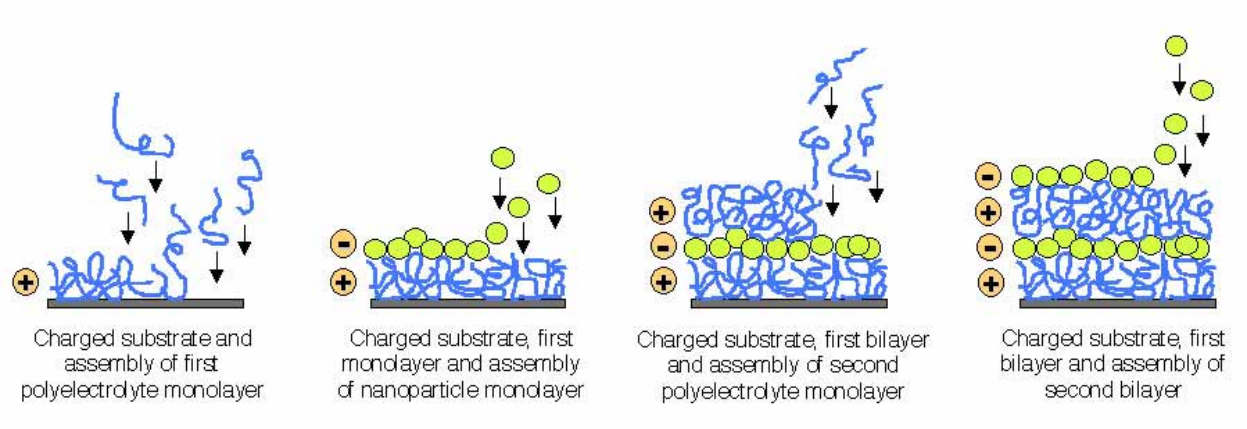

Figure 2-2. Basic ESA schematic for the buildup of multilayer assemblies by consecutive adsorption of cationic polyelectrolytes and anionic nanoparticles.

2.1.4 Characterization techniques

The ESA thin films were characterized and evaluated to determine structural, optical and secondary characteristics with emphasis on uniformity, film thickness, layer-by-layer linearity, surface morphology, thermal properties and optical characteristics, using the following materials analysis tools.

UV/vis spectroscopy • Multilayer ESA films were characterized using a Hitachi Model U-2010 UV/vis spectrophotometer to monitor film growth and uniformity, and determine the transmission and absorption spectral characteristics of films. Values reported are the average of measurements taken at three locations on each sample. The optical

absorbance plots measured at several points during film growth gave a good indication of film quality and uniformity.

Ellipsometry • Multilayer films assembled on single-crystal Si substrates were measured using a Rudolph Auto-EL ellipsometer to determine the film thicknesses and refractive index. The instrument was calibrated using a standard silicon wafer with SiO_2 thickness 1097 ± 3Å and index 1.462 ± 0.002. The reported values in this study were the average of measurements taken at three locations, twice each. Thickness was a critical parameter in both the linear and nonlinear optical experiments.

Atomic force microscopy (AFM) • A Digital Instruments NanoScope AFM was used in TappingMode™ to image the surface morphology of films with atomic resolution, utilizing topology and phase imaging in combination. Surface roughness analyses allowed the comparison and evaluation of different dipping techniques.

Contact angle • To determine the wettability and quality of monolayer and multilayer films, contact angle measurements were made using a Rame-Hart NRL Contact Angle Goniometer Model 100-00. The wettability of a film is dependent on the structure of the outermost few angstroms and thus can be used to verify the requisite reversal of surface charge with the addition of each monolayer in an ESA film. The measurements were taken at room temperature; the temperature was not controlled and so varied from 20-25°C. The drop volume was 4 μL and was placed on the film surface using a microliter syringe. The measurements were taken within 1 minute of drop application. The tangent to the drop was estimated visually. Each reported value was the average of 6 measurements taken on both sides of three drops.

Fluorescence spectroscopy • A Hitachi F-4500 Fluorescence Spectrophotometer to determine film emission characteristics to evaluate their suitability for related optoelectronic applications. In addition, fluorescence spectra of novel polymer Polydye films were examined to illustrate the superposition of the characteristics of the two polymer film components.

2.2 Substrate variability

Initial experiments of this study developed methods to deposit commercially available organic dyes onto multiple substrates of different sizes, different shapes and different materials. The purpose of this demonstration was to show that ESA processing can be used to apply films of uniform thickness and properties on surfaces of small and large, flat, curved, and geometrically complicated substrates. Substrates utilized included glass, quartz, single-crystal silicon, plastic and transparent conductive substrates.

ESA processing was used to apply coatings to several glass substrates of different sizes and shapes. For these first simple experiments, colorful rather than transparent coatings were fabricated to allow simple visual inspection during and after the multi-step dipping process. A number of different polymers were used to demonstrate their suitability for incorporation in ESA

films. Figure 2-3 shows standard 1"x3" silica glass microscope slides with 32 bilayer orange Poly S-119, violet Poly R-478 and Direct Red 75 ESA films. Poly(diallyldimethylammonium chloride) (PDDA) was used as the polycation in all three. Microscope slides were used for a large percentage of the testing in this study because they were inexpensive and easy to handle and store.

Figures 2-4 and 2-5 illustrate that films may be applied to larger substrates using the ESA method. The larger, 5.2"×7.6" flat glass plate is coated with a film of Poly S-119 and poly(allylamine hydrochloride) (PAH); the 5" diameter circular pyrex plate is coated with Direct Yellow 50 (Sigma) / PAH. Due to the size of these specimens, their uniformity could not be quantified. Visual inspection indicates uniformity of the coating over the surface of the substrates and equal coverage of the sides of the plates.

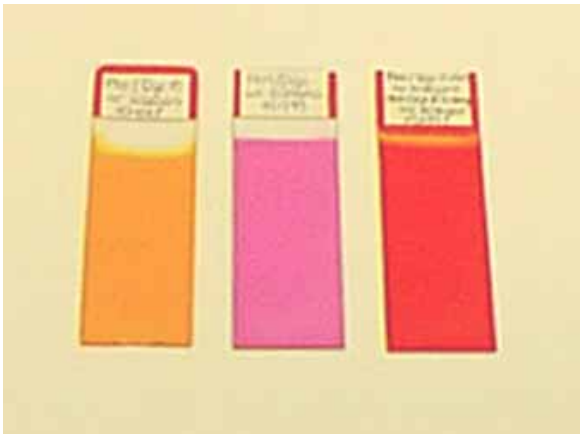

Figure 2-3. 32 bilayer Poly S-119, Poly R-478 and Direct Red 75 ESA films on glass microscope slides.

Figure 2-4. 50 bilayer Poly S-119/PAH ESA film on silica glass plate; demonstrates ability to coat larger substrates.

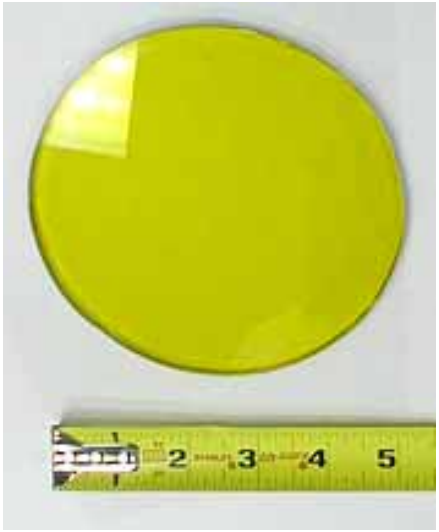

Figure 2-5. 70 bilayer Direct Yellow 50/PDDA ESA film on 5" glass substrate; demonstrates ability to coat larger substrates.

Figure 2-6 illustrates electrostatic self-assembly on curved substrates. Here a 1.8"-diameter concave/convex glass lens has been coated with 45 bilayers of Poly R-478/PDDA to demonstrate ESA coating coverage over a curved surface. The curvature of the surface can be seen from the shape of the reflections of the laboratory lighting.

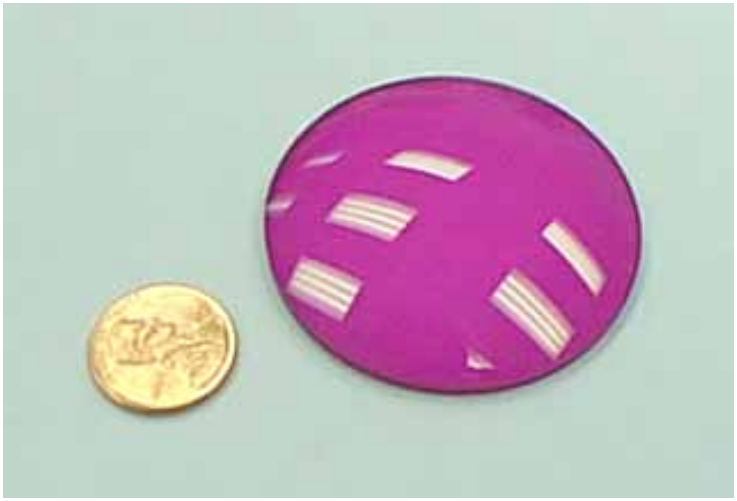

Figure 2-6. 45 bilayer Poly R-478/PDDA ESA film on a concave/convex glass lens; demonstrates ability to uniformly coat curved surfaces.

A substrate with a more complicated, multi-faceted shape is shown in Figure 2-7. Here a 2" length x 0.75" side equilateral glass prism has been coated with 45 bilayers of Alcian Blue 8GX/poly (sodium 4-styrenesulfonate) (PSS). In this case, the dye was the polycation, while PSS was the passive polyanion. Again, the ESA process allows the uniform coating of all surfaces of the substrate.

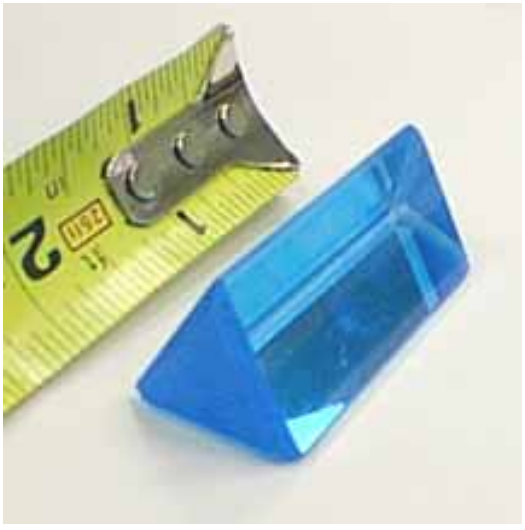

Figure 2-7. 45 bilayer Alcian Blue 8GX/PSS ESA film on equilateral glass prism.

An important advantage of the ESA process over other thin film methods is that it can be applied equally well in large scale and micro- or nanoscale applications. The deposition of ESA films on very small objects is illustrated in Figure 2-8, which shows 40 bilayer coatings of Alcian Blue 8GX/Polystyrene, Poly R-478/PDDA, and P-S119/PDDA on 125 micron-diameter glass optical fibers. The ability to coat fibers and specialized optical fiber components with such electro-optic materials will be important to the development of optoelectronic devices such as fiber polarizers [1] and sensors [2]. Films have also been deposited on small non-silica components. Figure 2-9 shows a 40 bilayer film of Poly R-478/PDDA and a 16 bilayer film of Poly S-119/PDDA on etched single-crystal silicon (Si) dies used by Litton Polyscientific in the manufacturing of optical fiber bypass switches. This suggests the use of ESA-processed active electronic materials on semiconductor substrates, or other small components requiring precise control of film parameters.

In order to demonstrate electro-optic film characteristics, ESA films need to be deposited on conductive substrates, such as the indium-tin-oxide (ITO) coated glass substrates shown in Figure 2-10. 100 and 200 bilayer films of Poly S-119 and Poly R-478 were assembled on the 1"x 3" substrates. For testing, electrodes are attached using conductive epoxy.

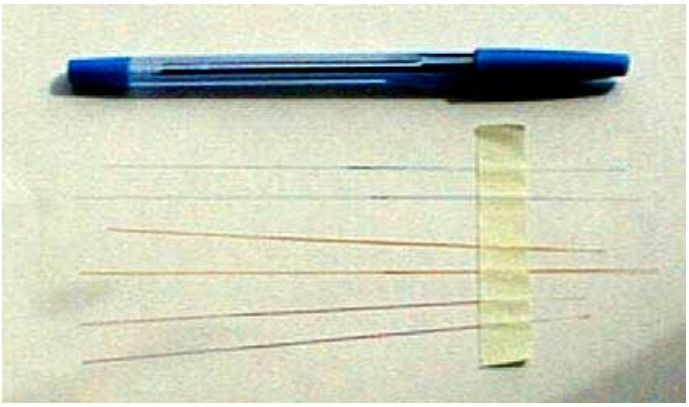

Figure 2-8. 40 bilayer Alcian Blue 8GX/PSS, Poly R-478/PDDA and Poly S-119/ PDDA ESA films on 125 μm-diameter glass optical fibers, below pen.

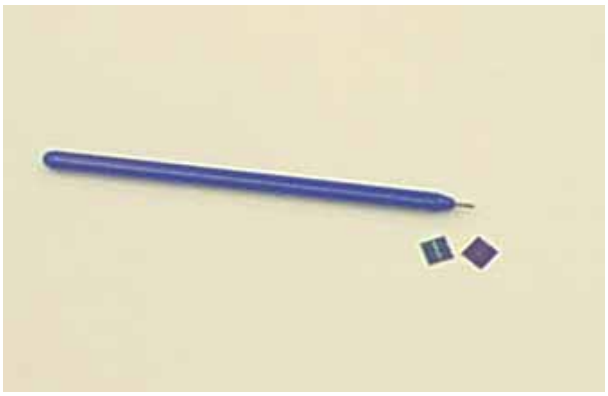

Figure 2-9. 40 Bilayer Poly R-478/PDDA and Poly S-119/PDDA ESA film on etched Si die; demonstrates ESA films on small non-glass substrate.

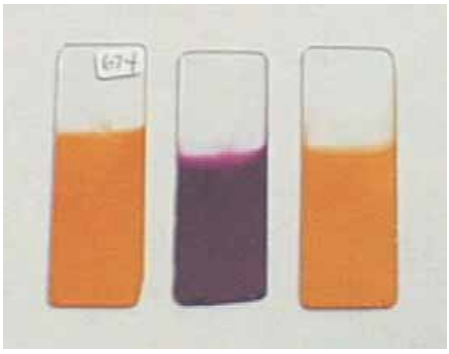

Figure 2-10. 100 bilayer Poly S-119 (right and left) and 200 bilayer Poly R-478 (center) ESA films on ITO-coated glass substrate.

The above experiments demonstrate that the ESA process can be applied equally well to substrates of almost any size or material and that the molecules self-assemble equally on all surfaces of the substrate. Uniform ESA films with greater than 2000 bilayers have been assembled in related ESA waveguide work.

2.3 Structural control

The final structure and characteristics of an ESA film are dependent on the composition of each monolayer, the conditions under which each monolayer was processed, and the order in which the monolayers are assembled. This section discusses variations in the process investigated as part of this dissertation, drying procedures, dipping time, selection of passive counterions and multilayer patterning using inorganic nanoparticles. The effect of solution concentration and salt concentration are investigated elsewhere [3, 4]. All these parameter variations should be considered both as methods in designing films and as conditions to consider to produce controlled experiments.

2.3.1 Drying procedures

In standard ESA processing, the film surface remains wet through all dipping steps. As part of the dipping parameter study, the effect on film characteristics of periodic drying to remove the water layer from the film surface was investigated. The resulting structures were evaluated using ellipsometry and UV/vis spectroscopy. Decher's group performed a similar study on PSS/PAH films using X-ray reflectivity [5]. For that film system, the results indicated that cyclic drying induced periodic modulation in the film's electron density and reduced the interfacial width between monolayers, but did not affect total film or individual bilayer thickness.

For this experiment, Poly R-478 / PDDA films were assembled on glass and single-crystal silicon substrates. From each pair, one specimen was dried in a stream of nitrogen gas after the deposition of each monolayer. The second specimen was dried only for measurement purposes; this is labeled "undried" in the plots that follow. Following each measurement, the undried film was "rehydrated" in a water bath for 15 minutes. However, previous studies [6] have shown that rehydration is not effective unless practiced using time scales on the order of days, rather than minutes. Therefore, the "undried" film can be considered as dried every 10 bilayers for comparison purposes. Identical concentrations, salt concentrations and dipping times were used for all samples.

Each bilayer in the dried film is thicker and more optically dense than the undried film. Ellipsometry data for dried and undried films are shown in Figure 2-11. A 20% increase in thickness is obtained by drying after each monolayer. The optical absorbance data (Figs. 2-12 and 2-13) shows only a 15% increase with the drying procedure. This suggests that the undried sample exhibits greater interpenetration between the monolayers since the optical absorbance peak at 522 nm is due solely to the Poly R-478 molecules, not the PDDA molecules. As each bilayer of the dried film was 20% thicker than the undried film, one may assume that 20% more molecules assembled in that bilayer. However, the UV/vis measurement indicates that the amount of Poly R-478 material in the film is only increased 15%. The remaining 5% increase accounts for the molecules which were interpenetrated with the wet, more loosely packed PDDA monolayers in the undried sample, and were separated above the PDDA monolayers in the dried sample. This concept is illustrated in Figure 2-14.

Note that this drying procedure is required at all measurement points and should be accounted for when planning film fabrication and evaluation. For example, a 100 bilayer film which has been dried for measurement every 10 bilayers will not be identical to a 100 bilayer film which has remained wet throughout the process, but will contain a periodic structure, with a period equal to the thickness of 10 bilayers.

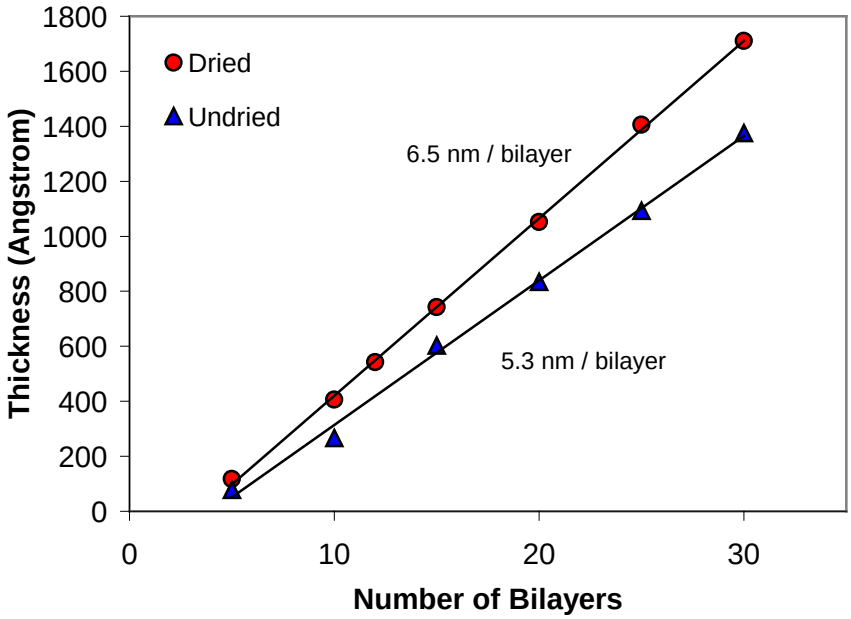

Figure 2-11. Ellipsometry comparison of Poly R-478/PDDA ESA films dried in a stream of nitrogen after deposition of each monolayer (Dried) and dried only for measurement purposes (Undried).

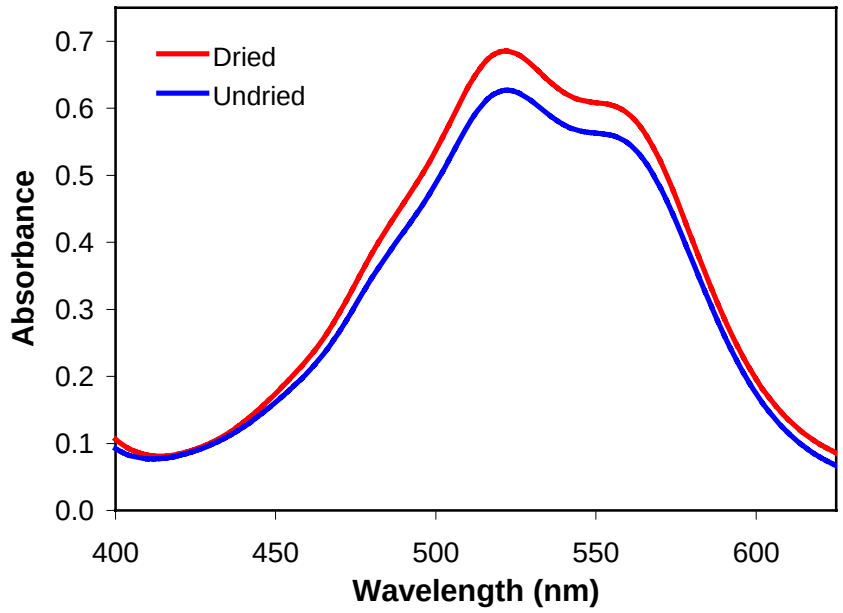

Figure 2-12. UV/vis absorbance spectra of 50 bilayer Poly R-478/PDDA ESA films dried in a stream of nitrogen after deposition of each monolayer (Dried) and dried only for measurement purposes (Undried).

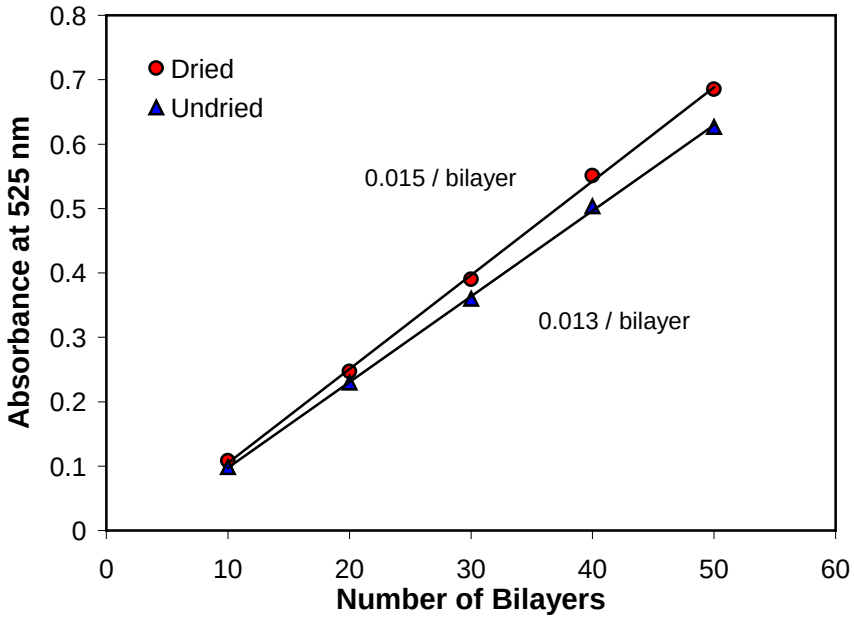

Figure 2-13. Absorbance peak comparison of Poly R-478/PDDA ESA films dried in a stream of nitrogen after deposition of each monolayer (Dried) and dried only for measurement purposes (Undried).

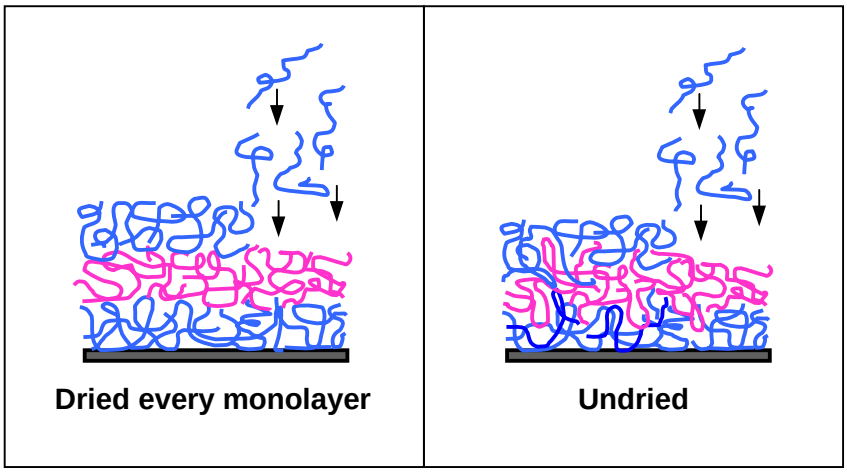

Figure 2-14. Effect of drying on layer interpenetration.

2.3.2 Dipping time

After immersing the substrate in solution, the polyelectrolyte molecules require a certain amount of time to move through the fluid, arrange themselves on the substrate and ionically bond to the surface monolayer. This process is both species and concentration dependent.

This fluid motion concept was investigated for the Poly S-119/PDDA film system, which was used for a number of the optical experiments in this work. Dipping times of 1, 5, 10 and 20 minutes were used to assemble 20 bilayer films on glass and silicon substrates. Concentration and pH values were identical for all eight samples, which were characterized using ellipsometry and UV/vis spectroscopy. The results are shown in Figure 2-15, 16 and 17. Note the reduced effect of each additional time increment.

Table 2-3 puts the data contained in the Figures 2-15, 16 and 17 in terms of a quantity that is more easily understood, time. For manufacturing, and to a lesser extent in research, this is a critical value. Both tables assume hand dipping methods, and the times required for bilayers and films account for the required rinsing steps as well as the dipping steps. A minimum of 1 minute is required for thorough rinsing by hand. Notice that although a 20 minute dipping time results in a 20% increase in thickness and optical density per bilayer, the time required per bilayer is increased by greater than 10 times. Therefore, the amount of time required to achieve specific film properties (i.e. 1 μm thickness or an optical density of 1) is greatly reduced by the use of 1 minute dipping time.

This study considered external characteristics of the bulk film. Further investigation should include consideration of the effect of reduced numbers of bilayers assembled using greater dipping times on the internal film structure, that is the structure of each monolayer and the interfaces between monolayers, in addition to the bulk film properties.

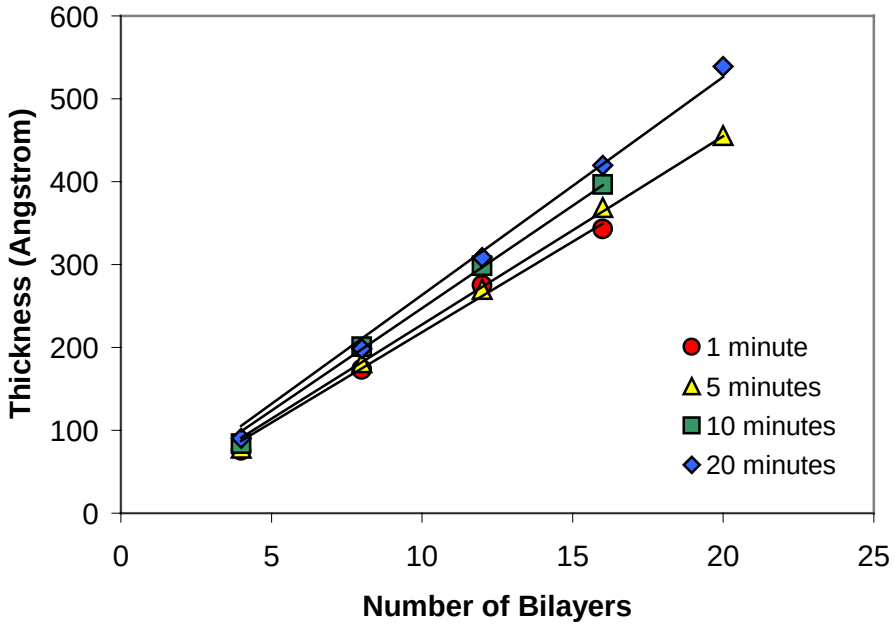

Figure 2-15. Ellipsometry comparison of PDDA/Poly S-119 ESA films fabricated using different dipping times.

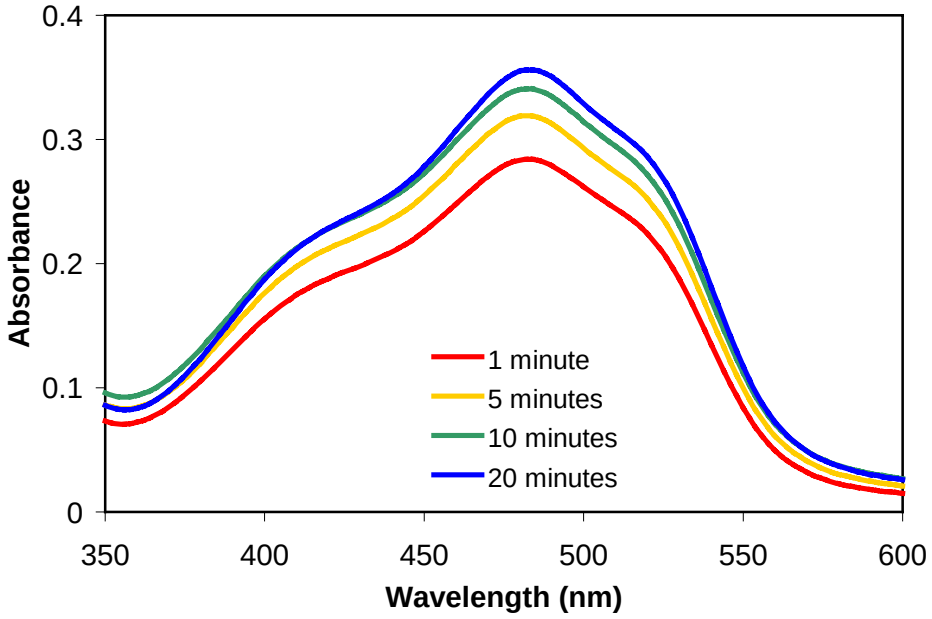

Figure 2-16. Optical absorbance comparison of 20 bilayer PDDA/ Poly S-119 ESA films fabricated using different dipping times.

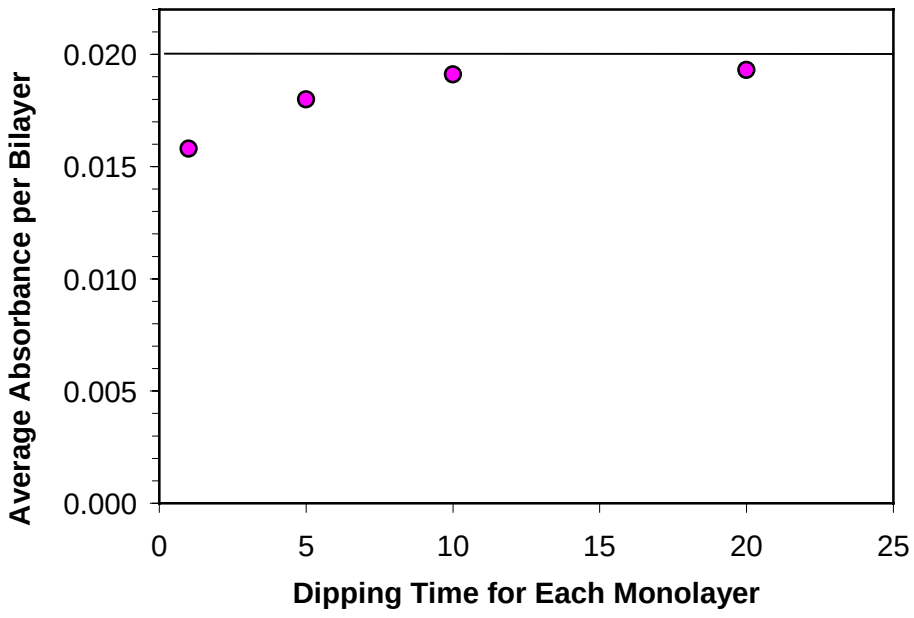

Figure 2-17. Effect of dipping time on average optical density per bilayer of PDDA/Poly S-119 ESA films fabricated using different dipping times.

Table 2-3. Effect of dipping time on film thickness and optical absorbance.

DIPPING TIME (min)		1	5	10	20
Average thickness per bilayer (Å)		22	23	25	26
Percent increase over 1 minute dipping		-	4%	13%	20%
Average optical density per bilayer (a.u.)		0.0158	0.0180	0.0191	0.0193
Percent increase over 1 minute dipping		-	14%	21%	22%
Single Bilayer	Minimum time required (min)	4	12	22	42
	Percent increase over 1 minute dipping time	-	300%	550%	1050%
1 μm film	Number of bilayers required	458	440	404	380
	Minimum time required (hours)	31	88	148	266
	Percent increase over 1 minute dipping time	-	288%	486%	871%
1 a.u. optical density	Number of bilayers required	63	56	52	52
	Minimum time required (hours)	4	11	19	36
	Percent increase over 1 minute dipping time	-	263%	455%	860%

2.3.3 Selection of passive counterions

The characteristics of thin films fabricated by the ESA process are dependent not only on the conditions under which each monolayer was processed, but also on composition of each monolayer, and the order in which the monolayers are assembled. This permits precise control over film properties. ESA films are assembled a single monolayer at a time, allowing the incorporation of a variety of molecules to allow the combination of multiple functionalities and characteristics in a single film. One example of this concept is the selection of the passive positive counterion in NLO thin films, which are discussed in detail in Chapter 4. The active molecule, containing the NLO chromophore, is anionic in this case. Two cationic counterion solutions were used in this study, polyallyamine hydrochloride (PAH) and polydiallyldimethylammonium chloride (PDDA). The choice controlled the resulting film thickness, refractive index and optical density.

30 bilayer films were assembled on glass and silicon substrates and the film growth monitored using ellipsometry and UV/vis spectroscopy. Anionic monolayers consisted of Poly S-119, Poly R-478 or PCBS; either PAH or PDDA was used for the cationic monolayers. Polyelectrolyte concentration, salt concentration and dipping time were constant for all samples. For all anionic molecules tested, the PDDA films exhibited greater thickness and optical density, as illustrated in Figures 2-18, 2-19 and 2-20. The absorbance peak at 525 nm in Figure 2-19 is due entirely to the Poly R-478 molecules in the film, not the PDDA or PAH molecules. This indicates that the selection of the cationic molecule controls not only its own adsorption characteristics, but also that of the anionic monolayer. It is the ionic *interaction between* the film surface polyions and the polyions in solution that determines the structure of the resulting new monolayer. These results are summarized in Table 2-4.

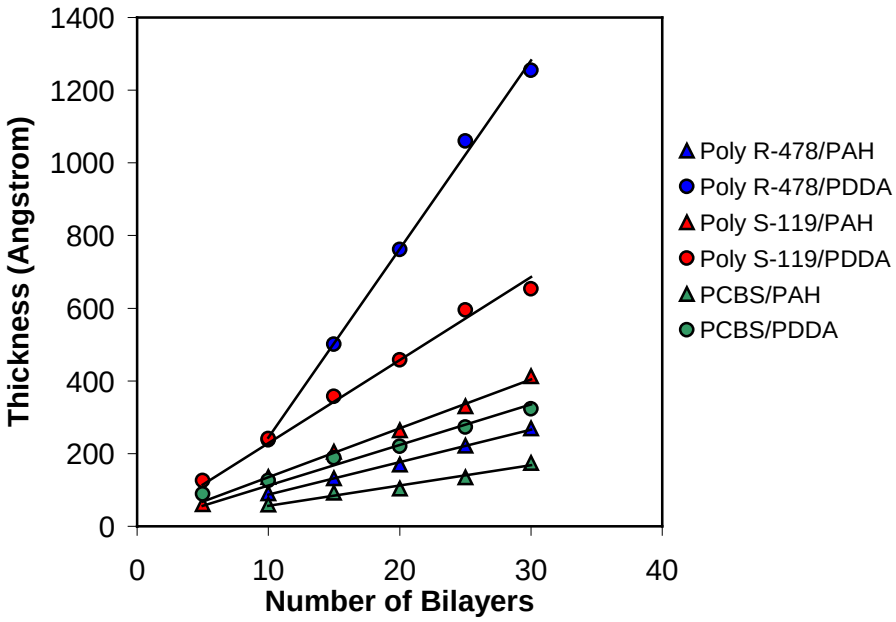

Figure 2-18. Comparative ellipsometry data for commercial NLO dye ESA films using PAH versus PDDA as the cationic layers.

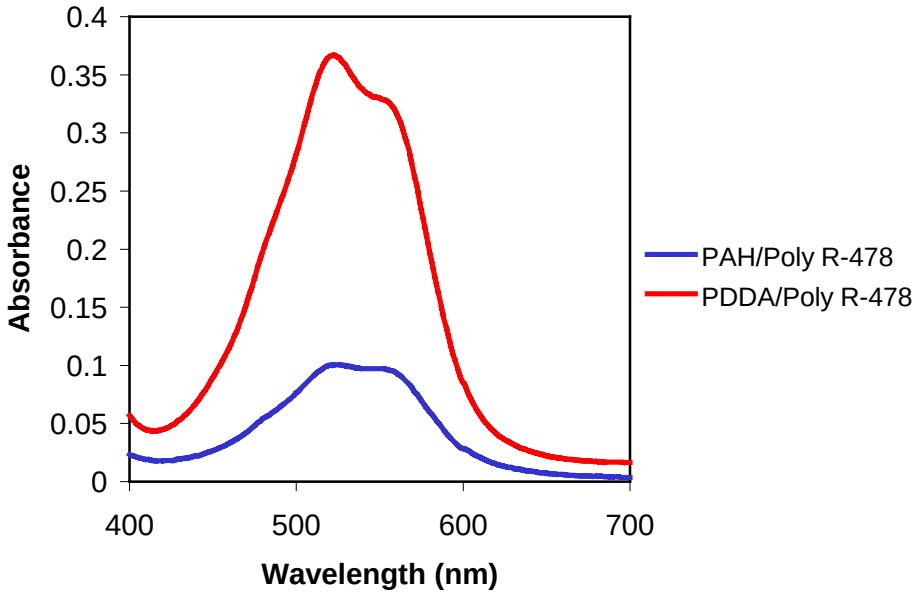

Figure 2-19. Optical absorbance spectra of 30 bilayer Poly R-478 films using PAH and PDDA as the cationic layer.

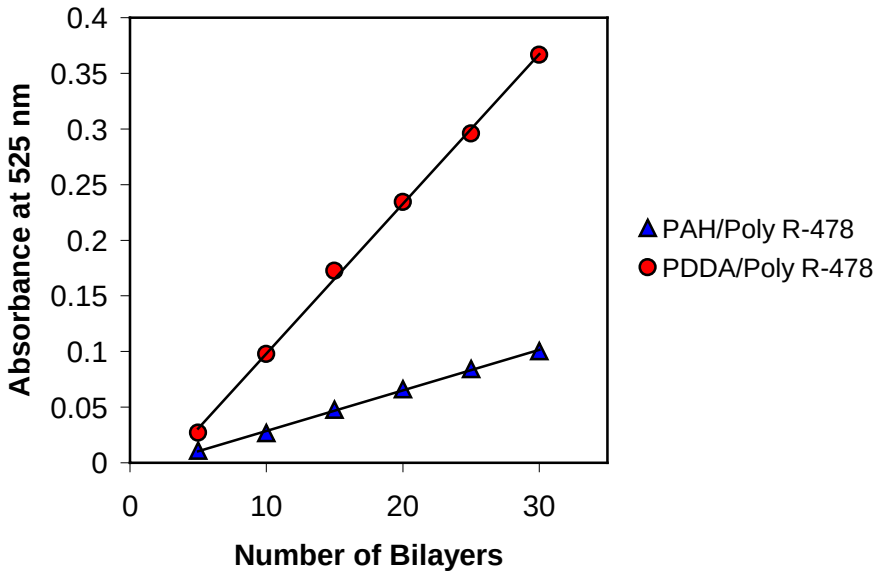

Figure 2-20. Comparative UV/vis spectroscopy data for Poly R-478 ESA films using PAH versus PDDA as the cationic layers.

Table 2-4. Comparison of the effect of counterion selection.

	Polyanion	Polycation		Percent increase
		PAH	PDDA	
Average bilayer thickness	**Poly R-478**	9	52	478%
	Poly S-119	13	23	77%
	PCBS	6	11	83%
Average optical density per bilayer	**Poly R-478**	0.0036	0.0135	275%

2.3.4 Incorporation of inorganic nanoparticles

As discussed in the previous section, film properties can be controlled by the selection of various passive polymer counterion layers. The incorporation of inorganic nanoparticles into alternate layers can also modify multilayer film characteristics. These effects are dependent on nanoparticle size and species as well as the spacing of nanoparticle monolayers within the film. This was investigated by incorporating platinum nanoparticles as part of multilayer structures in polymer ESA films.

The platinum nanoparticles were provided in solution by Dr. Yanjing Liu. They were analyzed using a Malvern Zetasizer 3000 system. The smallest measurable particle size using this system is 1.0 nm; this experiment approached that limit. 90% of the platinum nanoparticles were less than 1.3 nm, with a mean zeta potential of 37.2 mV. The zeta potential distribution is shown below in Figure 2-21, indicating a cationic solution. Zeta potential is the potential which is often most important in governing charge mediated particle interactions and thus the behavior of a suspension.

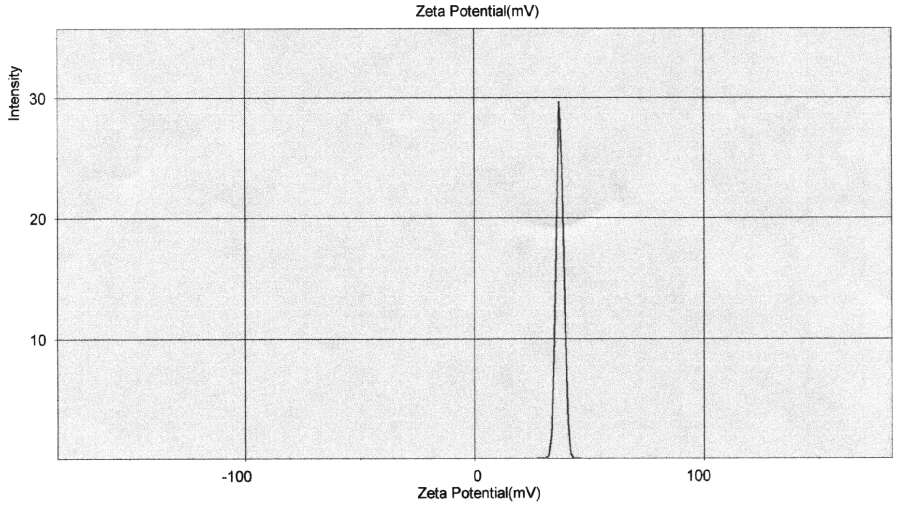

Figure 2-21. Zeta potential distribution of platinum nanoparticle solution.

Platinum/polymer dye films were deposited on N-(2-aminoethyl)-3-aminopropyltrimethoxy-silane (APS)-modified quartz substrates, producing multilayer structures of the form $[(\text{dye/PAH})_m\text{dye/Pt}]_n$, where m denotes the number of purely polymer bilayers between each bilayer containing platinum, and n denotes the total number of such multilayers in the film. n is also equivalent to the number of platinum monolayers contained in the film. (m+1) indicates the bilayer period between platinum monolayers. Films were prepared with m varying from 0 to 3 and n from 1 to 5, using three different dyes: Poly S-119, Poly{1-[4-(3-carboxy-4-hydroxyphenylazo)-benzenesulfonamido]-1,2-ethanediyl, sodium salt} (PCBS) and Direct Red 75.

Based on UV/vis spectroscopy data, each multilayer formed a discrete and reproducible unit for all values of m. The results indicated a linear increase in optical absorbance with the addition of each bilayer, as shown in Figures 2-22, 2-23 and 2-24 for Poly S-119 (m=0), PCBS (m=1), and Direct Red 75 (m=2) films. In comparing the resulting UV/vis data, it is important to keep in mind that every bilayer contained an anionic dye monolayer whether the cation was PAH or platinum. So each 20 bilayer Poly S-119 film contained 20 monolayers of Poly S-119 no matter how many platinum monolayers were included.

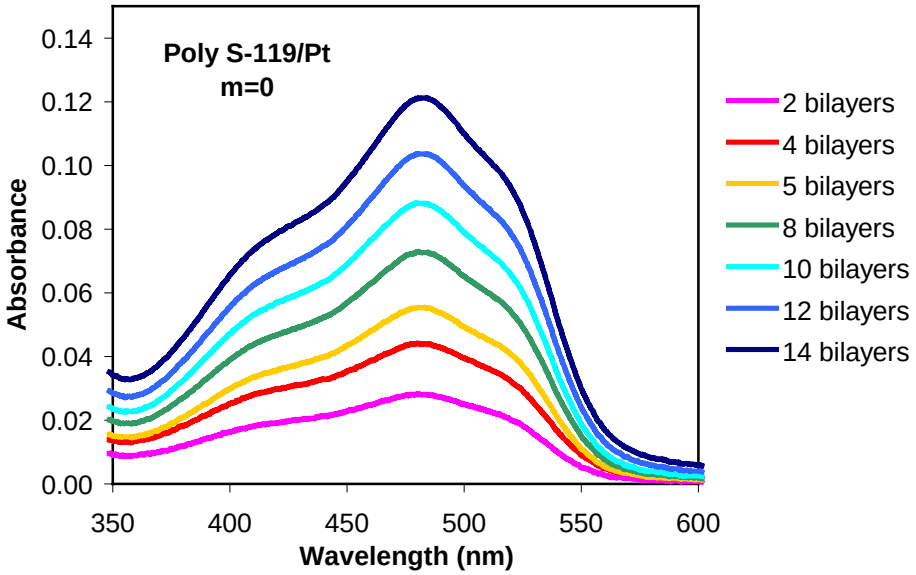

Figure 2-22. UV/vis absorbance for increasing numbers of bilayers of Poly S-119/Pt films; m=0 indicates platinum in every bilayer.

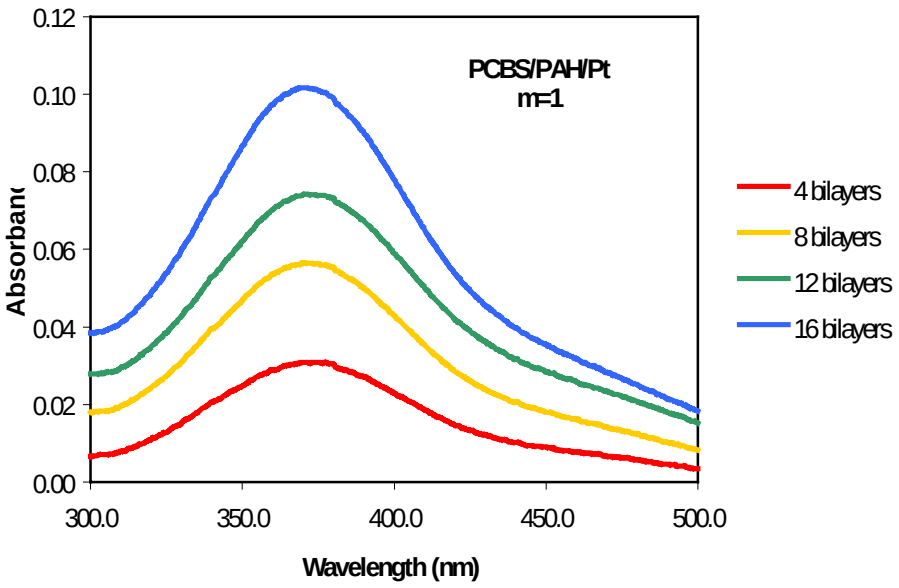

Figure 2-23. UV/vis absorbance for increasing numbers of bilayers of PCBS/PAH/Pt films; m=1 indicates platinum in every other bilayer.

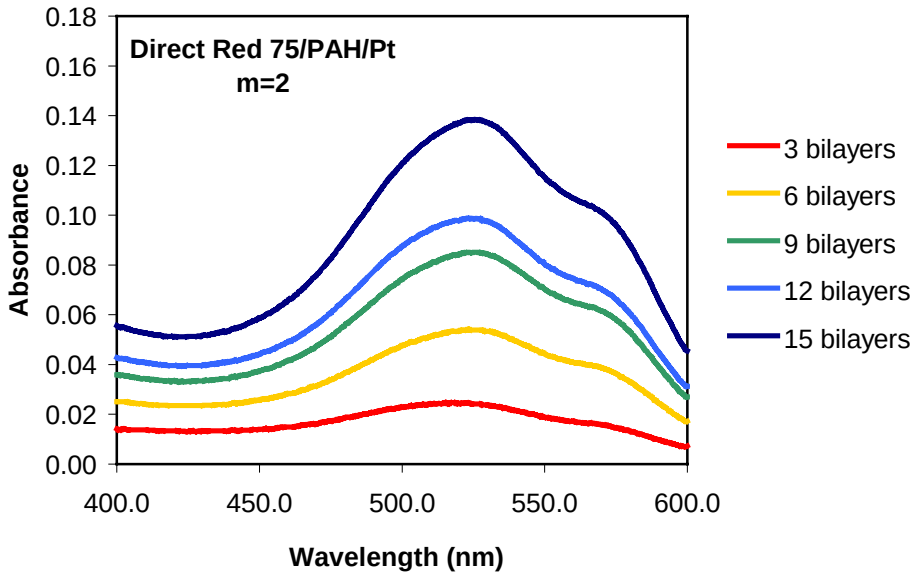

Figure 2-24. UV/vis absorbance for increasing numbers of bilayers of PCBS/PAH/Pt films; m=2 indicates platinum in every third bilayer.

For each dye molecule, a specific and unique pattern, i.e. the value of m, resulted in the maximum absorbance for the sample set, as illustrated in Figure 2-25. This absorbance enhancement by patterned layers containing metallic nanoparticles is therefore a species dependent effect. The source of this dependence is most likely the difference in bilayer spacing, and therefore spacing between each metallic layer, for each of the three dye species investigated. There was no change in the peak absorbance wavelength, and no secondary peaks due to any absorbance from the platinum. No resonance effects were observed in this experiment.

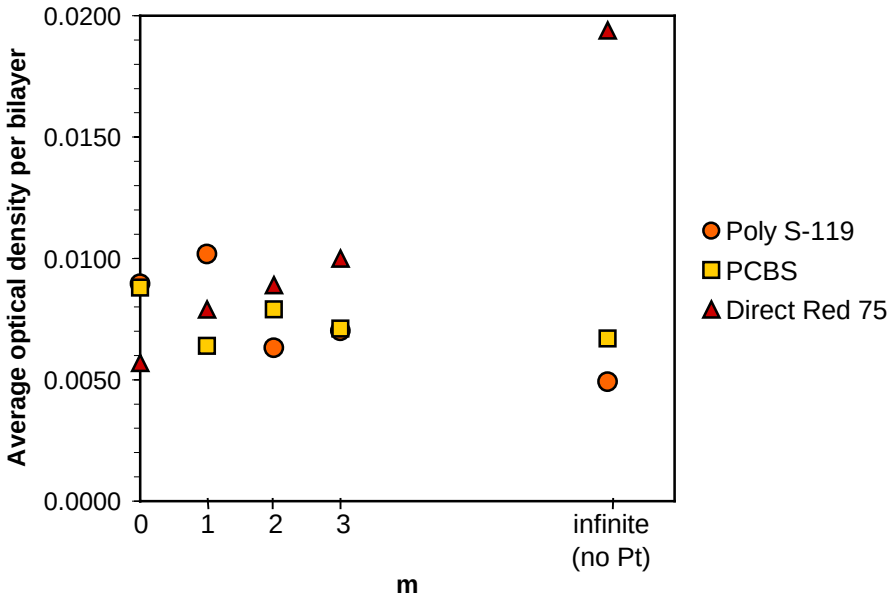

Figure 2-25. Effect of long-range ordering on thin film absorbance.

2.4 Environmental stability of ESA films

2.4.1 Thermal cycling

Good thermal behavior of ESA thin films was anticipated due to the incorporation of high temperature polymers as alternating monolayers in the film structure. As part of a study to determine ESA thin-films' ability to withstand thermal cycling and thermal shock, changes in the optical absorption properties of organic polymer dye thin films were observed before and after heating in air to temperatures of 120°C for periods up to 5 hours. Negligible change was detected.

Initial thermal testing was performed on several 40 bilayer Poly R-478/PDDA ESA films. Four identical samples were self-assembled on glass substrates to allow comparison of the effects of the different heating conditions, summarized in Table 2-5. Between each heat cycle indicated in

the third column of the table, the samples were cooled to room temperature for measurement. All heating was performed using a Thermolyne hot plate oven.

Before and after each heat cycle, the visible spectral absorbance was measured. The absorbance was observed to increase at most a few percent. Figures 2-26 - 2-29 illustrate the absorbance results of the four films tested, immediately after fabrication and drying in nitrogen gas, and after thermal cycling. The small variations evident may be due to changes in residual water content. This effect is discussed in more detail in Chapter 4. These initial results indicate that multilayer ESA film systems are stable up to temperatures of 120°C. This thermal stability is important for the linear and nonlinear optical applications discussed in this dissertation.

Table 2-5. Thermal cycling testing of 30 bilayer Poly R-478/PDDA ESA films.

SAMPLE NUMBER	CYCLE	HEATING CONDITIONS	PERCENTAGE INCREASE IN 522 NM ABSORBANCE PEAK OVER INITIAL VALUE
110	1	120°C, 1 hour	3.5 %
	2	120°C, 1 hour	3.0 %
	3	120°C, 1 hour	0.7 %
111	1	120°C, 1 hour	2.5 %
	2	120°C, 1 hour	3.8 %
	3	120°C, 1 hour	2.5 %
112	1	120°C, 2 hours	1.9 %
	2	120°C, 2 hours	2.0 %
113	1	120°C, 5 hours	2.0 %
	2	120°C, 5 hours	1.7 %

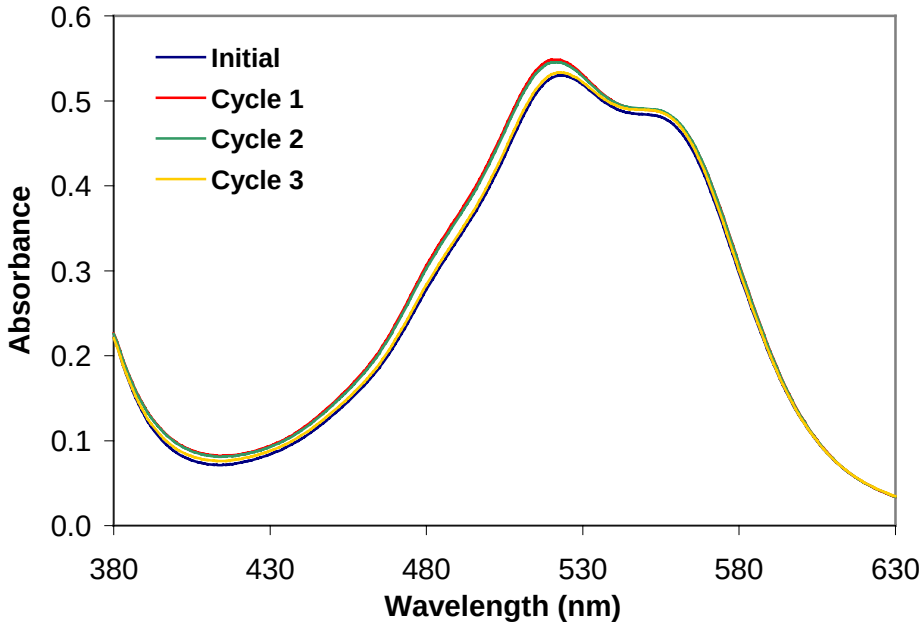

Figure 2-26. UV/vis absorbance spectra of #110, 40 bilayer Poly R-478/ PDDA ESA film before and after heating to 120°C in 1 hour cycles.

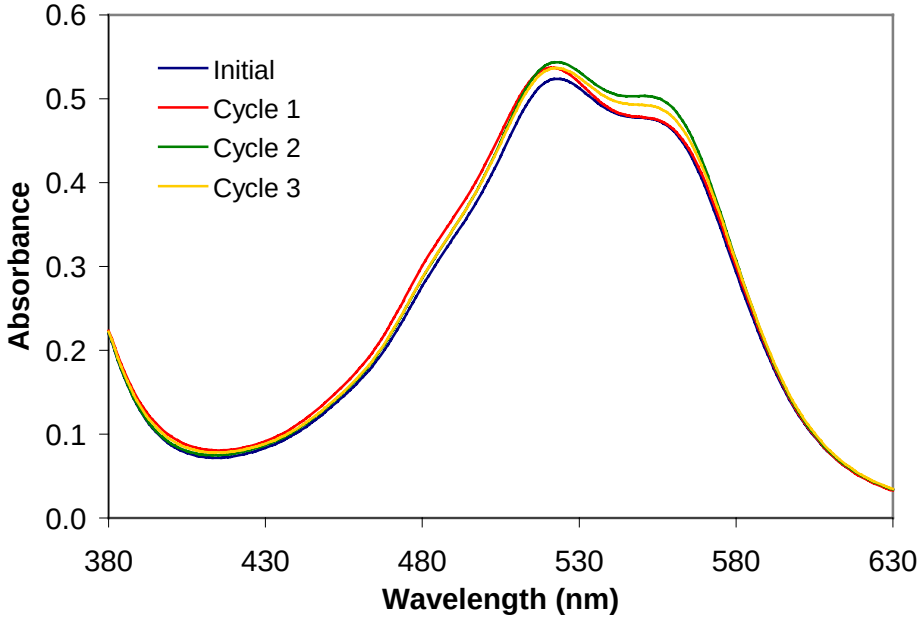

Figure 2-27. UV/vis absorbance spectra of #111, 40 bilayer Poly R-478/ PDDA ESA film before and after heating to 120°C in 1 hour cycles.

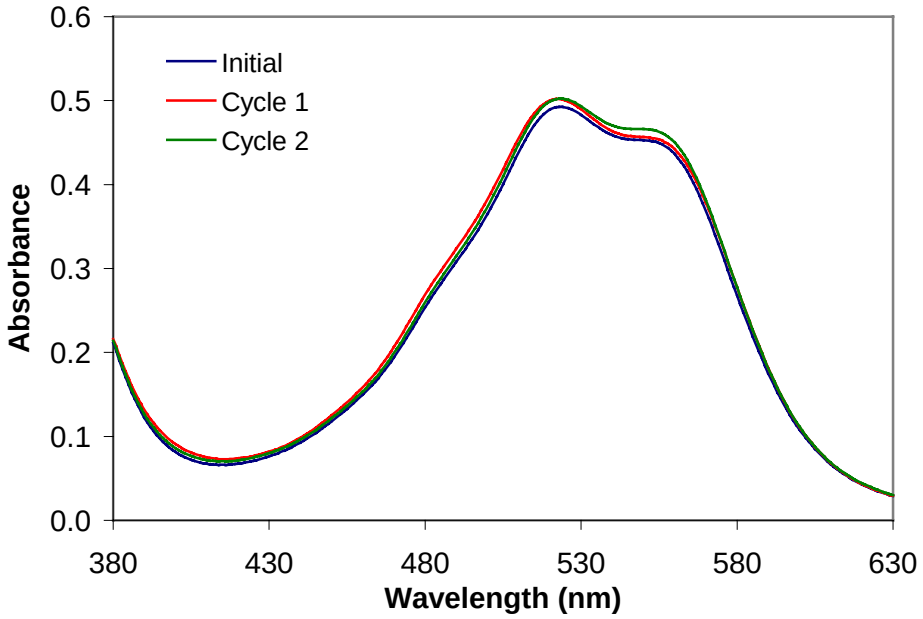

Figure 2-28. UV/vis absorbance spectra of #112, 40 bilayer Poly R-478/ PDDA ESA film before and after heating to 120°C in 2 hour cycles.

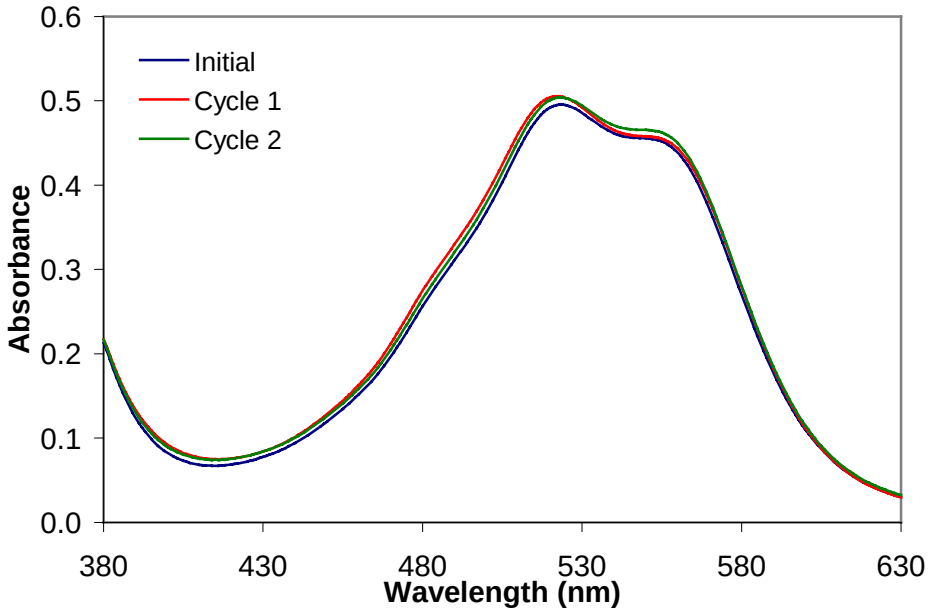

Figure 2-29. UV/vis absorbance spectra of #113, 40 bilayer Poly R-478/ PDDA ESA film before and after heating to 120°C in 5 hour cycles.

2.4.2 Water attack

To investigate the possibility of water attack on fabricated ESA films, a 40 bilayer PAH/Poly R-478 film was submerged in water for increasing periods of time and its UV-Vis absorbance spectrum monitored for any degradation. Absorbance spectra before and after submersion are shown in Figure 2-30. The sample was dried in a stream of nitrogen before placement in the spectrophotometer. After 21 hours submersion, negligible degradation of the spectrum was observed.

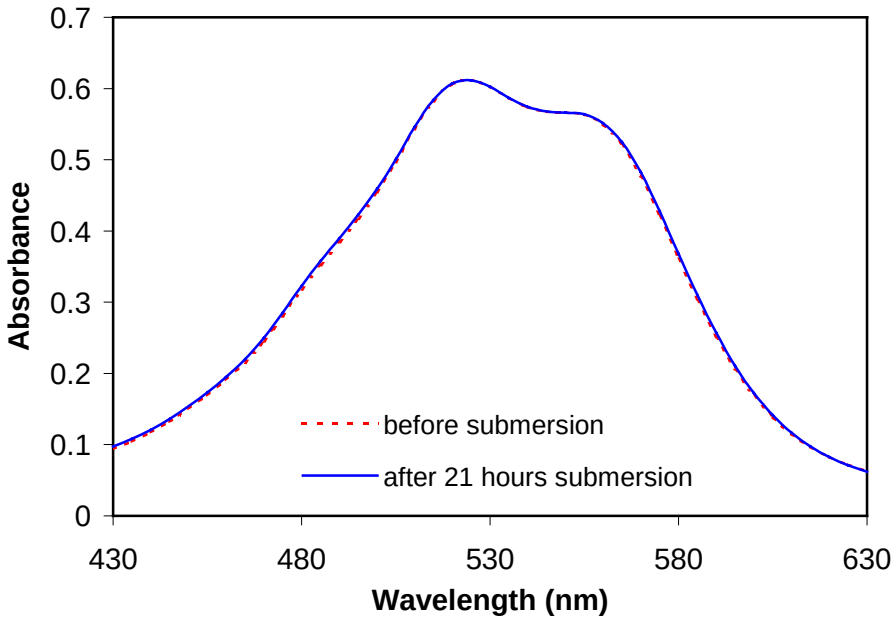

Figure 2-30. UV/vis absorbance spectra of 30 bilayer Poly R-478/PDDA ESA film before and after water submersion.

2.5 Process Automation

The samples characterized in this dissertation research were all fabricated using hand dipping methods. Automation of the ESA process will allow high-speed synthesis of identical films on multiple substrates. For manufacturing purposes, the advantage of such automation is obvious - higher throughput and lower costs. For research purposes, the simultaneous processing of multiple substrates will allow better-controlled comparative experiments.

As part of this study, the processing of ESA films was automated using a Zeiss slide stainer. To conserve ultrapure water, and therefore reduce cost, rinsing was accomplished using agitation within a still bath rather than a flow through tank. Several dielectric stack filters, including the two shown in Figure 2-31, have been fabricated using this semi-automated method, as well as

multiple nonlinear optical thin films. Excellent consistency between samples was obtained. The absorption peaks of the initial simultaneously auto-fabricated filters are shown in Figures 2-32, 2-33 and 2-34 at three different points in the assembly process. After 300 bilayers, a 3% difference in peak magnitude was observed (Table 2-6). The peak wavelength was identical in all measurements.

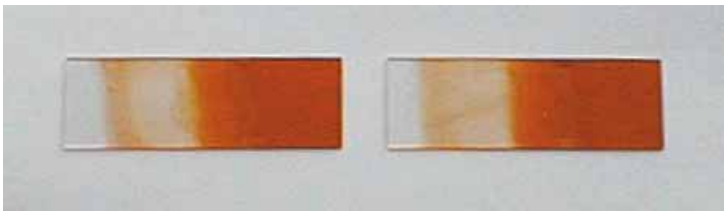

Figure 2-31. Initial automatically fabricated ESA dielectric stack filters.

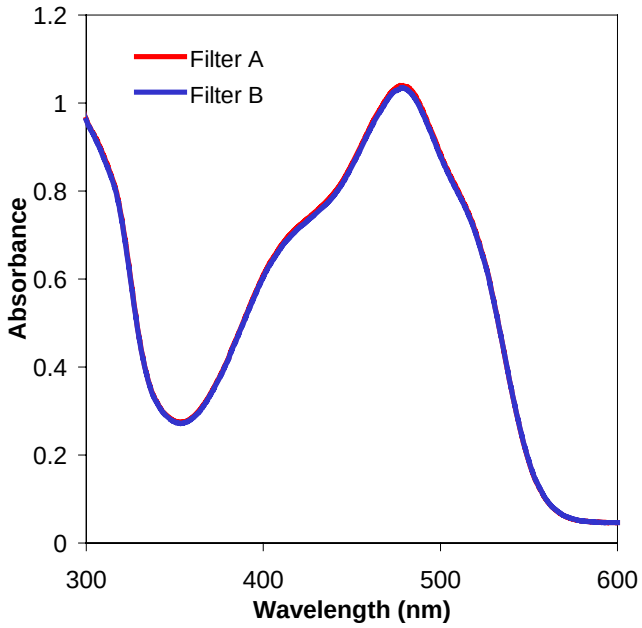

Figure 2-32. Optical absorbance spectra of two dielectric stack filters, consisting of 126 bilayers, fabricated simultaneously in the same batch using a semi-automated ESA process.

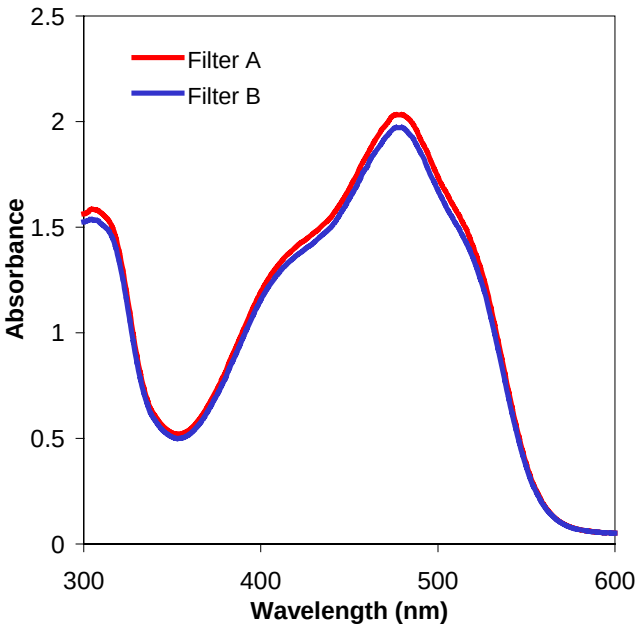

Figure 2-33. Optical absorbance spectra of two dielectric stack filters, consisting of 183 bilayers, fabricated simultaneously in the same batch using a semi-automated ESA process.

Table 2-6. Comparison of two filters fabricated in the same automatic batch.

NUMBER OF BILAYERS	% DIFFERENCE IN PEAK ABSORBANCE MAGNITUDE
126	0.5%
183	3.1%
309	2.7%

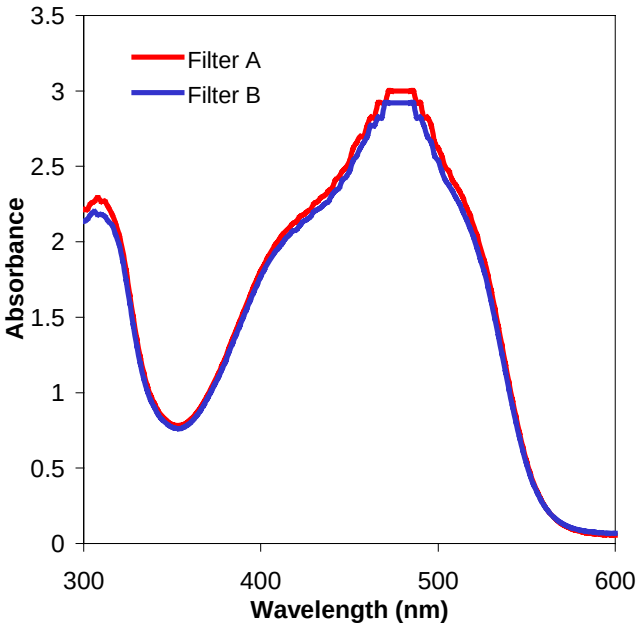

Figure 2-34. Optical absorbance spectra of two dielectric stack filters, consisting of 309 bilayers, fabricated simultaneously in the same batch using a semi-automated ESA process.

However, these initial samples exhibited some inhomogeneity across the film surface due to rinse water runoff problems. This problem was mostly alleviated by utilizing a temperature controlled airflow drying tank. As a final step, after rinsing, the samples are lowered into the airflow tank, which is maintained at 25 °C. In addition, the rinse times were reduced, while maintaining film quality, resulting in an overall process time reduction of 15%.

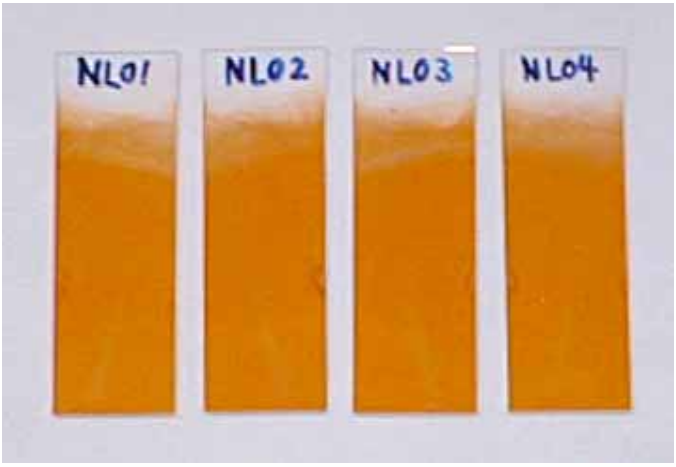

Figure 2-35. Single batch auto-fabricated ESA nonlinear optical thin films using the drying tank.

Future automation investigations will include comparison of film quality resulting from agitation within a still rinse bath system with that from a flow-through rinse system, and consideration of the water volume required for each method.

2.6 Summary

This chapter investigated methods and properties of the ESA process itself, in preparation for the self-assembly of the optical filters and devices discussed in Chapters 3 and 4. Each of the dip processing and film characterization methods was described in detail. These will be referred to in later chapters as a part of extensive thin-film experiments. ESA coating was demonstrated for various substrate sizes, shapes, and materials and the effect of processing variables on the resulting films investigated. For manufacturing and long-term applications of the filters and devices described in the remainder of this dissertation, studies of automation procedures and environmental ruggedness of ESA films were initiated.

2.7 References

1. P. Perumalsamy, *In-Line Fiber Polarizer*, M.S. thesis, The Bradley Department of Electrical Engineering, Virginia Polytechnic Institute & State University, Blacksburg, Virginia, April 1998.
2. F.J. Arregui, Y. Liu, K. Lenahan, C. Holton, I.R. Matias, R.O. Claus, "Optical Fiber Humidity Sensor Formed by the Ionic Self-Assembly Monolayer Process," *Proc. SPIE* Vol. 3670, Newport Beach, CA, March 1999.
3. Y. Liu, *Characterization and Patterned Polymer Films from a Novel Self-Assembly Process*, Ph.D. dissertation, Chemistry Department, Virginia Polytechnic Institute & State University, Blacksburg, Virginia, May 1996.
4. G. Decher and J. Schmitt, "Fine-Tuning of the film thickness of ultrathin multilayer films composed of consecutively alternating layers of anionic and cationic polyelectrolytes," *Progr. Colloid & Polym. Sci.* **89**, 160 (1992).
5. G. Decher, Y. Lvov, J. Schmitt, "Proof of multilayer structural organization in self-assembled polycation-polyanion molecular films," *Thin Solid Films* **244**, 772-7 (1994).
6. Y Lvov, G. Decher and H. Möhwald, "Assembly, Structural Characterization, and Thermal Behavior of Layer-by-Layer Deposited Ultrathin Films of Poly(vinyl sulfate) and Poly (allylamine)," *Langmuir* **9**, 481 (1993).

CHAPTER 3

Linear Optical Filtering in ESA Films

Optical filters or coatings can be defined as thickness-dependent refractive index systems which modify the properties of a surface to produce the desired optical characteristics. They can work over the entire spectrum, a broad range of wavelengths, or a very narrow band. Thin films have been used for this purpose since ancient times, when they were applied as glazes on ceramics. In a more scientific realm, optical interference filters have been studied since the early 1800s when the principle of the interference of light was first explained by Thomas Young. Fraunhofer fabricated the first recognized antireflection coatings as early as 1817. The theoretical basis for the analysis of such optical thin films was provided by James Clerk Maxwell's system of equations, first published in 1873. The traditional use of thin film coatings to enhance the performance of optical components was initiated by Lord Rayleigh's observation in 1886 that the surface corrosion of his lenses actually improved their performance by reducing reflection. Optical thin film use still centers on traditional optical components, such as telescopes, microscopes, binoculars, cameras, spectacles, etc., as well as new applications that have emerged with the growth of other technologies, e.g. solar cells, laser systems and automobile glasses (see, for example, Ref. 1,2).

Figure 3-1 illustrates the basic notion of a thin-film optical filter; the refractive index profile of the coating modifies the surface of the substrate to produce the required optical output. While it is relatively simple, with the computing power available today, to calculate the optical output of a given index profile, it is more useful to calculate the index profile required to produce a given spectral output. Several concepts are required to understand the nature of optical interference filter performance (after Ref. 3). The first is that the light amplitude reflected from an interface is dependent on the ratio of refractive indices of the materials on either side of that interface. For normal incidence, this can be simply expressed as

$$r = \frac{n_1 - n_2}{n_1 + n_2} \quad . \qquad \textbf{(3.1)}$$

The second concept is that a π phase shift occurs when the reflection takes place within the lower index material, and no phase shift occurs when the reflection occurs within the higher index material. The third is that incident light which is reflected from both the top and bottom surfaces of a thin film will recombine either constructively or destructively depending on the relative phase shift between the two. That is to say, it is possible that the combination of the two light beams may be darkness. This premise is difficult to accept without the wealth of mathematical theory and experimental proof that is available. The detailed mathematics behind these statements is thoroughly discussed in books by Heavens, Macleod, and Thelen [3-5].

The universally accepted [6] model of a single thin film is a homogeneous slab of material characterized by its optical constants, n and k, and a thickness, d. The quarter wave stack, multiple film layers of different refractive indices, all of optical thickness λ/4, is a basic building block for a number of different filter types and designs. For example, one of the oldest multilayer designs consists of an alternating high/low (HL) index quarter wave stack, producing a reflectance peak at the λ selected whose spectral characteristics are dependent on the indices of the HL layers. Antireflective (AR) coatings can also utilize variations of the quarter wave stack. AR was the principle objective of much of the early work in thin film optics and is still the most commonly used coating type today. Designs range from a single, low-index layer, producing a single reflectance minimum to complicated, multilayer systems with multiple mimina, depending on the substrate, the wavelengths involved and performance requirements. More detailed descriptions of the many optical interference filtertypes and relevant applications can be found in Ref. 1,7.

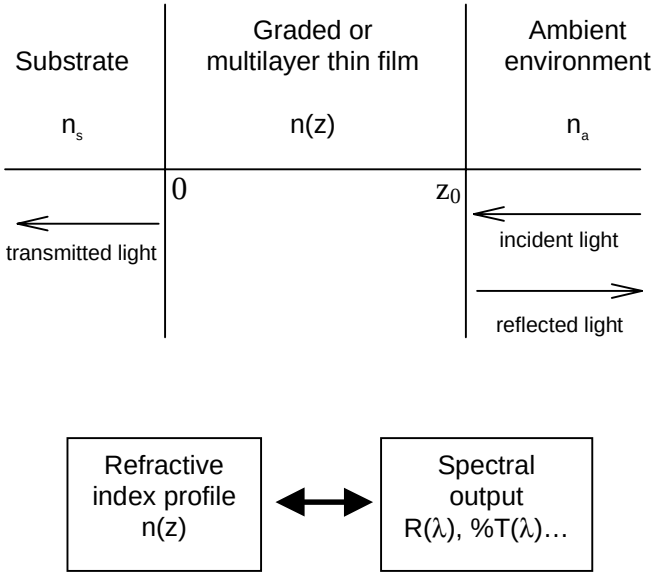

Figure 3-1. Optical thin film model (after Tikhonravov [8]).

Each application and substrate carry its own material requirements. For example, an antireflection coating designed for a high-index substrate will likely not work on a low-index substrate. The requisite optical characteristics are clearly index of refraction and transparency in the relevant spectral range. Practical application also requires mechanical properties such as hardness and abrasion resistance, as well as chemical and environmental durability. In addition, the deposition process required or eliminated by the materials must be considered. For example, plastic substrates will not survive the high temperature coating process required by some materials for uniform film coverage.

The optical thin film fabrication methods used commercially even today, vacuum evaporation and sputtering, were invented in the 19th and early 20th century and made viable in the 1930s by the invention of suitable vacuum pumps. The equipment required includes vacuum chambers and requisite pumps and pressure gauges, power supplies to vaporize the coating materials, and substrate holders and heaters. Vacuum evaporation consists of heating a charge using resistive, electron beam or laser beam heating. As the temperature rises, the material evaporates, rises and condenses onto the cooler substrate surface. Coating uniformity is dependent on a number of geometric considerations and the nature of this process results in a great deal of coating material waste, which must be cleaned from the vacuum chamber. The concept of sputtering is similar, except that the coating material particles are removed from a target through bombardment by ions or atoms. The substrates must be placed closer to the target in this case, and less material is wasted, but the process produces lower deposition rates.

The low packing density and columnar microstructure of films made by traditional vacuum deposition methods reduces film quality, e.g. intrinsic stress, transparency and durability [9]. This problem can be alleviated by increasing the energy of the particles arriving at the substrate surface, allowing the molecules to move around on the surface to find a low energy lattice site before being incorporated into the film, resulting in a denser and more durable film [10]. This can be accomplished by heating the substrates to temperatures of 200-300°C. Obviously, some substrates cannot tolerate this temperature range, limiting the number of materials that can be uniformly coated on plastics. Another issue that presents a difficulty is the potential mismatch in thermal expansion coefficients between the substrate and coating. This section is intended as a brief summary of current thin film technology. More detailed information on deposition methods and related issues can be found in books by Pulker, Macleod, and Rancourt [3,11,12].

Therefore, thin film optical design theory is well established, but the designs are limited by the materials and processes available. As an example, with no constraint on refractive index, one could theoretically produce an AR filter with zero reflectance at all wavelengths. According to Macleod, "the real limitation to what is possible in optical thin film filters and coatings is the capability of the manufacturing process to produce layers of precisely the correct optical constants and thickness" [3].

Electrostatic self-assembly processes offer significant advantages over traditional methods of optical thin film synthesis. Most importantly, the uniformity of each monolayer allows precise grading of bulk optical properties. Extremely homogeneous mixtures of inorganic nanoparticles, polymers and other molecules can be incorporated into each monolayer, allowing nanoscale control over refractive index through the film thickness. In addition, the

ionic bonding of molecules allows extremely uniform films to be deposited on substrates of arbitrary size and shape. The uniformity of coatings formed using vacuum deposition methods is dependent on the substrate size and topology [3,12]. ESA synthesis at room temperature and pressure allows coating of almost any substrate, including ceramics, plastics, metals, semiconductors or organic films, without a reduction in coating quality. The inherent multicomponent nature of ESA films permits a broad range of film functionality. The incorporation of a wide range of inorganic and organic molecules allows the molecular-level control of coating electronic, conductive, optical, magnetic, thermal and mechanical properties. Conventionally, exposure to high temperatures and corrosive and humid environments has a deleterious effect on thin film optical properties. The resistance of ESA films to chemical and environmental effects has been demonstrated in several studies, discussed in Chapter 2 and Ref. 13. Finally, the ESA process does not require the large equipment investment of vacuum processes; fabrication consists of repeatedly dipping the substrate into aqueous solution baths at room temperature. Equipment costs are therefore low and the process can easily be upscaled and automated.

The results in this chapter demonstrate the feasibility of the ESA process for the fabrication of many types of linear optical interference filters with enhanced properties. The chapter is organized as follows - Section 3.1 demonstrates the capability to vary the index of refraction of adsorbed multilayer thin films using two distinct methods, multilayer patterning and aqueous mixtures. This information was used to design and synthesize dielectric stack filters with several different reflecting wavelengths, discussed in Section 3.2. Most importantly, these filters demonstrate the ability to use the ESA method to control material properties through the thickness of several micron-thick multilayer films and therefore control the optical output. In Section 3.3, the filter work is extended to continuous index profile, or Rugate, type optical reflectance filters, demonstrating the ability to produce a graded index profile several microns thick. ESA-synthesis of multilayer AR coatings is discussed in Section 3.4. The linear optical filtering portion of this dissertation is summarized in Section 3.5.

3.1 Control of refractive index profile in ESA thin films

A critical step in this investigation was the identification, ESA synthesis, and characterization of optical thin-film materials, followed by control of the refractive index of thin films by combining multiple materials in a single ESA film. This was divided into two distinct tasks, namely

Task 1 - Select anionic and cationic polymers and nanoparticles which will produce single anion/single cation ESA films with a range of refractive indices, synthesize ESA thin films, and verify optical and structural characteristics.

Task 2 - Combine multiple anions and/or cations in a single film to *a)* control refractive index through the thickness of the film on a finer scale than is possible with single anion/single cation systems and *b)* prove the feasibility of graded index structures by varying the material combinations through the film thickness. Two separate methods were evaluated, multilayer patterning and aqueous mixtures.

Refractive index control was demonstrated, both in simple bilayer systems through selection of appropriate molecules, and in more complicated multilayer systems by incorporation of multiple anions and cations.

3.1.1 Single anion/single cation ESA films with uniform refractive index

In initial experiments, combinations of anionic and cationic solutions were identified to produce simple, single anion/single cation, or ABAB configuration, ESA films with a range of refractive indices. Four anionic and two cationic solutions were assembled in the AB combinations shown in Table 3-1. Fifty bilayer films were fabricated on silicon and glass substrates, incorporating the same anion and cation into every bilayer throughout each film thickness. As is characteristic for ESA films, the linear growth of both optical absorbance and film thickness with the number of layers indicates homogeneous deposition with each successive layer; each bilayer contributes an equal amount of material to the film, both in density and thickness. This is illustrated in Figures 3-2, 3-3 and 3-4 by UV/vis absorbance and ellipsometry measurements.

Table 3-1. Ellipsometry data for 50-bilayer ESA films of a single anion and single cation.

	ANION	CATION	n			AVERAGE BILAYER THICKNESS
			6328 Å	5461 Å	4050 Å	
1	Poly (sodium 4-styrene-sulfonate) (PSS) *	Polydiallyldimethyl-ammonium chloride (PDDA)	1.539	1.538	1.559	23 Å
2	Poly S-119 (Sigma)	PDDA *	1.682	1.799	1.535	28 Å
3	PCBS **	PDDA	1.532	1.547	1.571	13 Å
4	Direct Red 75 *	PDDA	1.767	1.629	1.662	12 Å
5	PSS	ZrO_2	1.567	1.580	1.601	12 Å

* from Aldrich

** Poly {1-[4-(3-carboxy-4-hydroxyphenylazo)-benzenesulfonamido]-1,2-ethanediyl, sodium salt} (Aldrich)

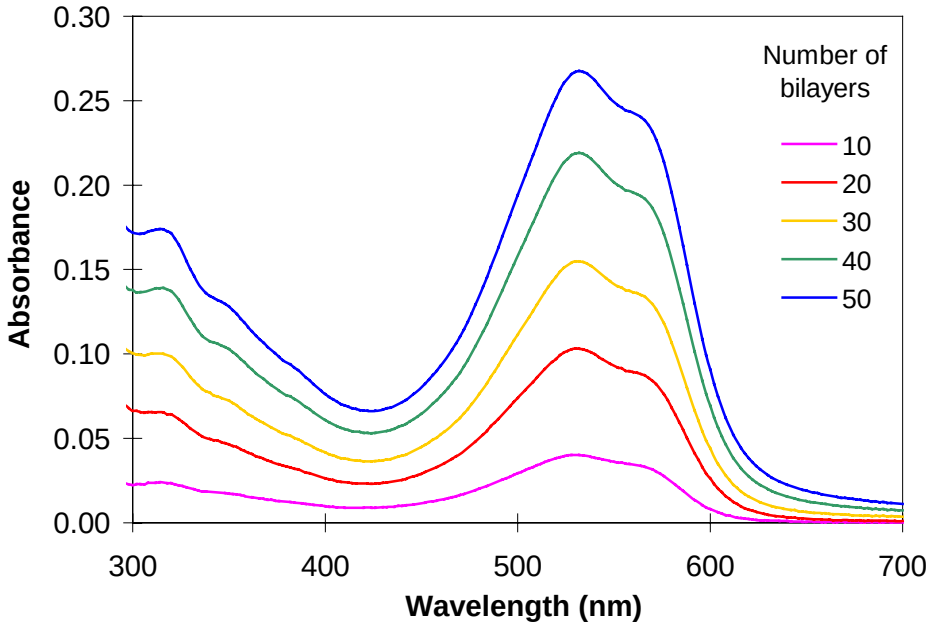

Figure 3-2. UV/vis absorbance of Direct Red 75 / PDDA ESA thin films with increasing numbers of bilayers.

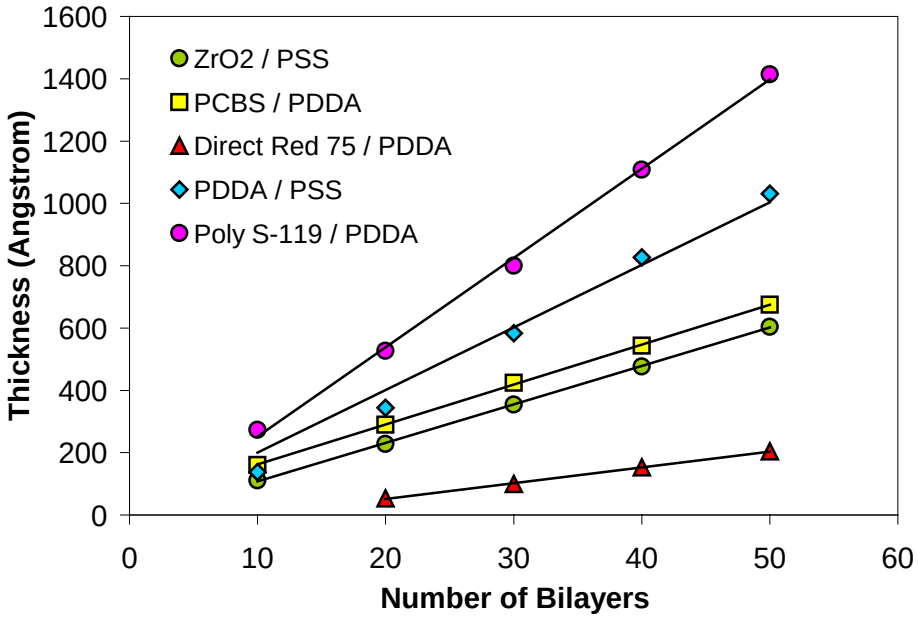

Figure 3-3. Film thickness with increasing numbers of bilayers for single anion/single cation ESA films.

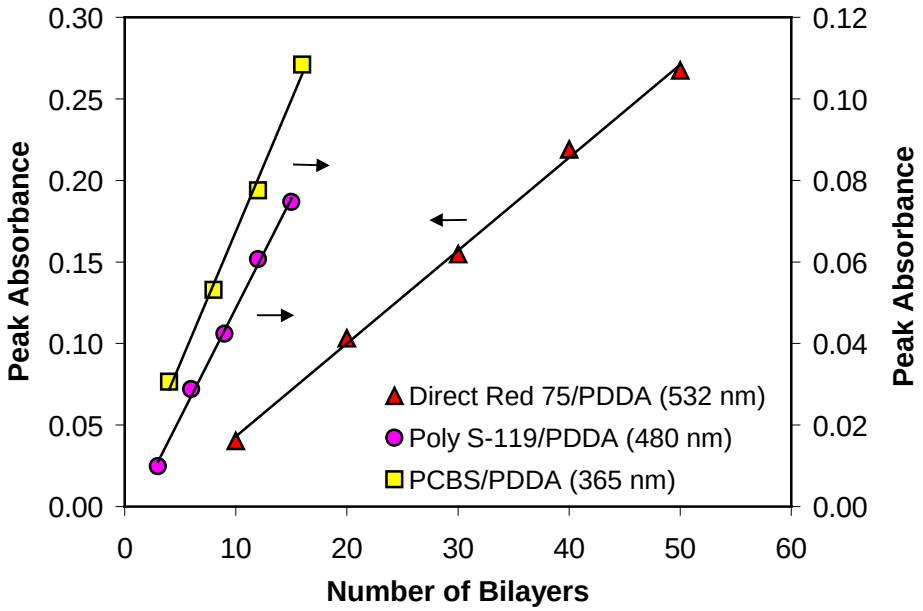

Figure 3-4. UV/vis absorbance increase during ESA film growth for single anion/single cation ESA films.

For the five combinations listed, average bilayer thickness ranged from 12 to 28 Å and each can be controlled by adjusting the dipping parameters, as discussed in Chapter 2. For most polymers studied, a small thickness dependence was found in the refractive index for the first few hundred Ångstrom of film growth, followed by saturation after approximately 40-50 bilayers. Examples of this initial thickness dependence are shown in Figure 3-5. It is believed this is due to an equipment limitation at film thicknesses less than 500 Å rather than a true material characteristic. It is not generally exhibited by films with bilayer thicknesses exceeding 20 Å.

To investigate the wavelength dependence of the film indices, ellipsometry measurements were taken using the three available wavelengths: 6328, 5461 and 4050 Å. These results are summarized in Table 3-1 for the five polyelectrolyte and nanoparticle combinations. Of all the films tested, PDDA/PSS films exhibited the most level dispersion spectrum.

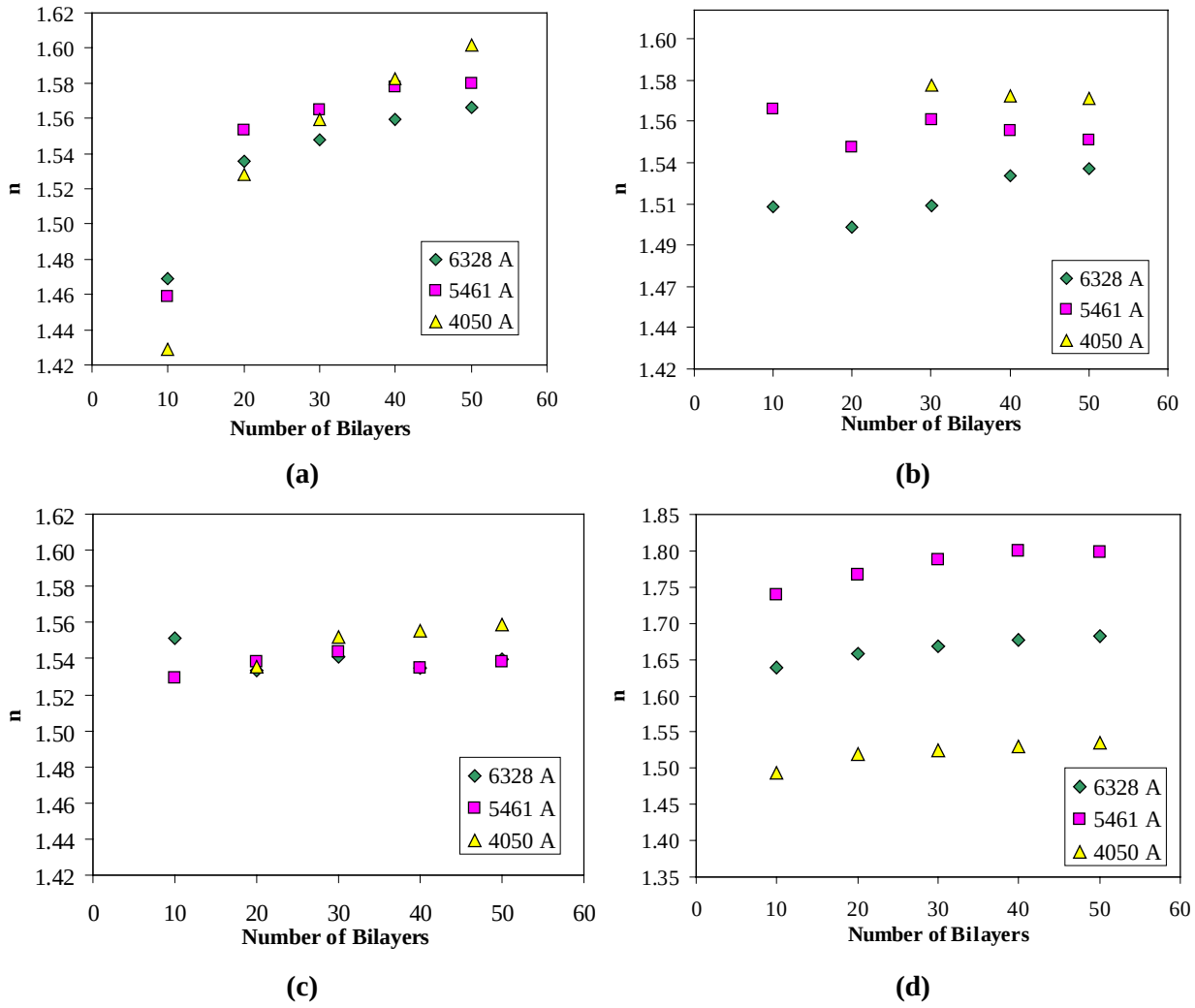

Figure 3-5. Thickness dependent refractive index for single anion/single cation ESA thin films; (a) ZrO_2 / PSS; (b) PCBS / PDDA; (c) PDDA / PSS; (d) Poly S-119 / PDDA.

3.1.2 Multilayer patterning method

In an effort to control the ESA film refractive index continuously across the range from 1.53 to 1.77, two bilayer combinations were chosen from Table 3-1, Direct Red 75/PDDA (X) and PSS /PDDA (Y) and mixed in varying proportions within a single ESA film. In this particular case, the cation, PDDA, remains constant throughout the film and only the anion varies from bilayer to bilayer. Figures 3-6 and 3-7 illustrate the concept of building up multilayers composed of predetermined patterns of X and Y, specifically a mixture of 33% X and 67% Y (XYY multilayer). As an example, to achieve a 10%/90% mix, one in ten bilayers contain Direct Red (X) as the anion, while the remaining nine contain PSS (Y). The percentage of X bilayers in a set of 50-bilayer films was increased from 0% to 100% and the refractive index monitored at several points during the film growth. Based on the assumption that the mixed films are a linear

combination of the individual X and Y films, the expected values for the range of percentages fabricated are listed in Table 3-2. These values have been calculated taking into account the difference in bilayer thicknesses between the two bilayer systems. For the two materials chosen for this experiment, there was a particularly large discrepancy between the bilayer thicknesses, i.e. 12 Å versus 23 Å, making the bilayer thickness allowance critical. These theoretical values are compared to those measured experimentally in Figure 3-11, on page 53.

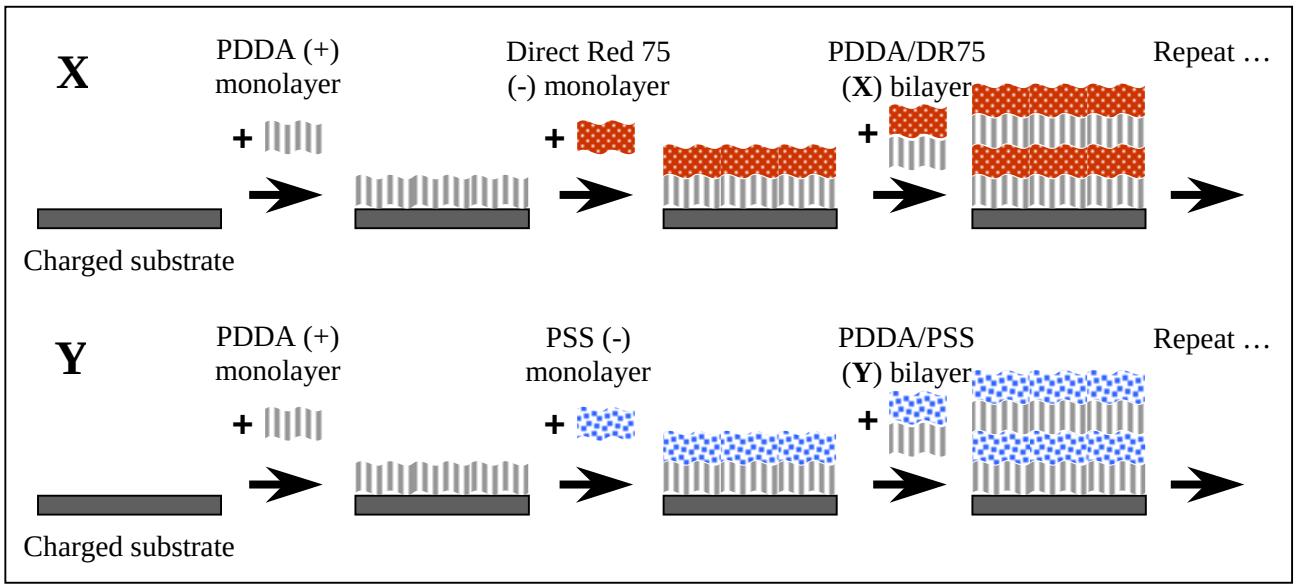

Figure 3-6. Self-assembly of Direct Red 75/PDDA (X) and PSS /PDDA (Y) films.

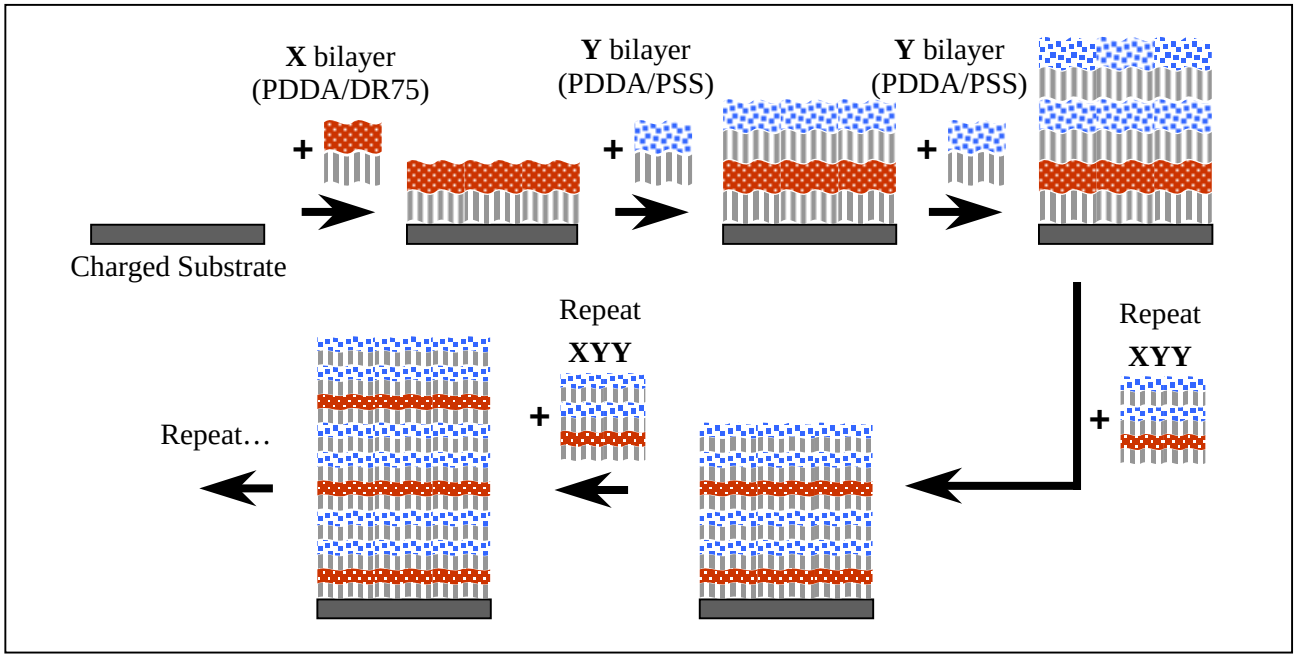

Figure 3-7. Example of the self-assembly of 33:67 mixture (XYY multilayer) ESA thin films. Variations in mixture ratio allow precise control and spatial grading of index of refraction.

Table 3-2. Expected ellipsometry values for patterned multilayer films consisting of PDDA/Direct Red 75 (X) and PDDA/ PSS (Y) bilayers.

%X Bilayers	%Y Bilayers	Refractive Index		
		6328 Å	5461 Å	4050 Å
0	100	1.539	1.538	1.559
25	75	1.563	1.548	1.570
33	67	1.573	1.552	1.574
50	50	1.598	1.562	1.586
67	33	1.633	1.576	1.602
75	25	1.656	1.585	1.612
100	0	1.767	1.629	1.662

The films were first characterized using both ellipsometry and UV-Vis spectroscopy to evaluate film structure and uniformity. The UV/vis absorbance spectra of 50-bilayer multilayer films with varying X percentages are shown in Figure 3-8a. Figure 3-8b illustrates the corresponding increase in optical density as the percentage of X bilayers is increased. As seen in (a), the absorbance peak at 532 nm does not appear in the 100% Y film; it is solely due to the increasing X content in the patterned multilayer films.

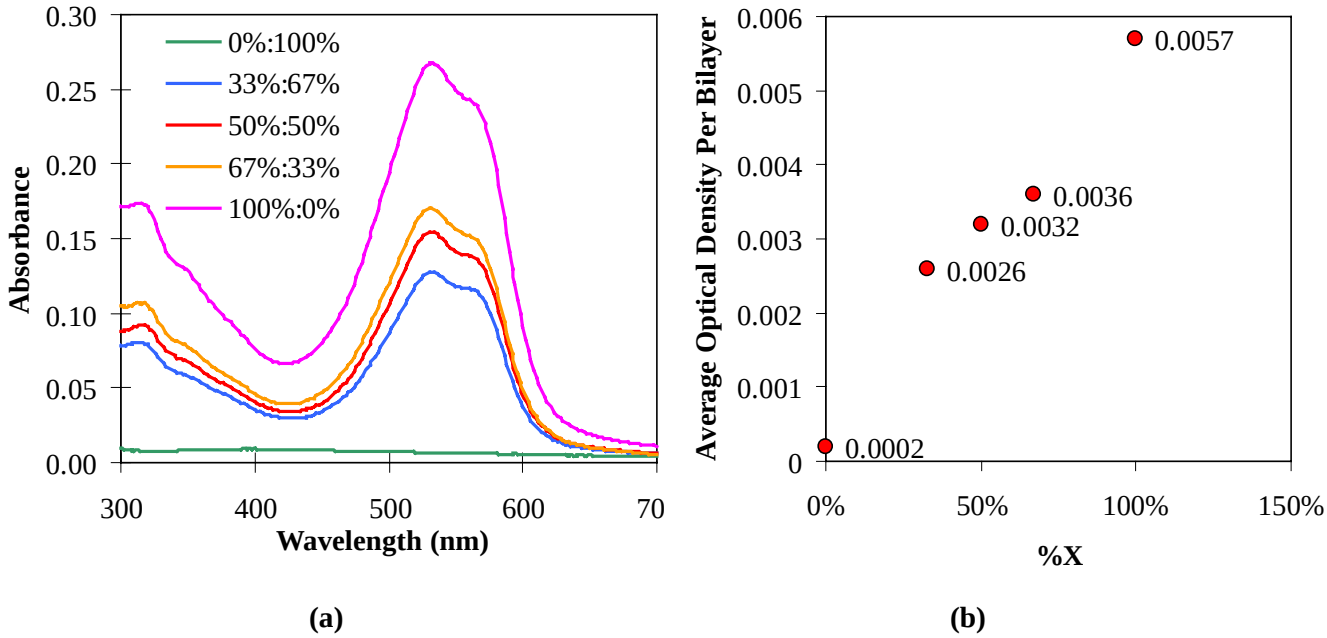

Figure 3-8. (a) UV/vis spectra and (b) average optical densities per bilayer at 532 nm for increasing X:Y [(PDDA /Direct Red 75):(PDDA/PSS)] ratios in 50-bilayer ESA films.

As expected for ESA films, both the absorbance and thickness increase linearly for each of the films fabricated (Figures 3-9 and 3-10), indicating that each multilayer is an identical, reproducible unit, and therefore a suitable ESA building block. The average bilayer thickness ranged from 12 to 23 Å, as predicted.

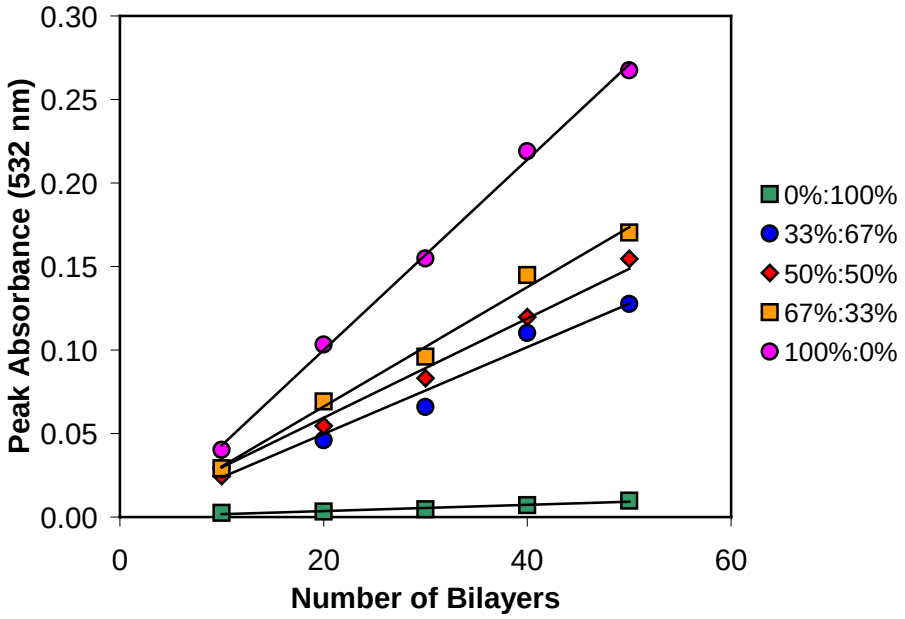

Figure 3-9. Peak absorbance of UV/vis spectra with increasing bilayers for varying X:Y [(PDDA /Direct Red 75):(PDDA/PSS)] ratios.

The refractive indices of the patterned X:Y multilayer films are shown in Figure 3-11, as well as those from a similar set of experiments combining organic materials with inorganic nanoparticles, using X and Y bilayers of (Poly S-119/PDDA) and (Poly S-119/platinum nanoparticles). Both experiments demonstrate that the refractive index of ESA thin films can be controlled by the use of appropriately chosen multilayer structures. The multilayer films are a nearly linear combination of the individual X and Y films. Using the same concept, it is possible to grade the index through the thickness of a film, n(x), by varying the X percentage through the thickness of a film, %X(z). This is the basis of thin-film refractive index control using the ESA process.

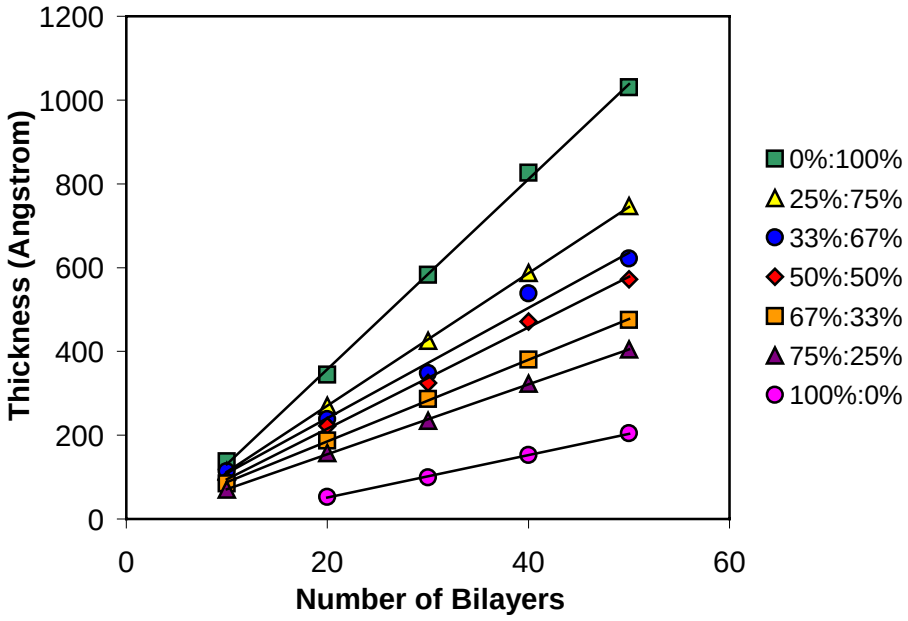

Figure 3-10. Film thickness vs. number of bilayers for varying X:Y [(PDDA /Direct Red 75):(PDDA/PSS)] ratios.

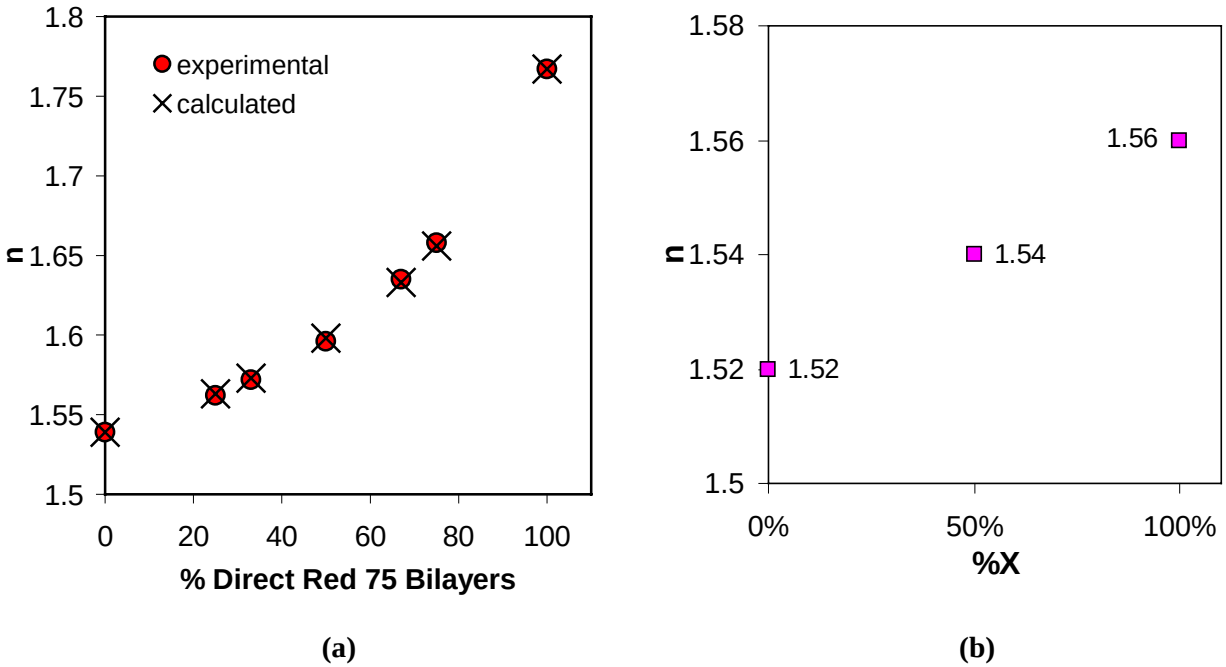

Figure 3-11. Bulk refractive index vs. percentage of higher index material for combinations of (a) two different polymers and (b) a polymer and inorganic nanoparticles.

3.1.3 Aqueous mixture method

An alternative method of refractive index control, using aqueous mixtures of the selected molecules, was also investigated. The molecules were mixed in aqueous form and assembled simultaneously from the resulting ionic solution. In this experiment the same cation, polydiallyldimethylammonium chloride (PDDA), was used for all specimens, while each anionic solution was composed of a mixture of Direct Red 75 and poly (sodium 4-styrene-sulfonate) (PSS), both obtained from Aldrich. Five samples were prepared, under identical conditions, with the percentage of Direct Red 75 in the mixture increasing by steps of 25%.

The thickness increased linearly for each of the films fabricated (Figure 3-12), with the average bilayer thickness ranging from 12 to 21 Å. The refractive index was again found to be thickness-dependent for the first few hundred Å of film growth, followed by saturation after approximately 40-50 bilayers, as illustrated in Figure 3-13 for measurements at 633 nm. The index range resulting from the mixture of the two materials is shown in Figure 3-14 for both 405 nm and 633 nm. For each mixed film, the refractive index is closer to that of a purely Direct Red 75/PDDA film than expected, due to the preferential adsorption of Direct Red 75 over PSS. The time constant for ionic self-assembly is not only dependent on the dipping parameters, but is also species dependent. In other words, in each bilayer, the PSS molecules were slower to adsorb, therefore more Direct Red 75 molecules assembled in each bilayer than would be expected based on the fractional solution contents.

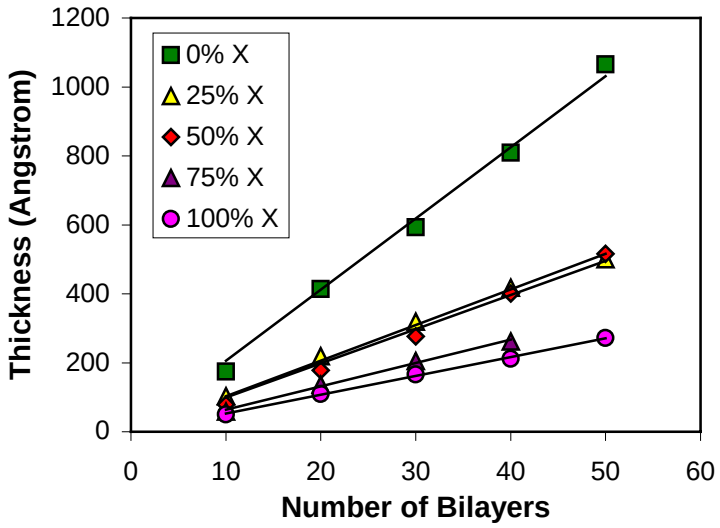

Figure 3-12. Film thickness for varying X:Y (Direct Red 75:PSS) ratios.

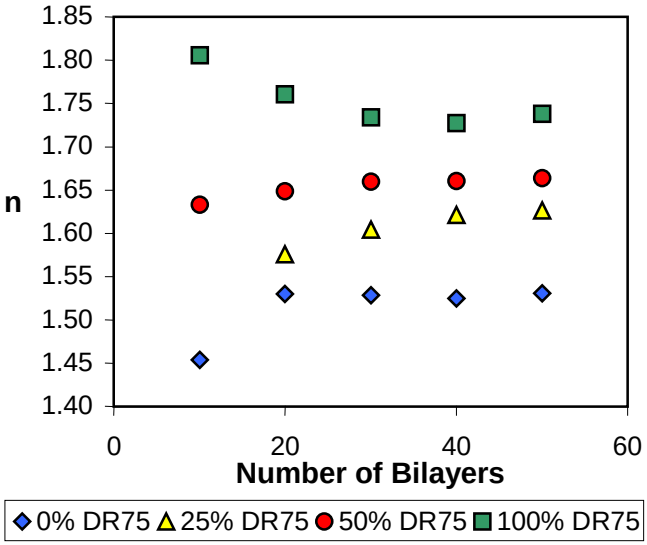

Figure 3-13. Thickness dependent refractive index at 633 nm.

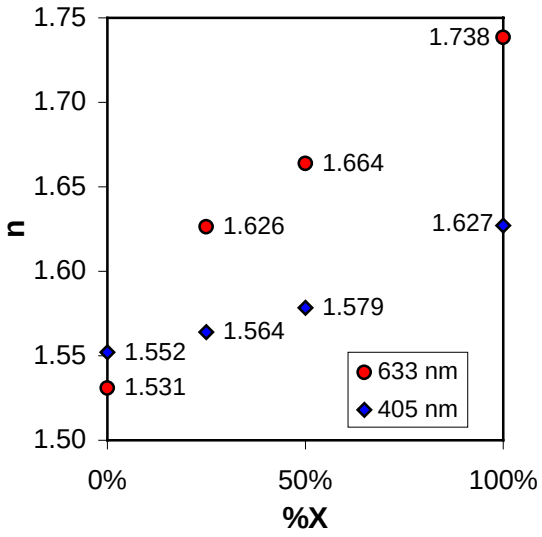

Figure 3-14. Refractive index vs. Percentage of X (PDDA/Direct Red 75) bilayers in 50-bilayer films.

Although this experiment demonstrated that the refractive index of ESA thin films can be controlled by using mixtures in the aqueous form, the multilayer method resulted in superior film quality. The mixture method produced less uniform films than the multilayer method as evidenced by greater deviations of the ellipsometry thickness measurements and AFM surface roughness analyses. In the latter, for the 50:50 mixed film, ΔZ across the surface was found to be 35 nm, while in the 50:50 multilayer film, ΔZ was only 21 nm. The AFM images, shown in Figure 3-15, also indicate that agglomerates may have formed in the mixed films, resulting in decreased homogeneity.

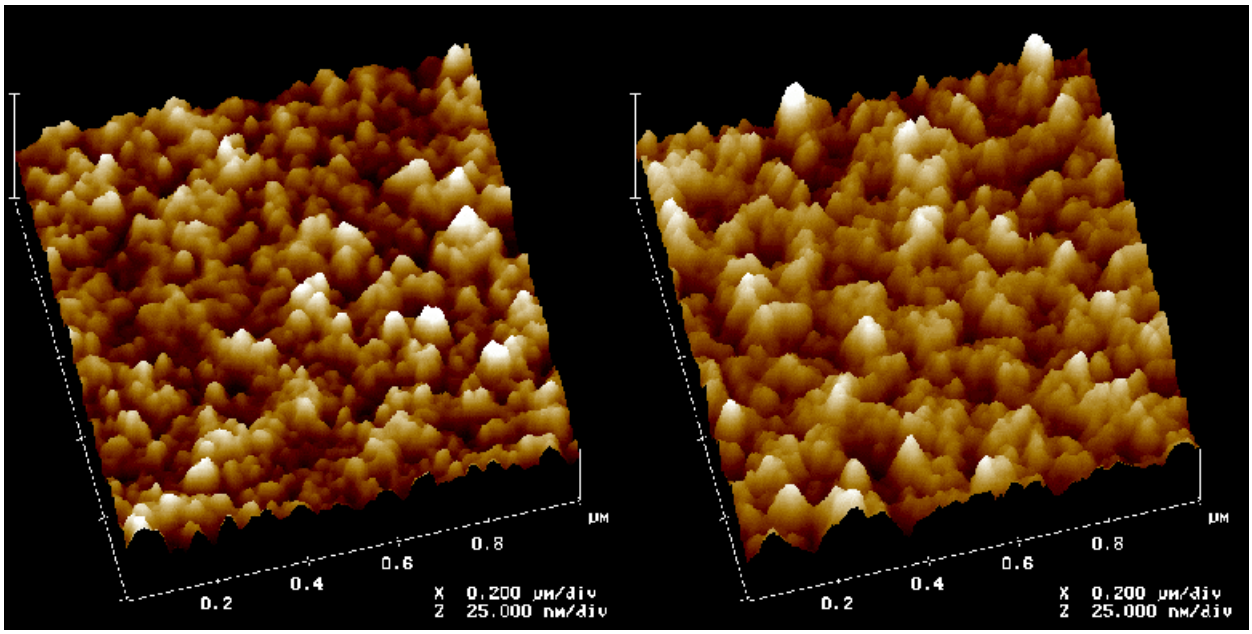

(a) **(b)**

Figure 3-15. AFM images of 50-bilayer ESA thin films fabricated using (a) the multilayer method and (b) the mixture method. Both samples contain a 50:50 Direct Red 75/PSS ratio.

3.2 Dielectric stack filters

Considering a single λ/4 film, it can easily be shown that constructive interference from reflections at both the top and bottom surfaces produces high reflectance at the top surface of the film [3,14,15]. This effect is enhanced by reflection from multiple layers since the light reflected from all interfaces within the film have equal phase when they reach the top surface of the film. A stack of alternating high (H) and low (L) index layers, each of optical thickness λ/4, is required. The first layer, next to the substrate and the outermost layer must be high-index. The maximum reflectance from a such film, consisting of *p* layers, has been previously calculated [14,16] and is given by

$$R_{\lambda/4} = \left(\frac{n_H^{p+1} - n_L^{p-1} n_S}{n_H^{p+1} + n_L^{p-1} n_S} \right)^2 \qquad \textbf{(3.2)}$$

where n_H, n_L and n_S are the high, low and substrate indices respectively. Note that the assumption that each layer is exactly λ/4 thickness is inherent in Equation 3.2. This indicates that film thickness control is far more critical in multilayer designs than single layer coatings. Rearrangement of Eq. 3.2 under the assumption of negligible absorption will show that each additional set of low and high index layers increases the reflectance by a factor of $(n_H/n_L)^2$ [13]. Figure 3-16 illustrates the change in spectral characteristics for such a dielectric stack with increasing numbers of λ/4 layers. This figure is presented here for general comparison with the

experimental spectra obtained from the stack filters fabricated in this study. The magnitude of peak reflectance as well as the number of sideband oscillations increases with increasing λ/4 layers. The spectral width of the reflectance peak is dependent on the ratio of refractive indices of the high and low index layers. In addition to film thickness and refractive index, low light scattering and good film adhesion are critical requirements for dielectric interference systems. Both of these are provided by the ESA processing method.

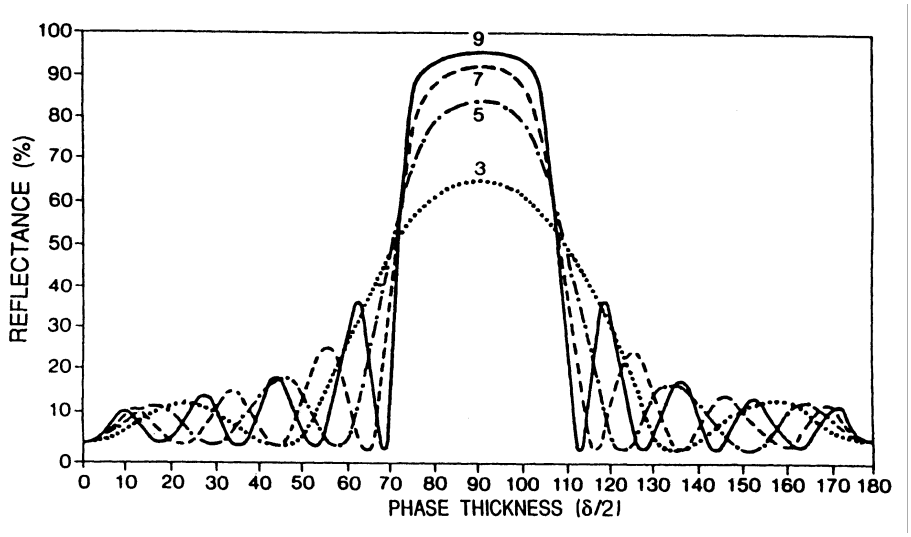

Figure 3-16. Theoretical reflectance spectra of multilayer stacks formed of alternating λ/4 layers of n_H=2.3 and n_L=1.38 on glass (n_S=1.52) as a function of phase thickness (2πnd/λ). The number of layers is indicated. (After Penselin and Steudel [17].)

Using the refractive index data discussed in the previous section, the initial ESA dielectric stack filters were designed and synthesized with two different reflecting wavelengths, demonstrating the ability to design and control the optical output through precise control of the refractive index profile. The high index λ/4 layers were composed of PDDA and Poly S-119 (Sigma), with n=1.68 at 633 nm, while the low index layers were composed of PDDA and PSS, with n=1.54 at 633 nm. Both the magnitude of the reflectance peak and the number of sideband oscillations increase with the number of layers, as predicted by theory [3]. The spectral width of the high-reflectance zone is dependent on the refractive index difference between the two layers, in this case, approximately 0.14.

The initial stack exhibited inconsistent reflectance wavelengths, as shown in Figure 3-17, which is most likely due to variations in thickness and index of the λ/4 layers. The specimen was dipped over a time period of several weeks, allowing the potential for variations in solution chemistry. Uniformity was greatly improved in the fabrication of the second stack filter, shown in Figure 3-18, with a reflection peak at 642 nm; note the more consistent peak wavelength. The optical thickness of each λ/4 layer is approximately 161 nm, as indicated in the index profile.

The filters discussed above were fabricated using hand dipping methods. However, the stack filter fabrication process has been automated, as discussed in Chapter 2.

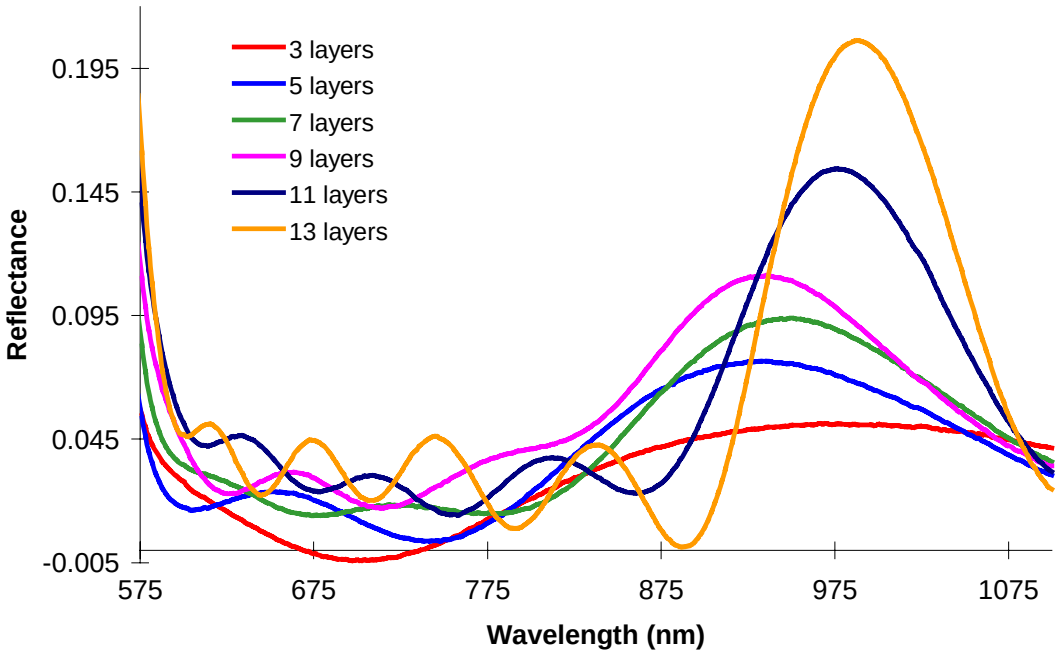

Figure 3-17. Prototype dielectric stack filter and spectral characteristics for increasing numbers of alternating λ/4 layers of PDDA/Poly S-119 and PDDA/PSS ESA thin films.

3.3 Rugate filters

Considering the complexity of the refractive index profiles involved, Rugate filter fabrication presents a greater challenge than that of dielectric stack filters, but also offers many advantages, including the elimination of high-ordered harmonics and the capability to superimpose multiple index profiles to produce multi-notch filters.

For this investigation, to demonstrate the feasibility of producing graded index ESA structures, a simple sine wave Rugate filter prototype was designed and synthesized (Fig. 3-19). The lack of apodization in the index profile of this simple design produces undesired sidelobes in the reflectance spectra, but this can be corrected in future designs, after the capability is demonstrated. The index grading within the filter was achieved using the multilayer technique discussed in Section 3.1. PDDA was used as the cation throughout the film. Low-index bilayers contained the polyanion PSS; high-index bilayers contained Poly S-119, resulting in a refractive index range from 1.54 to 1.68. For a reflectance peak at 780 nm, the index profile design is shown in Figure 3-20; the period was calculated to be 243 nm, using $\lambda_c=2n_ad$, where n_a is the average refractive index, assumed to be 1.61. However, this calculation assumes an infinite number of sinusoidal periods. Transitory effects as the initial periods are assembled create a shift in the peak reflectance wavelength, which saturates as the "infinite sinusoid" approximation

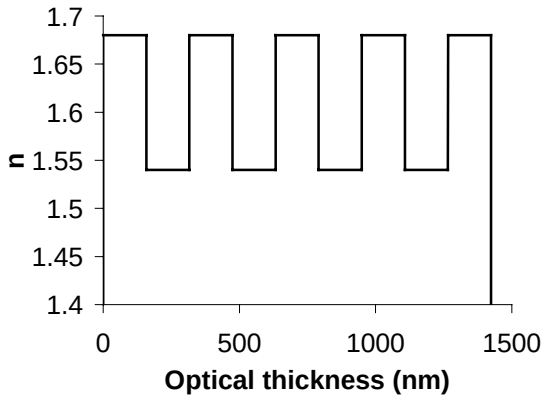

(a) **(b)**

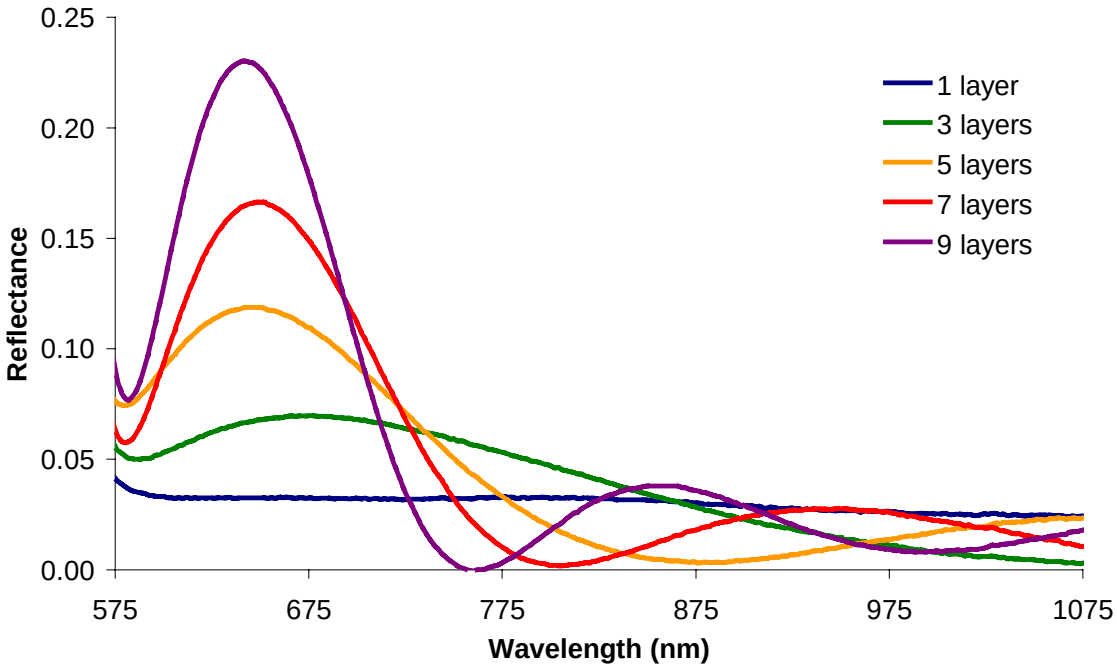

(c)

Figure 3-18. Dielectric stack filter (a) refractive index profile design (b) and experimental reflectance output for increasing numbers of λ/4 layers (c).

Figure 3-19. Prototype rugate filter.

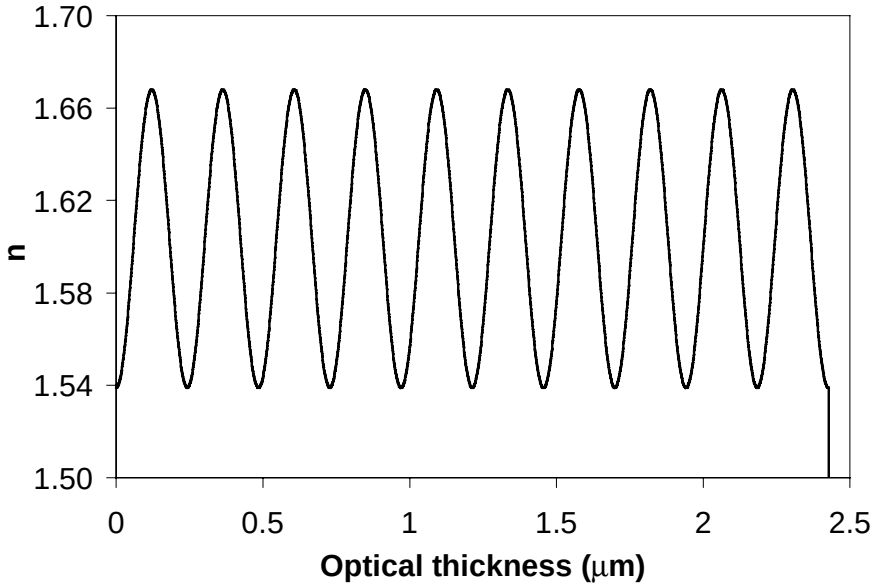

Figure 3-20. Rugate filter index profile design.

becomes valid. The filter was dipped by hand on a glass substrate. In total, ten periods were self-assembled.

The spectral characteristics of this prototype filter are shown in Figure 3-21 for increasing numbers of periods; the six plots are split only for the sake of readability. Note the shift of the reflectance peak to higher frequencies with the addition of greater numbers of periods. The drop in transmission below 600 nm is due to the absorption band of the Poly S-119 dye, not the reflectance of the interference filter. As illustrated in Figure 3-22, the peak wavelength saturates around 615 nm, which indicates a sinusoidal index profile of period 192 nm. More accurate bilayer thickness estimates are required for future designs.

While the index profile design of this filter was kept at a simple level, its synthesis demonstrates the capability to produce graded index optical filters and other graded index structures using the ESA process.

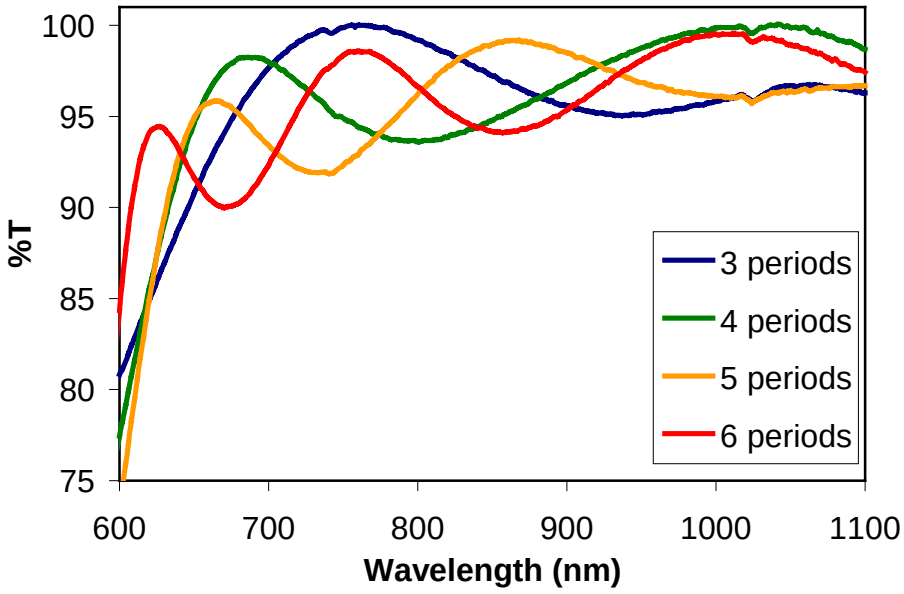

(a)

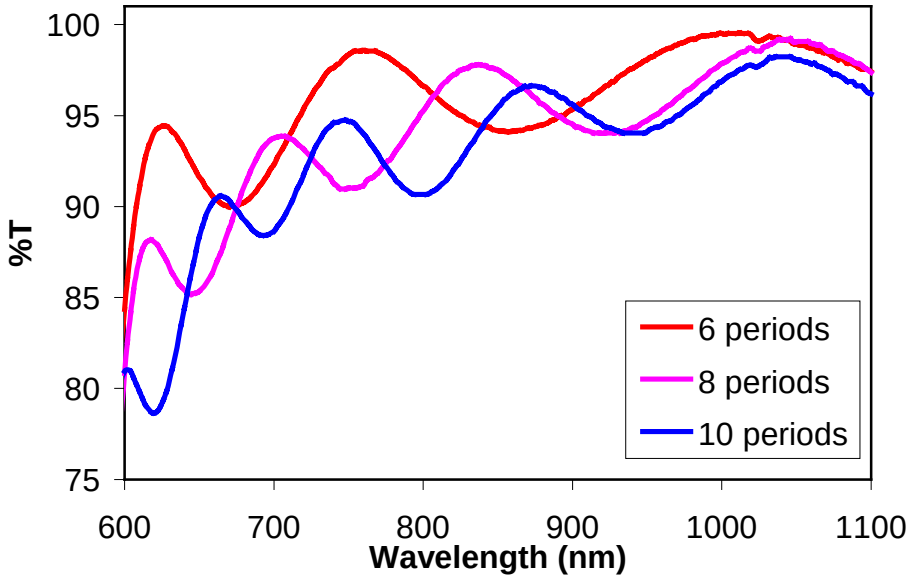

(b)

Figure 3-21. Transmission spectra of ESA rugate filter with increasing numbers of periods; (a) three, four, five and six periods assembled, and (b) six, eight and ten periods assembled.

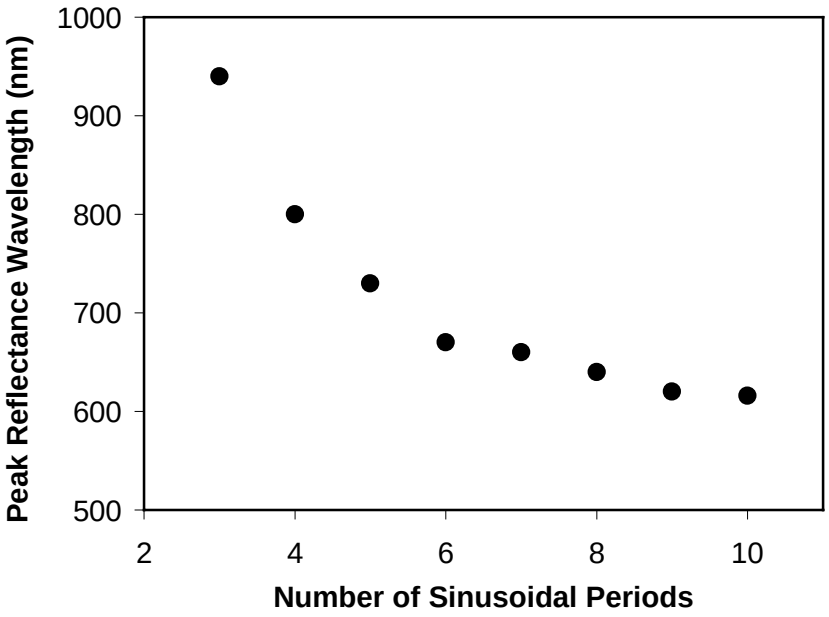

Figure 3-22. Peak reflectance wavelength of ESA Rugate filter as the index profile approaches the infinite sinusoid approximation.

3.4 Antireflection (AR) coatings

AR coatings were the goal of much initial work in thin film optics, and considering production volume, they still exceed all other types of coatings [3]. Their purpose is to reduce reflection, increase light transmission, and reduce glare. In simple applications, only surface reflection reduction is required; in others, increased transmission is the goal. Glare reduction improves the contrast of images in optical systems. AR coatings find application in almost any optical system, including cameras, binoculars, telescopes, microscopes, spectacle lenses, display windows, picture frames and laser systems, as well as applications which require increased light capture such as solar cells, detectors and magneto-optical devices.

As with the reflectance filters discussed in previous sections, AR coatings can consist of a simple single layer design, or a multilayer system. The selection depends on the substrate material, the wavelengths involved, and the film materials available. For this dissertation, multilayer ESA-formed AR coatings on polycarbonate substrates were investigated. According to Macleod, "design techniques for AR coatings on low-index materials are less well organized and involve much more intuition and trial and error than those for high-index materials [3]." This statement was verified in this study. Polycarbonate falls into the low-index substrate category with a refractive index of 1.586. As with other thin film fabrication approaches, the ESA technique is limited by the refractive index of available film materials. Single layer coatings would require film refractive indices of 1.26; no material is available in this range. Another obstacle was the absorbance range of the high-index materials available. As a result, reflection characteristics at wavelengths greater than 550 nm were studied, rather than 400-700 nm, the visible range. A

search for high-index water-soluble materials with negligible absorbance in the visible is currently ongoing.

Three design iterations were performed for a total of six prototype AR coatings. The first pair of coatings, designated A.1 and A.2, compared the performance of a quarter-quarter-quarter filter with that of a quarter-half-quarter with identical refractive indices. In labeling these filter index profiles, "quarter" indicates a film layer optical thickness of λ/4, where λ is the central wavelength of the range in question, in this case, 550 nm, and "half" then indicates a film layer thickness λ/2. For example, filter A.1 was a quarter-quarter-quarter filter with refractive indices 1.656, 1.68, 1.54. This means that layer 1, immediate to the substrate, was a film λ/4 thick with an index of 1.656; on top of that was layer 2, λ/4 thick of index 1.68, followed by layer 3, λ/4 thick of index 1.54. The index profile designs of AR filter designs A.1 and A.2 are illustrated in Figure 3-23; they are identical other than the thickness of Layer 2. Layer 3 in each was composed of PDDA as the cationic monolayers and PSS as the anionic. Layer 2, PDDA and Poly S-119. Layer 1 was synthesized using the multilayer patterning index control method discussed in Section 3.1.2; X bilayers were composed of PDDA/Poly S-119 and Y bilayers PDDA/PSS. The bilayer percentages are indicated in Table 3-3 below. Figure 3-24 shows the resulting transmission increase due to coatings A.1 and A.2 compared to that of a bare polycarbonate substrate.

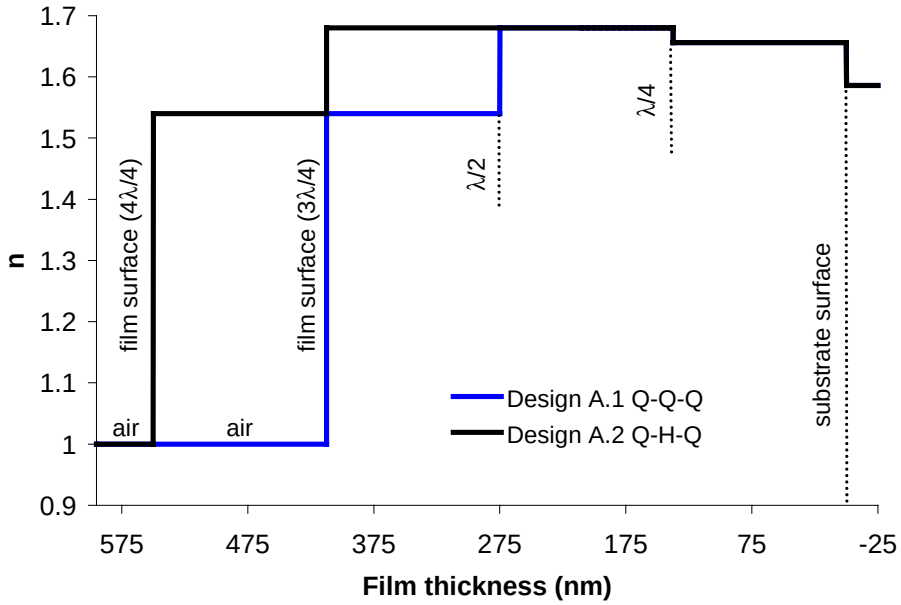

Figure 3-23. AR filter A.1 and A.2 refractive index profiles; the substrate surface, film/air interface, and λ/4 and λ/2 thicknesses are indicated. The filters are identical in the range 0-275 nm from the substrate surface.

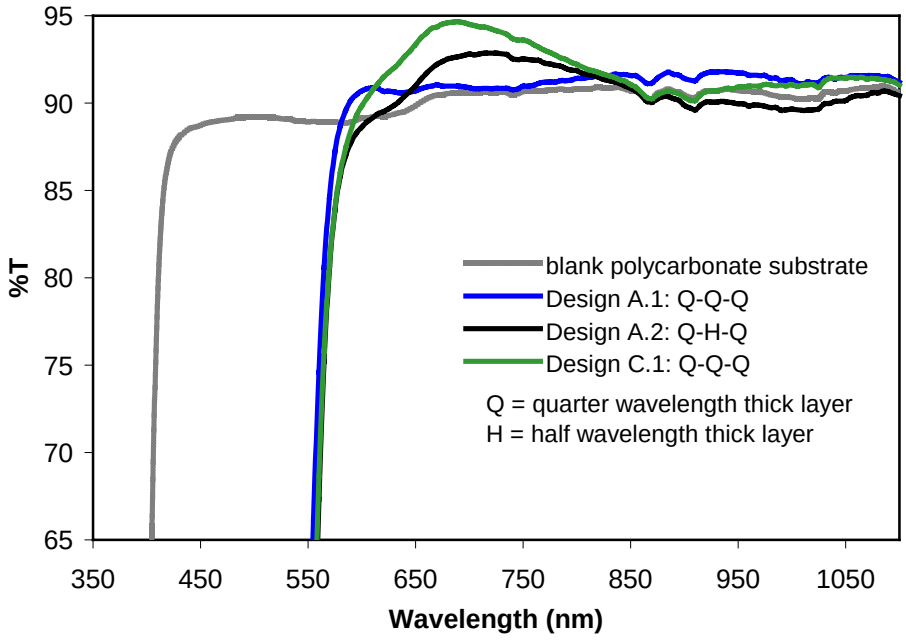

Figure 3-24. Percent transmission spectra of a bare polycarbonate substrate and polycarbonate substrates coated with AR filter designs A.1 and A.2.

Based on the results of iteration A, the quarter-quarter-quarter basic design was selected. Although the quarter-half-quarter filter produced the highest peak transmission at 92.9%, transmission was highly wavelength dependent, and was actually lower than that of the bare substrate at some wavelengths. For iteration B, the refractive index of layer 1 was varied above and below that of iteration A. Iteration C again varied this index, in the direction indicated by the results of iteration B, an increase. These four index profile designs are illustrated in Figure 3-25, as well as A.1. Layer 1 in each filter was fabricated using the multilayer patterning technique described above.

The transmission results for the five quarter-quarter-quarter filter designs are shown in Figure 3-26; the results from all 6 AR filters are summarized in Table 3-3. Of the index profile designs tested, design C.1 (Q-Q-Q, 1.67, 1.68, 1.54) produced the maximum transmission, up to a peak of nearly 95%, between 625 nm and 805 nm. Outside that narrow region, design B.1 (Q-Q-Q, 1.66, 1.68, 1.54) produced the maximum transmission over a much wider and flatter spectrum. C.1 transmission deviated as much as 5 % from the peak for wavelengths 600-1100 nm, while B.1 varied by less than 1% over the same region. The optimum choice is therefore dependent on the AR bandwidth required. The design will be greatly improved by the determination of a high index material possessing both negligible absorbance in the visible wavelengths and compatibility with ESA processing.

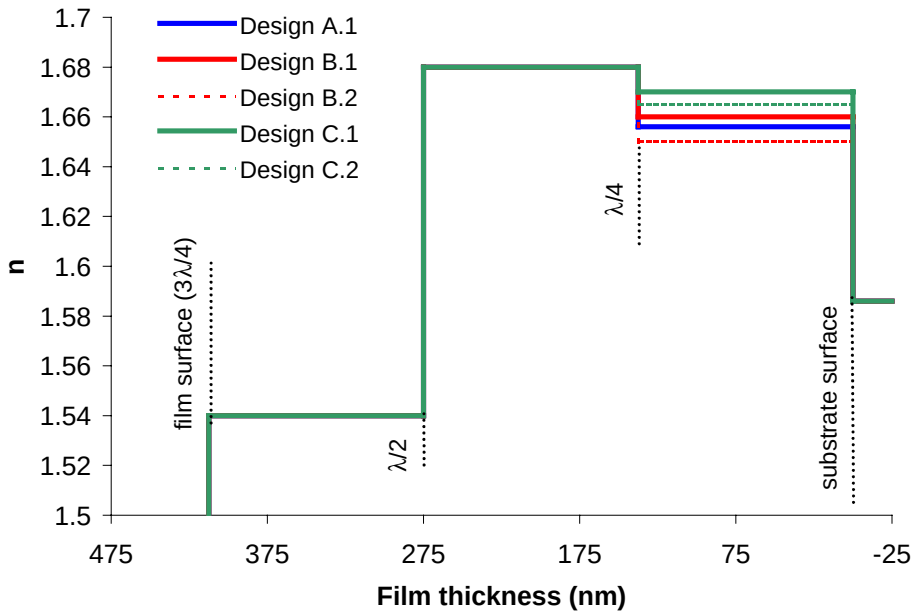

Figure 3-25. AR filter A.1, B.1, B.2, C.1 and C.2 refractive index profiles; the substrate surface, film/air interface, and λ/4 and λ/2 thicknesses are indicated. The filters are identical in the range from 138 nm to the film/air surface.

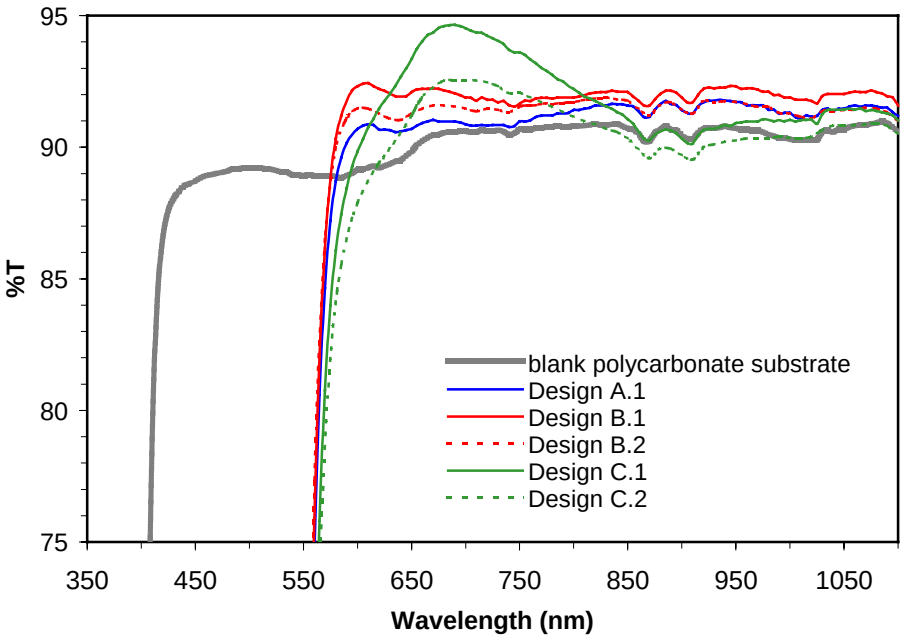

Figure 3-26. Percent transmission spectra of a bare polycarbonate substrate and polycarbonate substrates coated with AR filter designs A.1, B.1, B.2, C.1 and C.2.

Table 3-3. ESA-formed AR coating results (assembled on polycarbonate substrates).

FILTER	DESIGN	REFRACTIVE INDEX		% X (PDDA/ POLY S-119) BILAYERS	PEAK TRANSMISSION	PEAK %T WL	MAXIMUM Δ%T (600-1100 NM)
A.1	Q-Q-Q	Layer 1 2 3	1.656 1.68 1.54	80 % 100 % 0 %	91.8 %	935 nm	1.2 %
A.2	Q-H-Q	Layer 1 2 3	1.656 1.68 1.54	80 %	92.9 %	720 nm	4.2 %
B.1	Q-Q-Q	Layer 1 2 3	1.660 1.68 1.54	83 %	92.4 %	610 nm	0.9 %
B.2	Q-Q-Q	Layer 1 2 3	1.650 1.68 1.54	75 %	91.9 %	830 nm	0.9 %
C.1	Q-Q-Q	Layer 1 2 3	1.670 1.68 1.54	92 %	94.7 %	690 nm	4.8 %
C.2	Q-Q-Q	Layer 1 2 3	1.665 1.68 1.54	88%	92.6 %	695 nm	4.6 %
bare substrate (polycarbonate)		1.586		-	91.0 %	1085 nm	1.8 %

3.5 Summary

This chapter investigated the application of ESA processing to multilayer linear optical interference filters. Basic single anion/single cation ESA films were fabricated and characterized to provide a basis of optical materials from which filters could be designed. Using these materials, two methods of grading refractive index through the film thickness were demonstrated, multilayer patterning and aqueous mixtures. The aqueous mixture method, although feasible, presented several disadvantages; therefore multilayer patterning methods were used for the remainder of the experiments.

High and low index materials were chosen from the basis of optical materials identified in the first part of the chapter, and dielectric stack filters were fabricated, demonstrating the capability to produce step-index profile thin films. The study was then expanded to continuously-varying index profile Rugate reflectance filters. Finally, multilayer AR coatings were fabricated. These experiments have demonstrated for the first time the feasibility of using the ESA process for optical filters and other optical structures that require precise index profile control.

3.6 References

1. J.A. Dobrowolski, "Usual and Unusual Applications of Optical Thin Films - An Introduction," in *Handbook of Optical Properties Vol. 1: Thin Films for Optical Coatings*, ed. R.E. Hummel and K.H. Guenther, CRC Press, Boca Raton (1995).
2. Y. Taga, "Recent progress in coating technology for surface modification of automotive glass," *Journal of Non-Crystalline Solids* **218**, 335-41 (1997).
3. H.A. Macleod, *Thin-Film Optical Filters*, McGraw-Hill, New York (1989).
4. O.S. Heavens, *Optical Properties of Thin Solid Films*, Dover, New York (1965).
5. A. Thelen, *Design of Optical interference Coatings*, McGraw-Hill, New York (1989).
6. H.A. Macleod, "Optical thin film coating design," *Proc. SPIE* Vol. 2776, p. 2 (1996).
7. J.A. Dobrowolski, "Optical Properties of Films and Coatings," in *Handbook of Optics*, 2nd ed., Ed. M. Bass, McGraw-Hill, New York (1994).
8. A.V. Tikhonravov, "Some theoretical aspects of thin-film optics and their applications," *Applied Optics* **32**, no.28, 5417 (1993).
9. H.A. Macleod, "New techniques revolutionize thin-film optical coatings," *Laser Focus World* **28**, no. 11, 111 (1992).
10. H. Sankur, "Deposition of optical coatings by laser-assisted evaporation and by photo-assisted chemical vapor deposition," *Thin Solid Films* **218**, 161-9 (1992).
11. H.K. Pulker, *Coatings on Glass*, Elsevier, Oxford (1984).
12. J.D. Rancourt, *Optical Thin Films User Handbook*, SPIE Optical Engineering Press, Bellingham, Washington (1996).
13. Y. Liu, *Characterization and Patterned Polymer Films from a Novel Self-Assembly Process*, Ph.D. dissertation, Chemistry Department, Virginia Polytechnic Institute & State University, May 1996.
14. M. Ohring, *The Materials Science of Thin Films*, Academic Press, New York (1992).
15. K.D. Möller, *Optics*, University Science Books, Mill Valley, California (1988).
16. K.I. Chopra, *Thin Film Phenomena*, McGraw-Hill, New York (1969).
17. S. Penselin and A. Steudel, *Z. Phys.* **142**, 21 (1955).

CHAPTER 4

Second-Order Nonlinear Optical Behavior in ESA Films

The term "nonlinear optics" encompasses a range of extremely useful phenomena that occur as a consequence of the modification of the optical properties of a material by the presence of an optical field [1]. To examine the connection between this statement and the quantities that will be investigated in this chapter, we return to the well-worn Maxwell's equations and constitutive relations, particularly

$$\mathbf{D} = \varepsilon\mathbf{E} = \varepsilon_0\mathbf{E} + \mathbf{P}. \quad \textbf{(4.1)}$$

The constitutive parameter ε is, in general, a function of position within the material and the environment, i.e. applied field strength, polarization and frequency, expressed as

$$\varepsilon = (1 + \chi)\,\varepsilon_0 \quad \textbf{(4.2)}$$

In other words, the polarization or dipole moment density, **P**, is also a function of the applied field, via the electric susceptibility, χ, which describes how the material responds to the applied field. For linear optical materials, this relationship is as simple as

$$\mathbf{P}(t) = \chi^{(1)}\varepsilon_0\mathbf{E}(t). \quad \textbf{(4.3)}$$

For nonlinear optical materials, the equation can be expressed as a Taylor series expansion, or

$$\mathbf{P}(t) = \varepsilon_0\,(\chi^{(1)}\,\mathbf{E}(t) + \chi^{(2)}\,\mathbf{E}^2(t) + \chi^{(3)}\,\mathbf{E}^3(t)\,\ldots). \quad \textbf{(4.4)}$$

Second order nonlinear optical effects therefore require a nonzero $\chi^{(2)}$ characteristic and are dependent on the square of the applied field as follows.

$$
\begin{aligned}
E^2(t) &= (E^{dc} + E^{\omega}\cos\omega t)^2 \\
&= (E^{dc})^2 + 2(E^{dc}E^{\omega}\cos\omega t) + (E^{\omega})^2\cos^2\omega t \\
&= (E^{dc})^2 + \tfrac{1}{2}(E^{\omega})^2 + 2\,E^{dc}E^{\omega}\cos\omega t + \tfrac{1}{2}(E^{\omega})^2\cos 2\omega t
\end{aligned}
\qquad \textbf{(4.5)}
$$

The third term gives rise to the electro-optic effect, the fourth, second harmonic generation (SHG), which is the conversion of an optical wave from one frequency, ω, to twice that fundamental frequency, 2ω. This quantity is used to evaluate the $\chi^{(2)}$ characteristics of materials in this study.

ESA processing inherently yields noncentrosymmetric molecular structures that possess large $\chi^{(2)}$ second-order NLO response, without the need for electric field poling. As illustrated in Figures 2-1 and 2-2 for polymers and nanoparticles, molecules containing NLO chromophores can easily be incorporated in ESA films, as shown in Figure 4-1. Such structures have been shown to exhibit inherent long-term stability, in contrast to conventional poled polymers. Additionally, as discussed in previous chapters, ESA nonlinear optical thin films offer theadvantages of excellent homogeneity for low waveguide scattering loss, simplicity and low fabrication cost. ESA films greater than 10 microns thick can be produced with excellent uniformity and may be patterned in three dimensions to yield channel waveguides and other device structures. The purpose of this chapter is to describe the methods used to fabricate nonlinear optical thin films using the ESA process and demonstrate their second order characteristics.

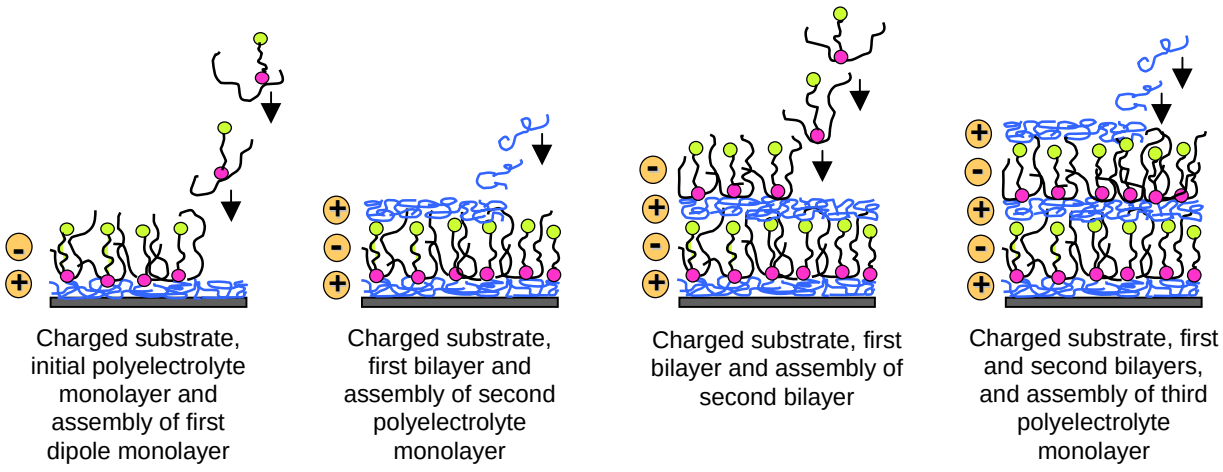

Figure 4-1. Basic ESA schematic for the buildup of noncentrosymmetric multilayer assemblies. Although this figure indicates a passive cation and chromophoric anion, either, or both of the alternating polyelectrolyte monolayers may contain the dipole element.

The chapter is organized as follows. A background of material systems used for second order nonlinear optical applications is reviewed in Section 4.1. Section 4.2 presents the characterization of ESA films fabricated using commercially available NLO polymer dyes. Due

to these promising results, films composed of molecules specifically designed and synthesized to produce a net macroscopic dipole moment were investigated. The fabrication methods and characterization of these novel films are discussed in Section 4.3. Section 4.4 considers the thermal stability of ESA NLO films. The chapter summary follows in Section 4.5.

4.1 Second-order nonlinear optical materials

4.1.1 Material requirements

All materials exhibit nonlinear optical behavior. However, second-order nonlinear optical effects, such as harmonic generation, optical parametric oscillation, and the electro-optic effect, are quadratic in the applied fields, as discussed above. Symmetry considerations therefore require that a material must be noncentrosymmetric in order to possess a nonzero $\chi^{(2)}$ [1].

In addition to the obvious requirement of as high as possible $\chi^{(2)}$ value, to be applied practically, NLO materials must satisfy numerous secondary requirements. As with most other optical processes, low absorption at the wavelengths of interest and low light scattering are essential. Other requisite properties can be divided into two areas - mechanical and chemical characteristics, and application-dependent requirements. The former includes homogeneity, processability, and optical, thermal, chemical and environmental stability. The latter, while variable, can encompass transparency, refractive index, dielectric constant, phase matching characteristics, and integration compatibility with other components.

Inorganic, ferroelectric crystals such as lithium niobate, potassium dihydrogen phosphate (KDP), and beta-barium borate (BBO) currently set the standard in second-order nonlinear optical devices. They offer the significant advantages of high NLO coefficients, excellent transparency, high optical quality, and optical and environmental robustness. However, growth of high-quality crystals is difficult, time-consuming, and expensive. (See for example, Ref. 2.)

Organic materials offer a number of advantages over inorganic crystals for $\chi^{(2)}$ applications [3-6]. A primary benefit is their versatility; organic synthesis techniques are capable of modifying molecular structures for increased nonlinear response as well as optimizing secondary properties, often labelled "molecular engineering." This is combined with easy and low-cost fabrication on a large choice of substrates [7] and simple patterning techniques by photobleaching. Organics also offer, in general, high mechanical strength as well as excellent environmental, thermal and chemical stability and high transparency. Optical damage thresholds can be greater than 10 GW/cm^2 for polymer materials [8]. Low dielectric constants result in lower RC time constants, allowing electro-optic modulation at higher frequencies. Ultrafast response times are possible as a result of nonresonant NLO mechanisms, due to the π bonding structures of organic materials. For the non-chemistry oriented, a brief discussion of π electrons follows.

The wide range of useful properties of organic molecules is due, for the most part, to the versatility of the carbon (C) atom, which can form different types of stable covalent bonds to both other C atoms and atoms of other elements. Single bonds between C and another atom are σ bonds; they form the framework of the molecule. Electrons in σ molecular orbitals tend to

stay along the interatomic axis, or along the bar of the dumbbell, if you will. When a C atom forms a double or multiple bond with another atom, only one of those bonds can be a σ bond. The remainder are π bonds, a weaker bond type, and the corresponding electrons are called π electrons. The π molecular orbitals consist of delocalized electronic charge distributions above and below the interatomic axis. Electrons in these orbitals are not associated with a single pair of nuclei, but are mobile and easily polarizable. They can move over large distances with even weak perturbations. The ease of this redistribution is described by the molecular hyperpolarizability, β.

NLO effects originate in the nonlinear response of a material to an applied E-field. Molecules that are noncentrosymmetric (lacking a center of symmetry) can possess a dipole moment. When an E-field is applied, the mobile charges are displaced, modifying the dipole moment. For small fields, the induced polarization of the molecule can be expressed (see Ref. 3, 4)

$$\vec{p} = \mu_0 + \alpha \cdot E + \beta : EE + \gamma \vdots EEE + \ldots \ , \qquad \textbf{(4.6)}$$

where μ_0 represents the ground state dipole moment, α the linear molecular polarizability, β the molecular hyperpolarizability, γ the second-order hyperpolarizability, and E the local field strength. These parameters characterize the isolated molecule.

Organic materials are molecular materials; the intermolecular forces are far weaker than the intramolecular forces. The bulk material NLO response is then dependent on the individual molecular structure rather than the crystal lattice structure. This is what differentiates organic NLO systems from inorganic. Macroscopic second-order nonlinear optical coefficients can therefore be expressed as a function of the individual molecular characteristics. In terms of second harmonic generation, the measuring stick used for the studies in this dissertation, the bulk quantity is the second-order nonlinear susceptibility, $\chi^{(2)}$, and the molecular quantity is the microscopic hyperpolarizability, β, related by [3-5]

$$\chi^{(2)}(-2\omega;\omega,\omega) = N\beta F(\omega)F(\omega)F(2\omega)O(\theta,\varphi) \qquad \textbf{(4.7)}$$

where N corresponds to the number density of molecules, O represents an orientation factor, or projection of β onto the bulk coordinate system, and F is a local field factor. The effect of both N and O quantities are addressed in the evaluation of ESA NLO films in Sections 4.4 and 4.5 in the form of chromophore density and tilt angle. More detailed explanations of the nonlinear optical molecular mechanisms can be found in Refs.6 and 8.

4.1.2 Organic material systems

Due to the advantages discussed above, organic crystals have been considered as a replacement for inorganic crystals. However, organic crystals suffer from the same drawback as their inorganic counterparts - they are difficult and expensive to grow. In addition, the weakness of the intermolecular forces compared to the intramolecular forces in some organic crystals results in low mechanical and optical resistance [9], and optical quality, reproducibility and integrability

requirements are difficult to satisfy [3]. Based on current results, organic crystals will not offer a viable alternative to inorganic technology.

An appealing alternative that offers the advantages of a delocalized π electron system and molecular engineerability combined with relatively inexpensive technology is poled polymers. These consist of a glassy polymer thin film that incorporates an NLO chromophore in a guest-host configuration or as a main-chain or side-chain substituent [10-12]. In the isotropic amorphous state, there is no $\chi^{(2)}$ response because of the random orientation of the chromophores. Orientational order is induced by heating the film above its glass/rubber transition temperature and applying an external electric field. The film is cooled back to room temperature before removing the field to freeze in the resulting dipole alignment. Two main poling techniques are generally utilized, parallel plate electrode poling and corona poling [4]. Although conceptually simple, this poling process is complex in practice.

Poled polymers have not achieved effective commercial development due to the lack of stability of the induced noncentrosymmetric state. A rapid decay of the $\chi^{(2)}$ response is observed immediately after poling, followed by a continued, more gradual decay back to the isotropic state due to both thermally activated rotational motion of the chromophore within the polymer and relaxation of the polymer within the glassy matrix [5, 13-17]. In Eq. 4.7, this relaxation corresponds to a reduction in the orientation factor, $O(\theta,\varphi)$. This decay is increased at elevated temperatures.

Langmuir-Blodgett films, described in Chapter 1, have been investigated for NLO applications [18, 19]. $\chi^{(2)}$ values as high as 500 pm/V have been reported [6], however, lack of molecular order beyond the first few monolayers and poor optical quality [3, 4] make the current state of L-B film technology unsuitable for practical applications.

The ESA technique has the potential to yield $\chi^{(2)}$ thin films with all the advantages inherent in organic NLO materials without requiring additional processing or exhibiting decay of the response. In addition to the advantages discussed in previous chapters, ESA processing of NLO thin films for optical waveguide devices has the following major advantages over traditional methods for the implementation of $\chi^{(2)}$ waveguides.

- Self-assembly into a noncentrosymmetric, $\chi^{(2)}$ structure without the need for additional processing.

- Long-term stability of the $\chi^{(2)}$ response. Because ESA-formed molecular structures are the thermodynamically stable states of the system, the structural ordering of the self-assembled film will not decay over time [20].

- Synthesis at room temperature and pressure - processing requires neither the high temperature and difficult crystallization methods of inorganic crystals, nor the elevated temperature and high electric field processing of poled polymers.

Due to the combination of these materials and processing advantages, ESA offers the potential for major changes in the manufacturing and application of $\chi^{(2)}$ waveguide devices. The

following sections describe the synthesis, characterization and evaluation of novel ESA NLO thin films. Initially, this research was performed using commercially available NLO polymer dyes to demonstrate the feasibility of the concept. The work was then expanded to incorporate organic molecules specifically designed and synthesized for ESA NLO applications. Although the organic synthesis of these molecules is not a part of this work, the structures are included in this chapter since the ESA processing and film characterization are critical elements.

4.2 Commercial dye molecules

Initial nonlinear optical experiments involved demonstration, through second harmonic generation (SHG) measurements with fundamental wavelengths 1064 and 1200 nm, that the ESA technique can produce a noncentrosymmetric arrangement of nonlinear optical chromophores to yield thin-films with $\chi^{(2)}$ values comparable to that of quartz. The first ESA NLO films were synthesized using commercially available polymer dyes, specifically, Poly S-119, Poly R-478, and PCBS, described in Table 4-1, as the polyanion, with poly(allylamine)hydrochloride, which has no $\chi^{(2)}$ response, as the polycation. The samples tested consisted of 68, 70 and 50 bilayers, respectively. The results illustrate that the strong internal electric fields of the ionic layers lead to alignment of polar NLO chromophores and the resulting noncentrosymmetric films possess a substantial $\chi^{(2)}$.

4.2.1 Structural and optical characterization

The films were first characterized structurally and optically to verify optical transmission characteristics, uniform growth and film thicknesses. Figures 4-2, 4-3, and 4-4 show the UV/vis absorbance of Poly S-119, Poly R-478 and PCBS films on glass substrates at several points during the self-assembly process. This measurement is a good indication of the consistent density of the chromophore through the thickness of the film. The linear growth characteristics obtained from both UV/vis spectroscopy and ellipsometry are illustrated in Figures 4-5 and 4-6. These verify that each bilayer is an identical, reproducible building block, contributing an equal amount of material to the film. The uniform distribution of chromophores thus obtained, both across the film surface and through the film thickness, allows precise control of the film properties on a nanometer scale.

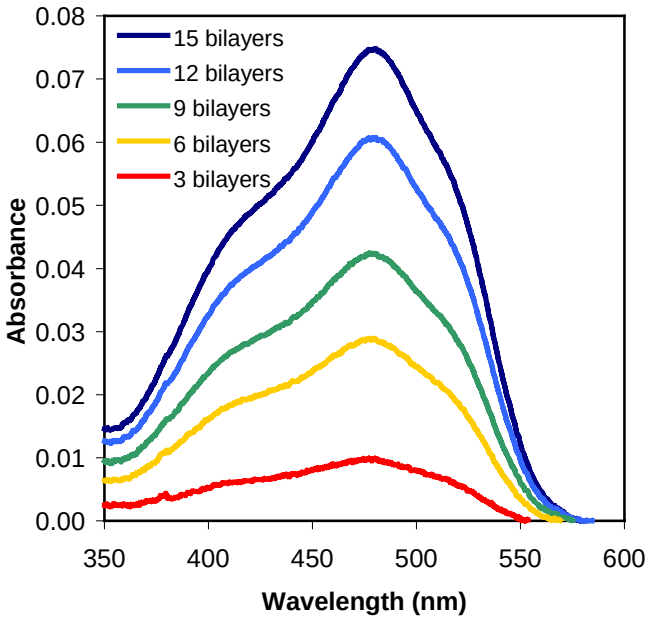

Figure 4-2. UV/vis absorbance spectra of Poly S-119/PAH ESA films with increasing numbers of bilayers.

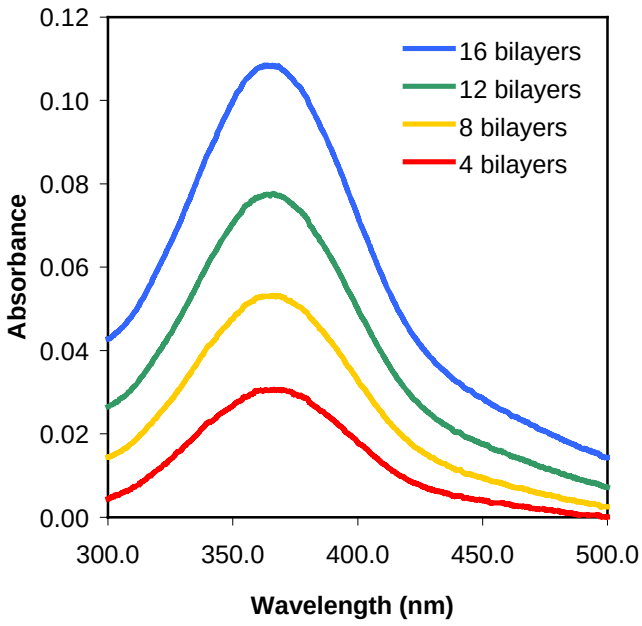

Figure 4-3. UV/vis absorbance spectra of PCBS/PAH ESA films with increasing numbers of bilayers.

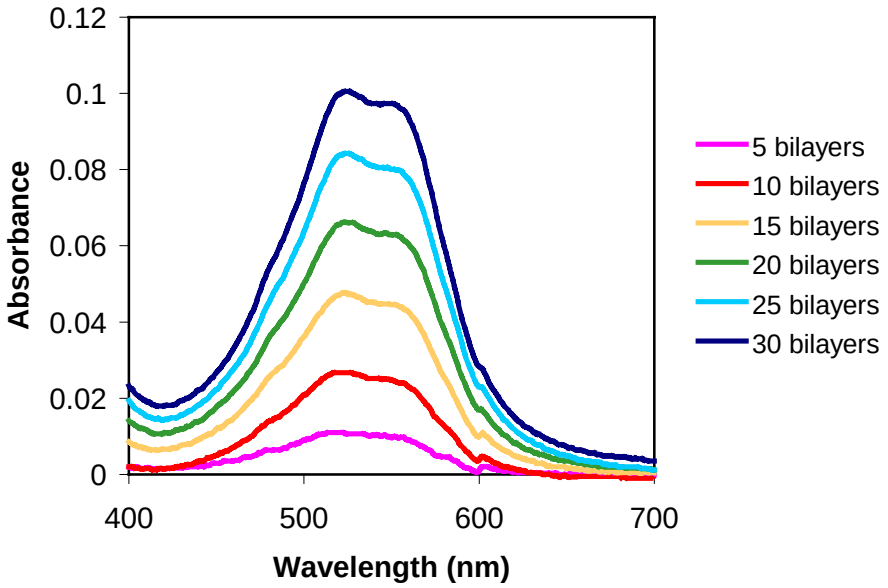

Figure 4-4. UV/vis absorbance spectra of Poly R-478/ PAH ESA films with increasing numbers of bilayers.

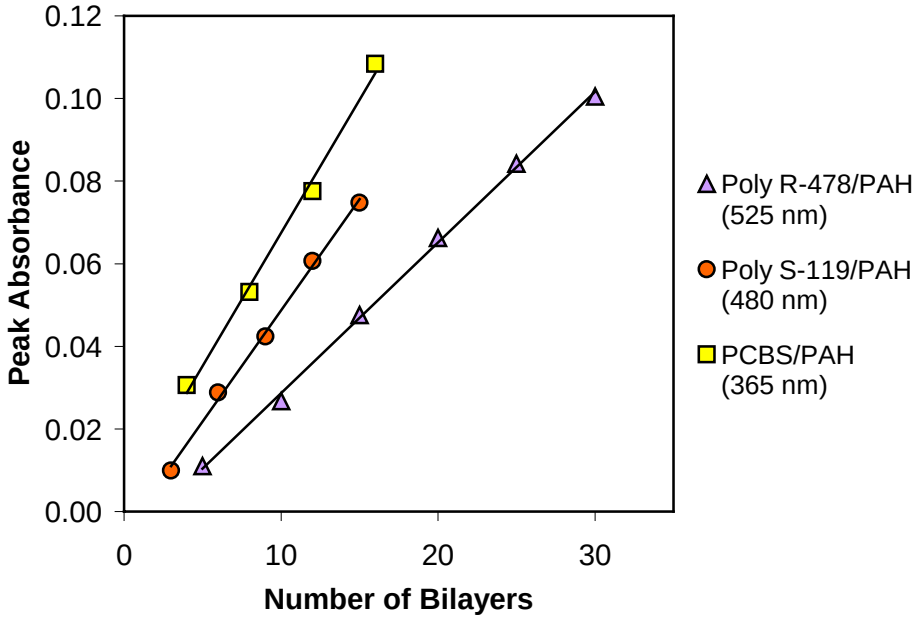

Figure 4-5. UV/vis absorbance increase during ESA NLO polymer film growth.

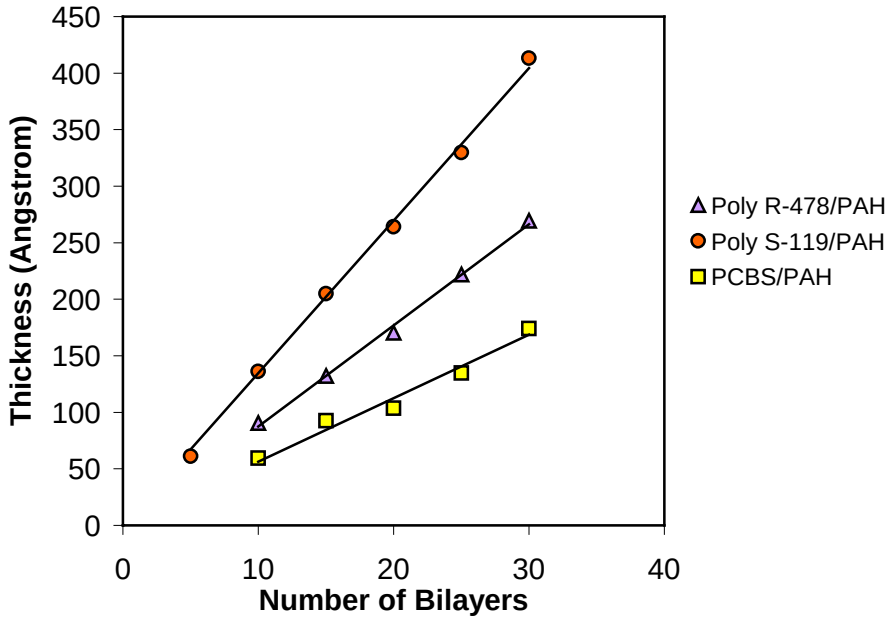

Figure 4-6. Film thickness increase during ESA NLO polymer film growth.

Table 4-1. Commercial NLO dyes used in second harmonic generation experiments.

DYE MOLECULE:	Poly S-119	Poly R-478	PCBS
OBTAINED FROM:	Sigma Chemical	Sigma	Aldrich
STRUCTURE	Poly(vinylamine) backbone Azo chromophore Orange dye	Poly(vinylamine) sulfonate backbone Anthrapyridone chromophore Violet dye	Poly{1-[4-(3-carboxy-4-hydroxyphenylazo)-benzenesulfonamido]-1,2-ethanediyl, sodium salt} Orange-yellow dye
BILAYER THICKNESS	13 Å	9 Å	6 Å
SHG FILM THICKNESS	68 bilayers 88 nm	70 bilayers 63 nm	50 bilayers 39 nm
MEASURED $\chi^{(2)}$	**0.56 pm/V**	**0.53 pm/V**	**0.90 pm/V**

4.2.2 Second harmonic generation (SHG) experimental setup

The SHG experiments were initially performed using the 1064 nm fundamental wavelength of a Q-switched Nd:YAG laser. However, since the films were strongly absorbing at the second harmonic, 532 nm, the remaining experiments used the 1200 nm output from a broadband BBO optical parametric oscillator (OPO), which was pumped by the 355 nm third harmonic of the Nd:YAG, as described previously [21]. A 700 nm high pass filter was used to remove the 504 nm OPO signal beam from the 1200 nm idler. The fundamental beam, weakly focused onto the sample, was measured using a beamsplitter and photodiode. Incident intensity and polarization were controlled by Glan-laser polarizing prisms. A spike filter ensured that the photomultiplier tube (PMT) measured only the intensity of the second harmonic light at 600 nm.

4.2.3 SHG results

Initial experiments used a 68 bilayer Poly S-119/PAH ESA film of thickness approximately 90 nm [21]. The film was rotated 45° away from normal incidence about the vertical axis and the incident light was p-polarized. Figure 4-7 illustrates the dependence of the SHG signal intensity as a function of the incident fundamental intensity. The solid curve in Figure 4-7 is a best fit to the data of the form $I_{2\omega} = A(I_{\omega})^b$, where $I_{2\omega}$ and I_{ω} are the second harmonic and

fundamental intensities, respectively, yielding a value of b = 2.02, in excellent agreement with the expected quadratic dependence on fundamental intensity.

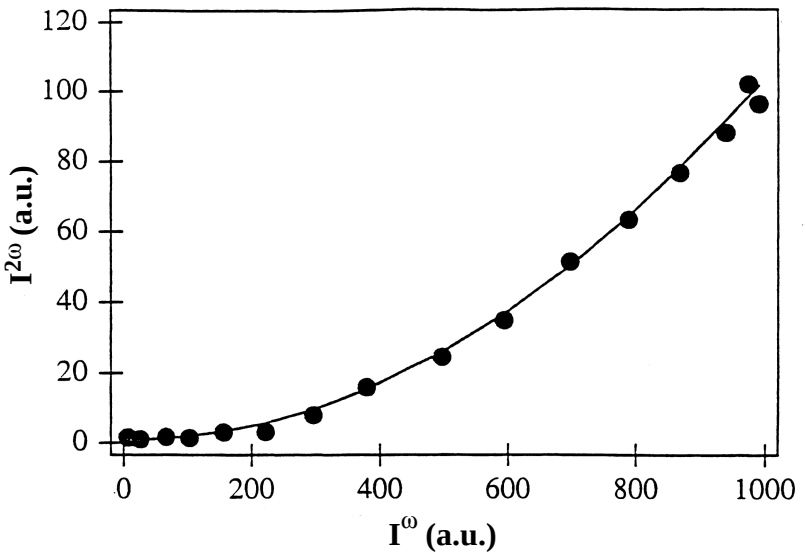

Figure 4-7. Dependence of the 600 nm second harmonic intensity on the 1200 nm fundamental intensity for a 68 bilayer Poly S-119/PAH ESA film.

Through comparison with the Maker fringes generated by a thin quartz wedge, the $\chi^{(2)}$ of the 68 bilayer Poly S-119 film was determined to be 0.70 times as large as the value of quartz. Using the standard quartz value of $\chi^{(2)} = 0.80$ pm/V ($d_{11} = 0.40$ pm/V), the $\chi^{(2)}$ of the Poly S-119/PAH film is thus 0.56 pm/V. The $\chi^{(2)}$ of other ESA thin films could then be quickly determined by comparison to the 68 bilayer Poly S-119 film, as shown for Poly R-478 in Figure 4-8. Since the thickness of the ESA films tested is much less than the second harmonic coherence length (10-20μm), the observed second harmonic intensity should increase quadratically with the thickness of a given material. In this limit, the $\chi^{(2)}$ value is determined by

$$\chi^{(2)} = \chi^{(2)}_{ref} \sqrt{\frac{A}{A_{ref}}} \frac{l_{ref}}{l} \qquad \textbf{(4.8)}$$

where A is the coefficient of the fit to the second harmonic intensity as a function of fundamental intensity and *l* is the path length through the sample, or film thickness. The SHG experiments were repeated for PCBS and the results are shown in Table 4-1.

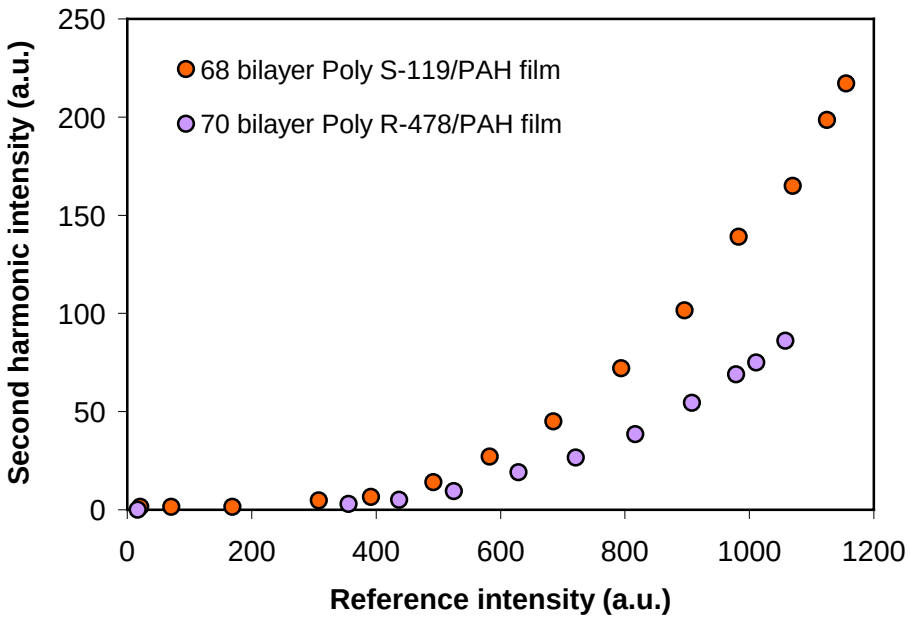

Figure 4-8. Comparison of second harmonic intensities observed for a 70 bilayer Poly R-478/PAH ESA thin film and the reference 68 bilayer Poly S-119/PAH ESA thin film.

4.3 Newly synthesized NLO polymer dyes (Polydyes)

The previous section discussed ESA NLO films that were fabricated using commercial ionic polymer dyes, Poly S-119, Poly R-478 and PCBS. While these materials possess the appropriate functionality for the ESA deposition process, they do not include chromophores with substantial β NLO molecular susceptibility. The polar ordering of molecules that occurs due to the inherent nature of the ESA process suggests that a number of similar NLO thin-films may be synthesized, using both other standard chromophore dyes, and molecules specifically designed to yield an enhanced macroscale net dipole moment. Consequently, several new NLO polymers, including poly(methacrylic acids), polyphenylene oxides and polyesters, have been designed and synthesized, and noncentrosymmetric thin films fabricated using the ESA process. While this investigation does not include the organic synthesis of these molecules, their processing, self-assembly, and characterization are an important segment. This section presents results that demonstrate the second-order nonlinear optical behavior of ESA films assembled from these Polydye materials.

4.3.1 Structural and optical characterization

A total of nine new Polydye molecules, shown in Figure 4-9, have been synthesized and self-assembled since the inception of this project. Representative chemical structures of these polymers are shown in Figure 4-10. Processing difficulties prevented complete evaluation of several of these dyes; the remaining results are discussed below. UV/vis spectra of the first seven Polydye aqueous solutions are shown in Figures 4-11 and 4-12.

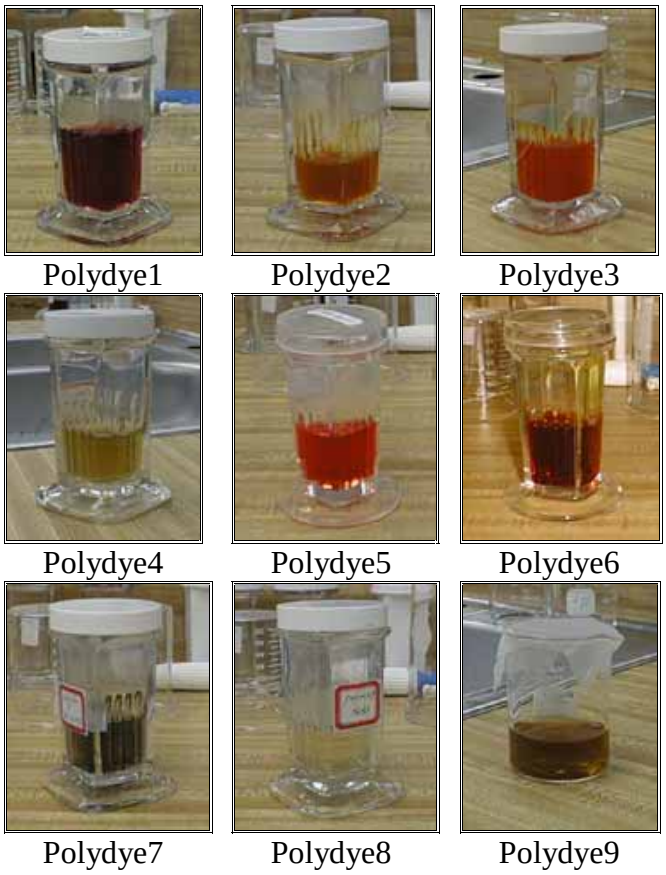

Figure 4-9. Polydye solutions synthesized for ESA of second order NLO thin films.

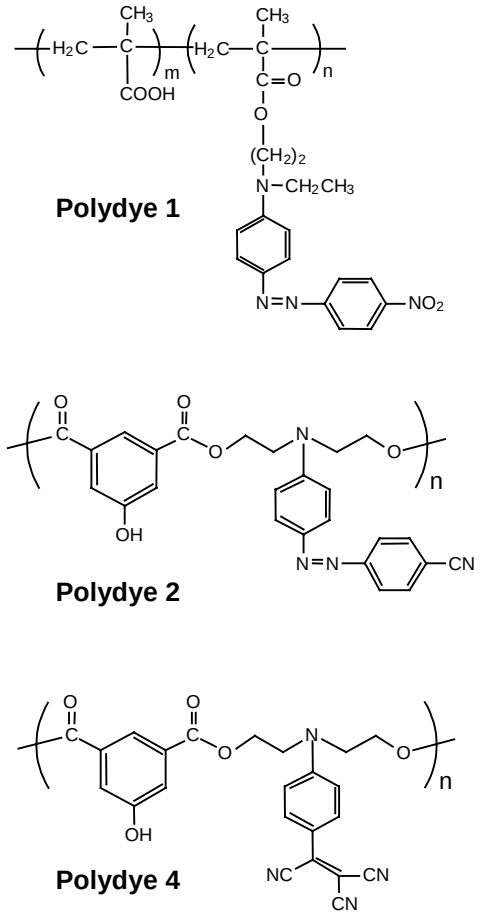

Figure 4-10. Chemical structure of Polydye1, Polydye2, and Polydye4.

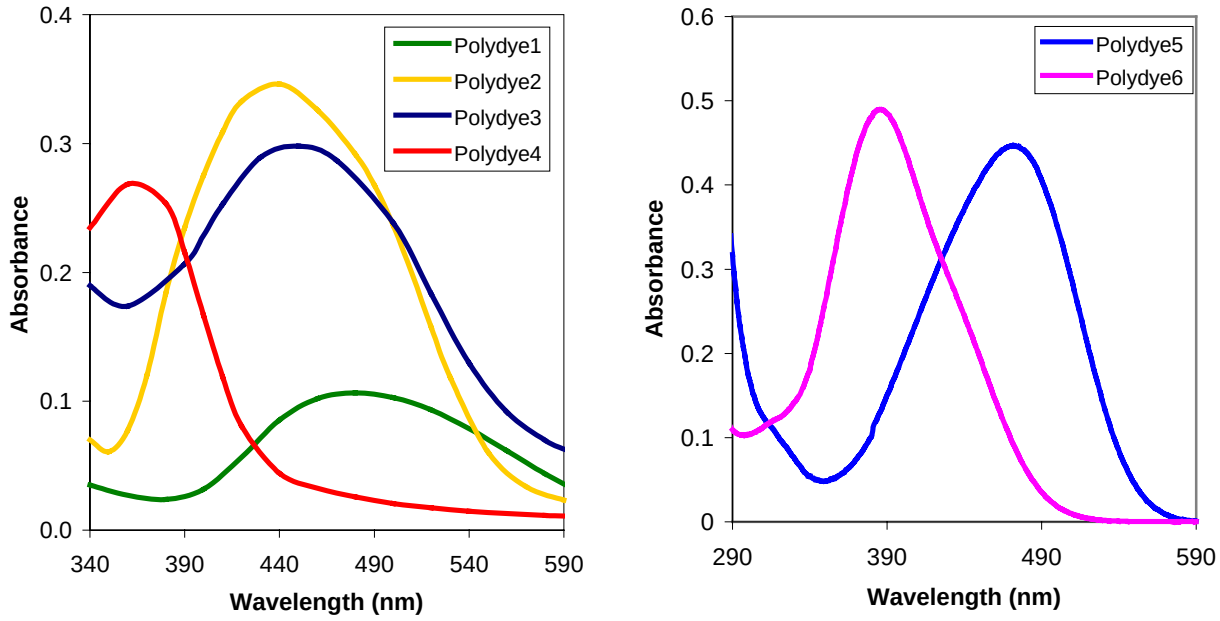

(a) **(b)**

Figure 4-11. UV-vis absorbance spectra of (a) Polydye1 - Polydye4 and (b) Polydye5 and Polydye6 aqueous solutions.

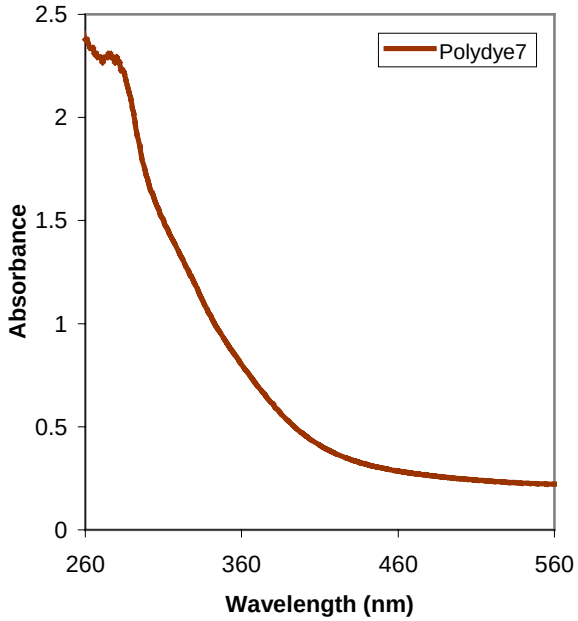

Figure 4-12. UV-vis absorbance spectrum of Polydye7 aqueous solution.

Multilayer Polydye thin-films were self-assembled on glass substrates with polydiallyldimethyl-ammonium chloride (PDDA) as the passive polycation layer. Uniform Polydye films with up to 88 bilayers were fabricated.

As discussed in Chapter 2, appropriate deposition conditions must be established for each new polymer in order to obtain the necessary surface charge reversal with the assembly of each monolayer. Required solution concentration, pH and dipping time are determined for uniform, homogeneous film growth. Establishing the requisite conditions for self-assembly of these Polydye molecules was a substantial part of this investigation. The parameters determined for the films used in this study are listed in Table 4-2. PDDA solutions were used at a concentration of 10.4 mg/ml; PSS solutions at a concentration of 2 mg/ml. Solution pH values were matched to the appropriate Polydye solution. Acceptable conditions were not able to be determined for Polydye5 and Polydye6.

Table 4-2. Polydye concentrations and dipping conditions.

POLYCATION	POLYANION	POLYDYE CONCENTRATION (MOL / L)	DIPPING PH	DIPPING TIME (MIN)
PDDA	Polydye1	1×10^{-2}	8	3
PDDA	Polydye2	1×10^{-2}	9.5	3
PDDA	Polydye3	1×10^{-2}	8	3
PDDA	Polydye4	1×10^{-2}	10	5
Polydye5	PSS	-	-	-
PDDA	Polydye6	-	-	-
PDDA	Polydye7	7×10^{-3}	8	3
PDDA	Polydye8	5×10^{-3}	8	5
PDDA	Polydye9	1×10^{-3}	8	1

Correct film buildup is most easily verified by a linear increase in optical absorbance in combination with visual inspection. For optical applications, self-assembly in itself, i.e. an increase in film thickness, is not sufficient. Uniform self-assembly is required both through the film thickness and across the film surface. Films that appear "cloudy," or nontransparent, to the eye will exhibit scattering, which is indicated quantitatively by a nonlinear decrease in optical transmission. For example, the absorbance spectra from an initial attempt to assemble Polydye9 is shown in Figure 4-13. An acceptable pH to allow ionic self-assembly was established, verified by the increase in optical absorbance on the left. However, visual inspection revealed a cloudy, opaque film and the absorbance peak appeared to increase nonlinearly as illustrated on the right in Figure 4-13. This scattering was due to agglomerates formed in the aqueous solution as a result of the high concentration. Reducing the concentration to 10% of the original (1×10^{-3}

M) alleviated this problem. In like manner, dipping parameters for each molecule were individually established to produce uniform Polydye ESA films assembled on glass and silicon substrates.

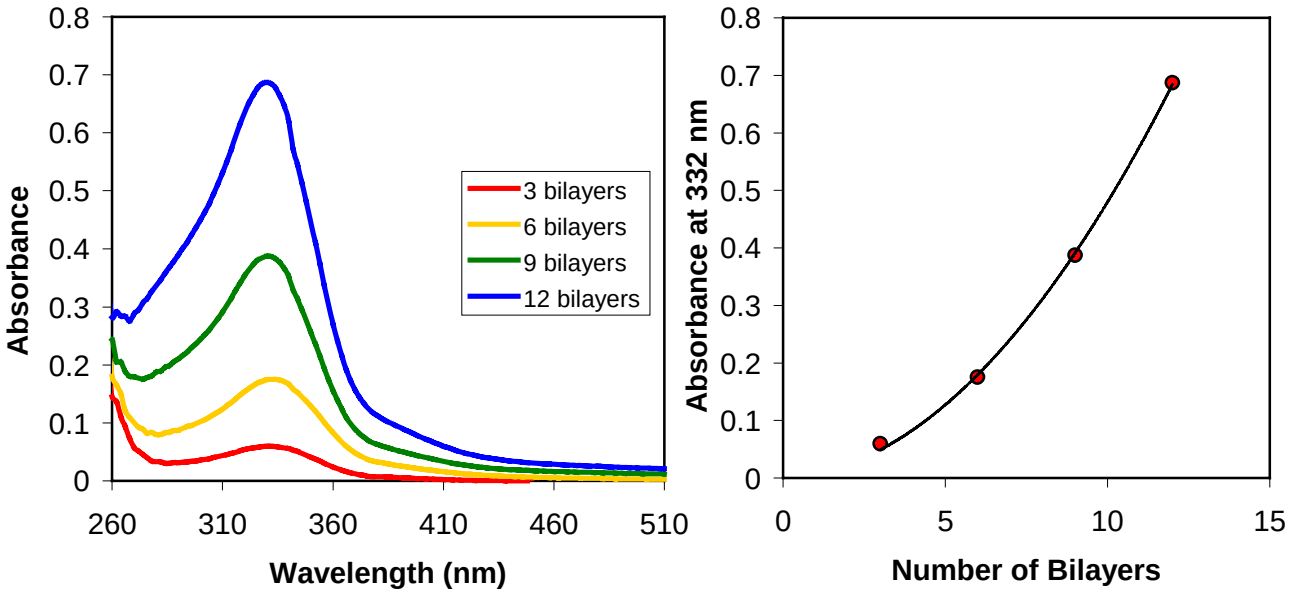

Figure 4-13. Optical absorbance spectra of inhomogeneous/agglomerated Polydye9 ESA films of increasing numbers of bilayers.

Polydye1 consistently exhibited self-assembly difficulties in the first few bilayers. However, once full substrate coverage was established, after approximately 12 bilayers, linear deposition ensued. This is discussed in more detail in Section 4.3.3.

UV/vis spectroscopy was used to identify the absorption and transmission characteristics of the Polydye thin films as well as to quantify the growth of the multilayer structures. As can be seen from the optical absorbance spectra measured during the growth of the nine PDDA/Polydye films (Figs. 4-14 to 4-22), linear growth was established for all but Polydye5 and Polydye6. This is more clearly illustrated in Figure 4-23, demonstrating that each bilayer contributes an equal amount of material to the thin-film growth. In addition, the maximum differences between data collected at different locations across each film is at most a few percent, indicating excellent uniformity of the films (Fig. 4-24). The ESA method therefore produces novel Polydye thin films that are homogeneous through the film thickness as well as across the width and length of the film.

For the Polydyes measured, the film thickness increased linearly with the addition of each bilayer, as shown in Figure 4-25. The special case of Polydye1 again is discussed below. This thickness measurement was required for $\chi^{(2)}$ calculations, as explained in Section 4.2. As discussed in Chapter 2, adjusting the dipping parameters, e.g. polyelectrolyteconcentration, pH, salt concentration, may control the slope of each line, or the average bilayer thickness.

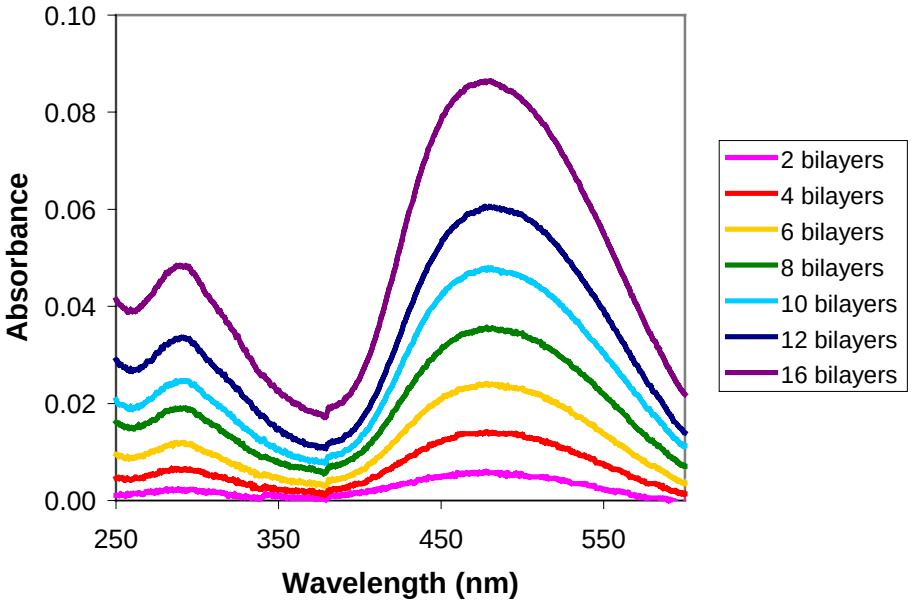

Figure 4-14. Optical absorbance spectra of Polydye1 ESA films of increasing numbers of bilayers.

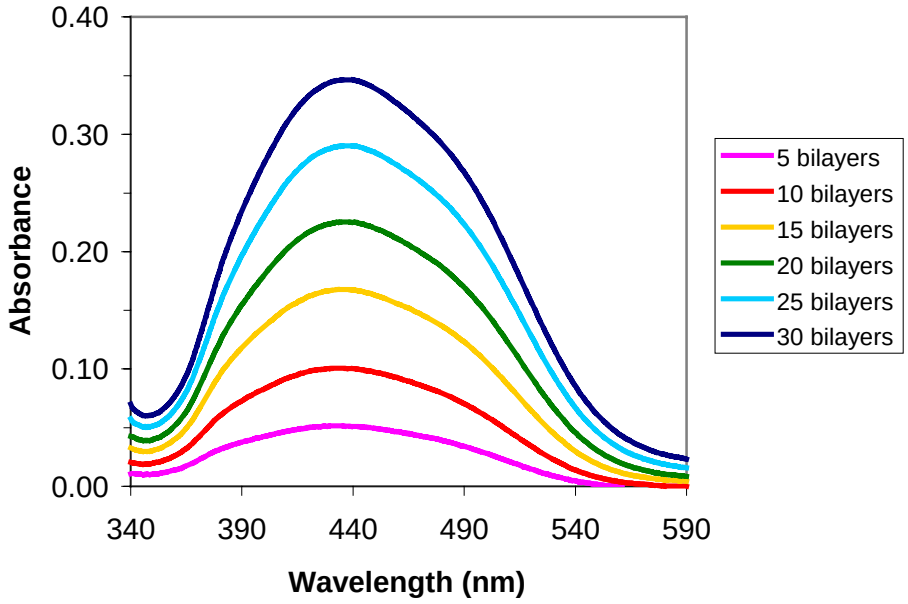

Figure 4-15. Optical absorbance spectra of Polydye2 ESA films of increasing numbers of bilayers.

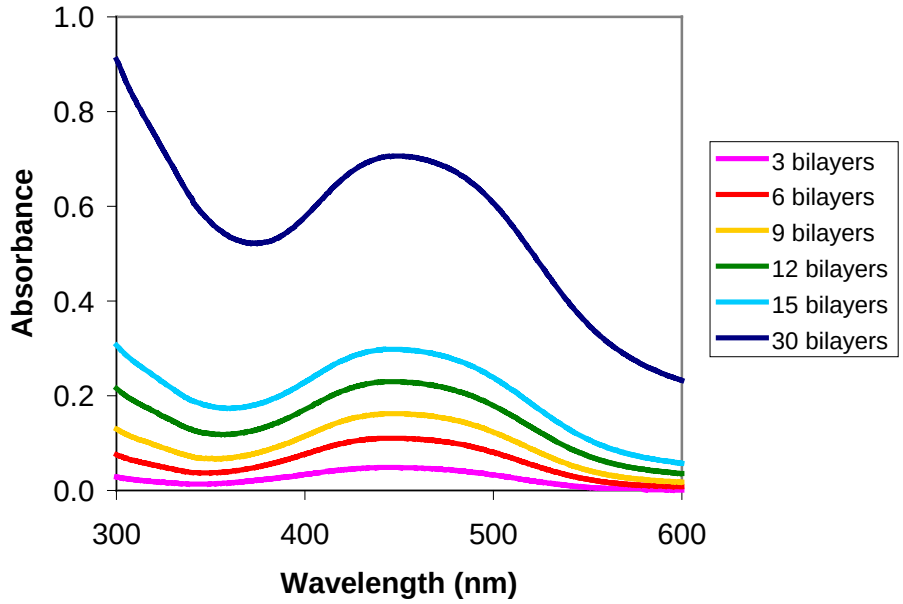

Figure 4-16. Optical absorbance spectra of Polydye3 ESA films of increasing numbers of bilayers.

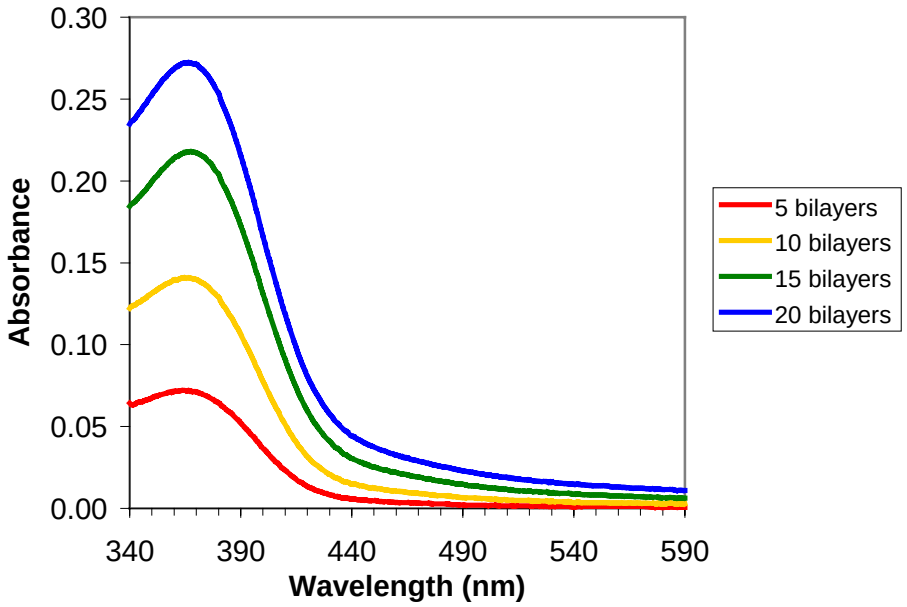

Figure 4-17. Optical absorbance spectra of Polydye4 ESA films of increasing numbers of bilayers.

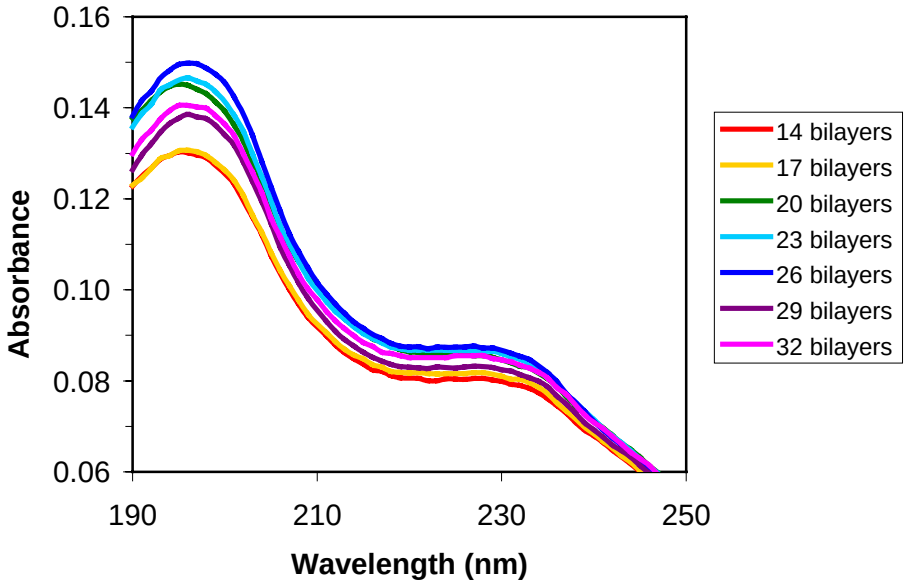

Figure 4-18. Optical absorbance spectra of Polydye5 ESA films of increasing numbers of bilayers on a quartz substrate.

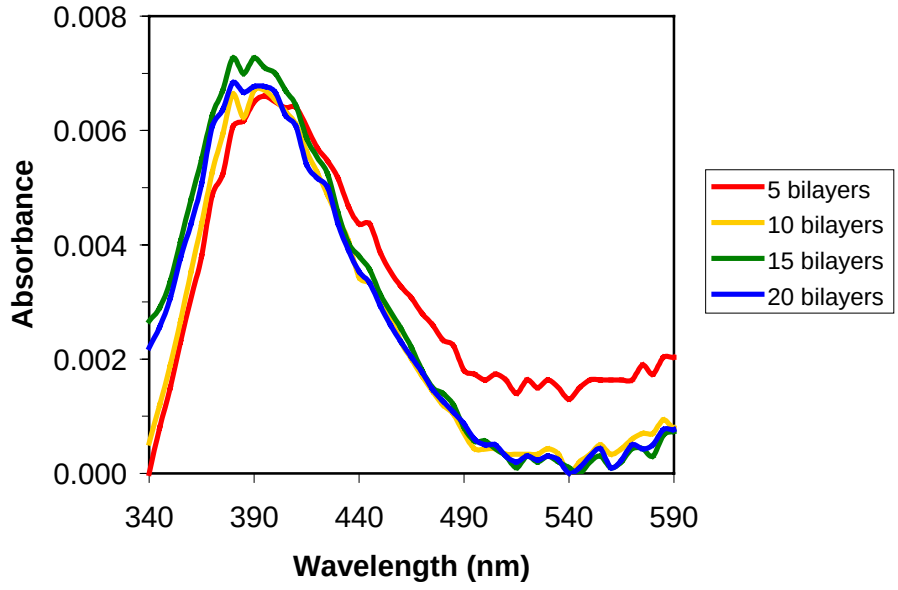

Figure 4-19. Optical absorbance spectra of Polydye6 ESA films of increasing numbers of bilayers.

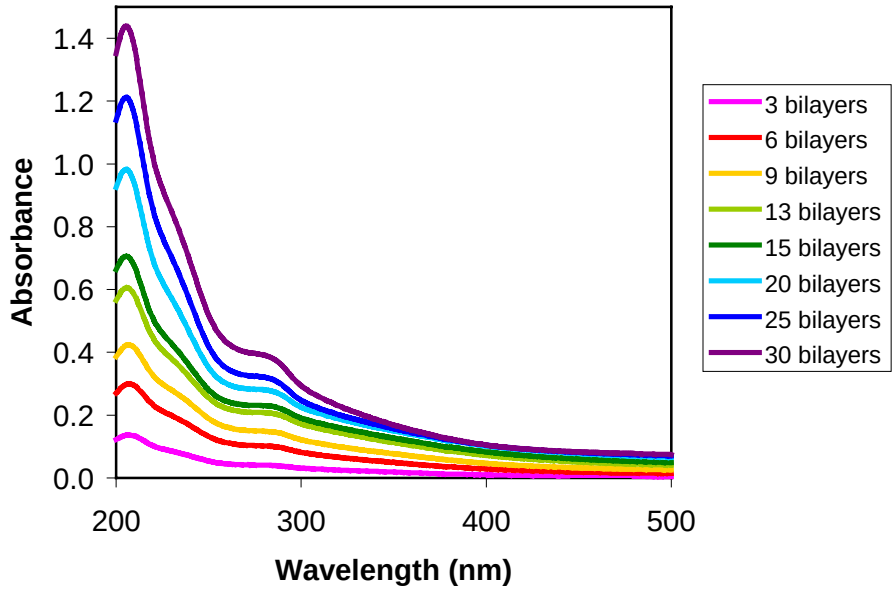

Figure 4-20. Optical absorbance spectra of Polydye7 ESA films of increasing numbers of bilayers on a quartz substrate.

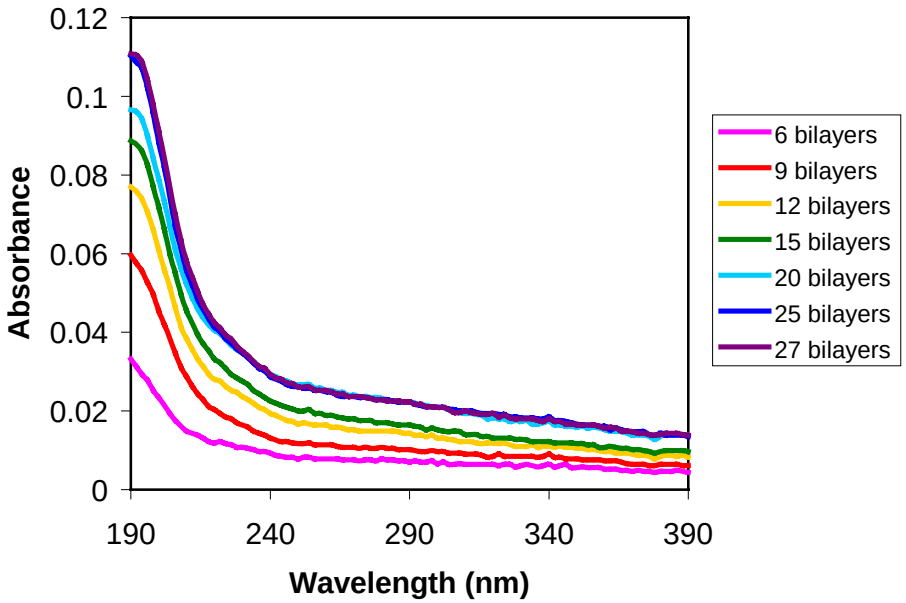

Figure 4-21. Optical absorbance spectra of Polydye8 ESA films of increasing numbers of bilayers on a quartz substrate.

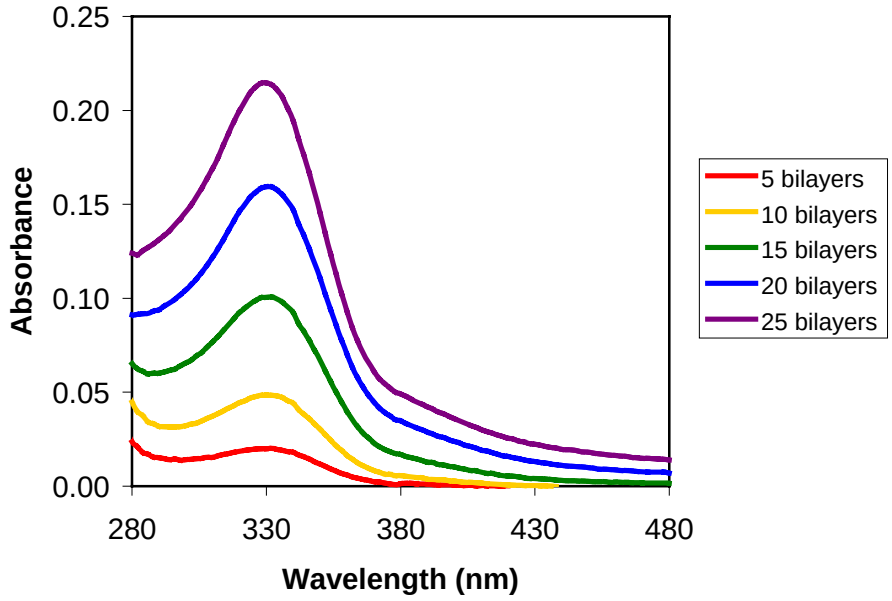

Figure 4-22. Optical absorbance spectra of Polydye9 ESA films of increasing numbers of bilayers on a quartz substrate.

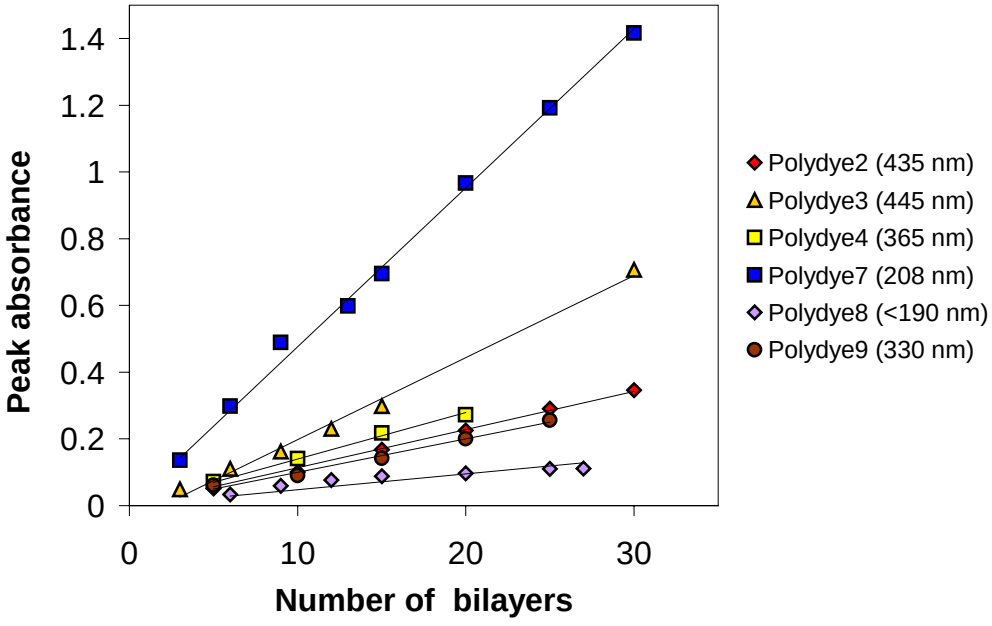

Figure 4-23. Peak UV/vis absorbance increase during Polydye film growth.

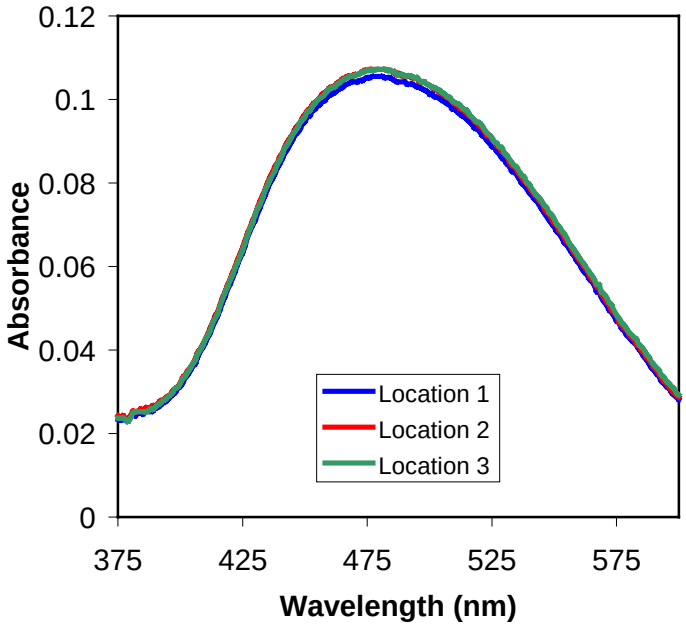

Figure 4-24. UV/vis absorbance at three separate locations on Polydye1 ESA film.

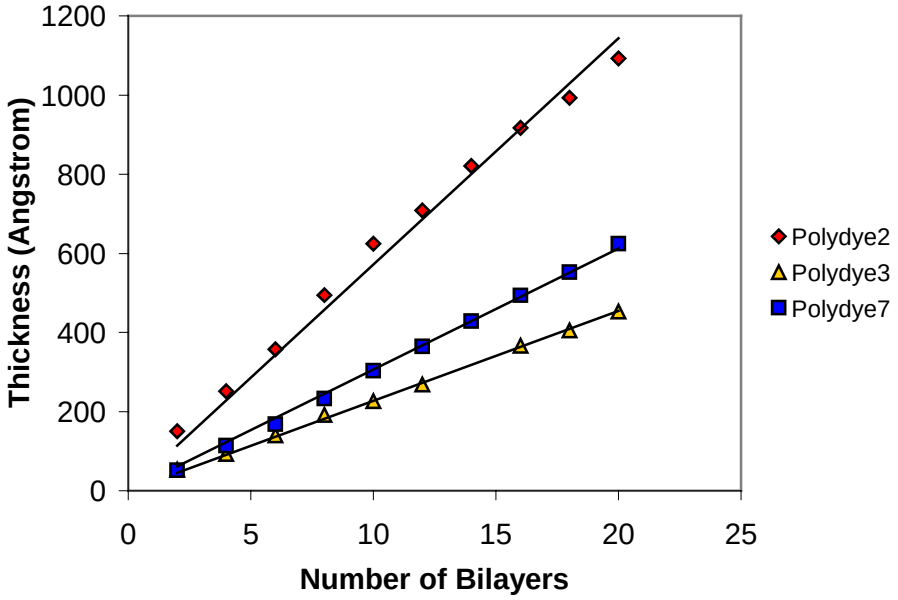

Figure 4-25. Film thickness increase during Polydye2, Polydye3 and Polydye7 film growth.

The optical and structural characterization data for all nine Polydyes is summarized in Table 4-3. It is interesting to note that higher optical density/greater absorbance does not correspond to greater thickness. The increased optical density is not necessarily due to a thicker layer of dye molecules, but in some cases, a denser layer of molecules.

Table 4-3. Polydye characteristic comparison.

Polymer Dye	Peak Absorbance	Average Optical Density at Peak Wavelength (per bilayer)	Average Bilayer Thickness
Polydye1	480 nm	0.006 **	39 Å **
Polydye2	435 nm	0.011	57 Å
Polydye3	445 nm	0.022	23 Å
Polydye4	365 nm	0.014	
Polydye5	195 nm	-	-
Polydye6	390 nm	-	-
Polydye7	208 nm	0.048	31 Å
Polydye8	<190 nm	0.003	
Polydye9	330 nm	0.010	

** after initial 12 bilayers

4.3.2 Polydye1 characterization

Although only 15 bilayers were assembled, the initial Polydye1 sample was extremely inhomogeneous, resulting in substantial scattering loss. Testing continued due to the high $\chi^{(2)}$ value measured for one portion of the film (See Section 4.3.3) and modification of the dipping parameters produced Polydye1 films that exhibit the homogeneity typical of ESA films. Although the resulting $\chi^{(2)}$, 1.7 pm/V, was only 47% of the initial promising Polydye1 value, it was still greater than that obtained using commercial polymers. This can be explained by examining the absorption spectra of the two films, which have the same number of bilayers. The peak absorbance of the first, inhomogeneous film was 0.14 while the peak absorbance of the homogeneous film was 0.03, indicating a reduction in chromophore density by a factor of 4.5.

Even with the new dipping parameters, Polydye1 still consistently exhibited self-assembly difficulties in the first few bilayers. However, once full substrate coverage was established, after approximately 10 bilayers, linear deposition ensued. In other words, the initial bilayer thicknesses were reduced compared to those in the remainder of the film. This initially became evident in the ellipsometry measurements and was confirmed using UV/vis spectroscopy and atomic force microscopy. The ellipsometry data for a Polydye1 sample assembled on a single

crystal silicon substrate is shown in Figure 4-26. Only after the first 20-25 nm of film growth does the thickness consistently increase. Similar absorption results are shown in Figure 4-27. Note the change in substrate coverage in the AFMs shown in Figures 4-28, 4-29 and 4-30. After two bilayers of PDDA/Polydye1 are assembled, substrate irregularities are evident; they are somewhat covered after ten bilayers and completely concealed after 18 bilayers, where equilibrium layer thicknesses have been established.

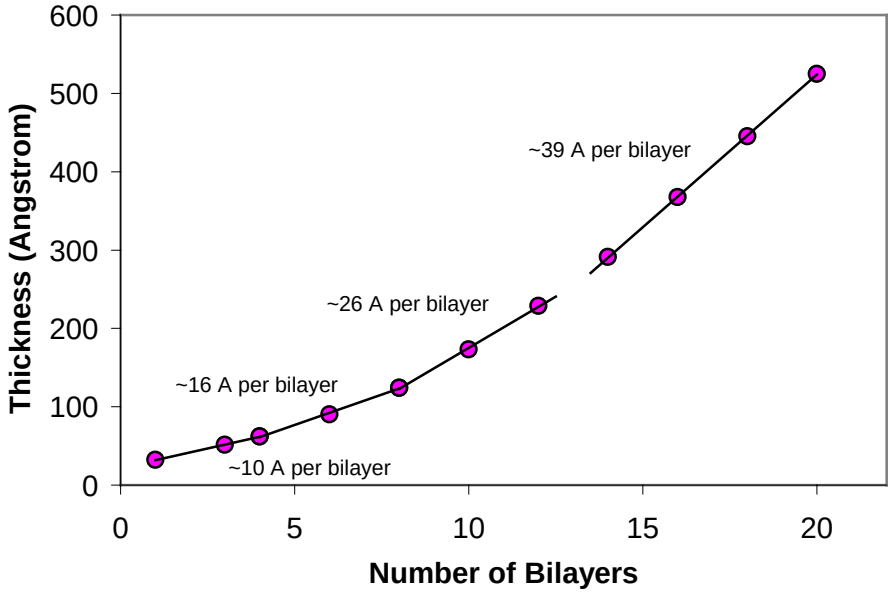

Figure 4-26. Film thickness increase during Polydye1 film growth.

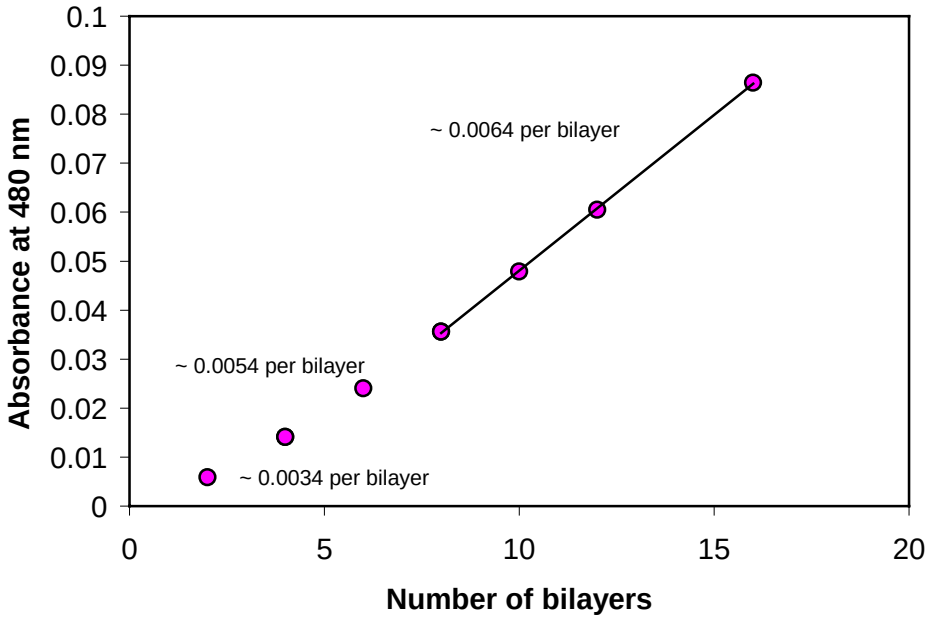

Figure 4-27. Peak UV-vis absorbance increase during Polydye1 film growth.

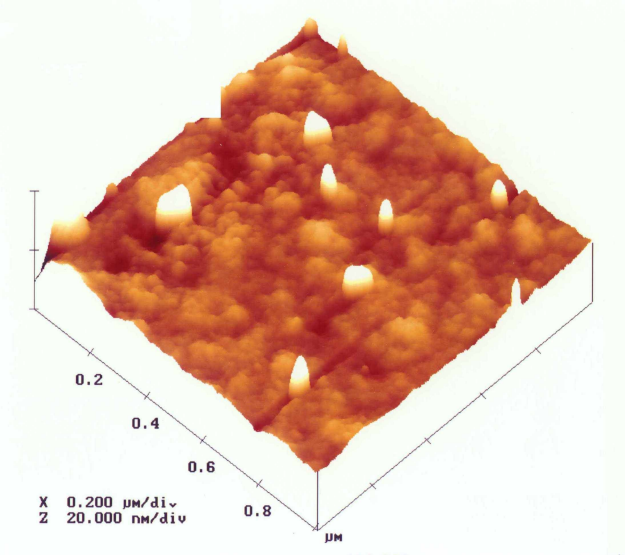

Figure 4-28. AFM image of 2 bilayer Polydye1/PDDA film

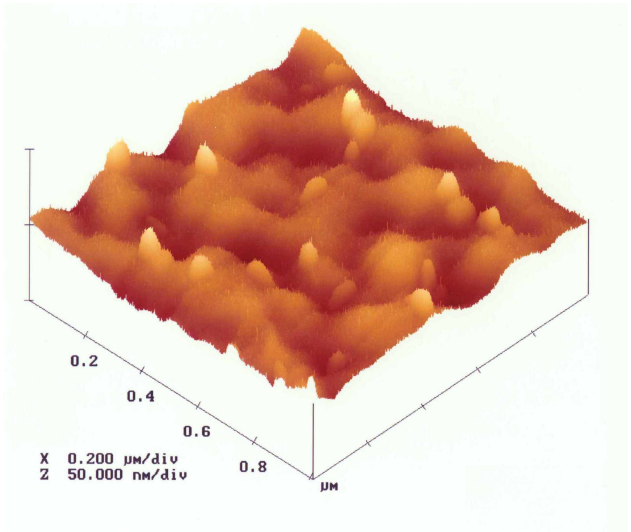

Figure 4-29. AFM image of 10 bilayer Polydye1/PDDA film

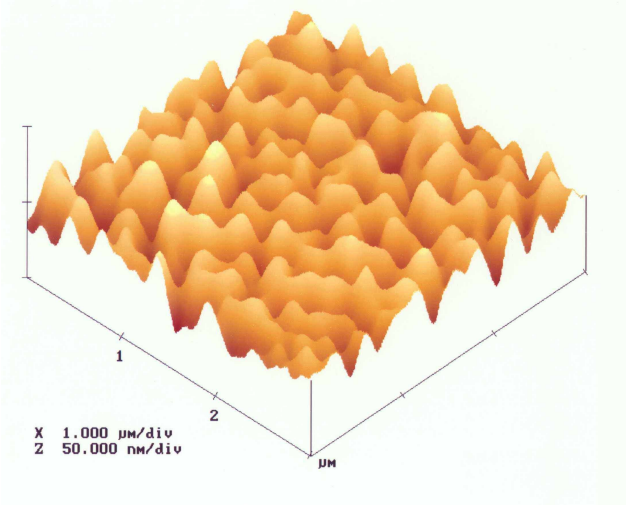

Figure 4-30. AFM image of 18 bilayer Polydye1/PDDA film

Similar results have been observed by other groups, where the layers deposited close to the substrate have smaller thicknesses and equilibrium layer thickness is reached several layers away from the surface. In an investigation of PSS/PAH films, Decher et al. found the initial layer thickness to be less than half that of the equilibrium thickness [22,23]. This can be explained as follows. The film functionality is determined by the surface charge density. The thickness of the first few layers will be then affected by the charged substrate surface, whose charge density can be assumed to be larger than that of the polymer film surface after a number of layers have been deposited [after Ref. 24]. This effect was found to be influenced by the solution concentration, becoming more evident at higher concentrations [25]. In summary, the substrate surface does influence film growth for the first few layers deposited, but the effect is

eliminated as film continues to grow. One possible solution to this difficulty may be drastically increased dipping times in the first ten bilayers.

4.3.3 Second harmonic generation (SHG) results

Second harmonic generation experiments were carried out using a 1200 nm fundamental wavelength in the same setup described earlier for commercial NLO polymers [21]. The second harmonic intensities generated by three different Polydye films are compared to that of the 68 bilayer Poly S-119 film in Figures 4-31, 4-32 and 4-33, which illustrate the quadratic dependence of the 600 nm second harmonic intensity on the 1200 nm fundamental input intensity. The $\chi^{(2)}$ of the Polydye films was determined by the same method described above, fitting the second harmonic generation data to $I_{2\omega} = A\ (I_{\omega})^2$, where $I_{2\omega}$ and I_{ω} are the second harmonic and fundamental intensities, respectively.

The Polydye1 film denoted "A" was the initial inhomogeneous 15 bilayer film discussed above. The Polydye1 (B) film, although homogeneous, possessed a much lower chromophore density, as evidenced by its lower $\chi^{(2)}$ value. Both Polydye1 films and the Polydye2 film, although thinner than the Poly S-119 film, exhibited higher second harmonic intensities. The $\chi^{(2)}$ of the Polydye1 (A) film was found to be 3.6 pm/V, an increase of more than a factor of six over that of the ESA films of commercially available NLO polymers. The $\chi^{(2)}$ values for other Polydyes were similarly determined and are shown in Table 4-4.

Table 4-4. Second order nonlinear comparison of Polydyes.

SAMPLE	NUMBER OF BILAYERS	FILM THICKNESS	$\chi^{(2)}$ (pm/V)	INCREASE OVER COMMERCIAL POLYMER ESA FILMS	
				Poly S-119	**PCBS**
Poly S-119	68	197 nm	**0.56**	-	
PCBS	50	65 nm	**0.9**	-	
Polydye1 (A)	15	43 nm*	**3.6**	640%	400%
Polydye1 (B)	15	35 nm	**1.7**	300%	90%
Polydye2	52	296 nm	**0.34**	(-40%)	(-60%)
Polydye3	30	69 nm	**0.48**	(-15%)	(-50%)
Polydye4	50	145 nm*	**<0.1**	(-80%)	(-90%)
Polydye7	30	93 nm	**<0.2**	(-65%)	(-80%)

*assumed value

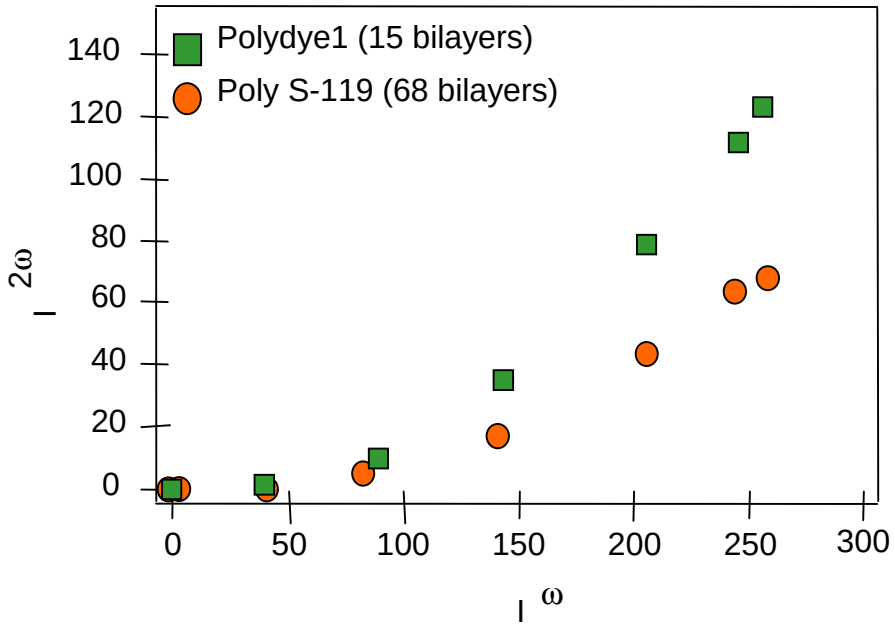

Figure 4-31. Comparison of second harmonic intensities observed for 15 bilayer Polydye1 (A) ESA thin film and a 68 bilayer Poly S-119 ESA thin film.

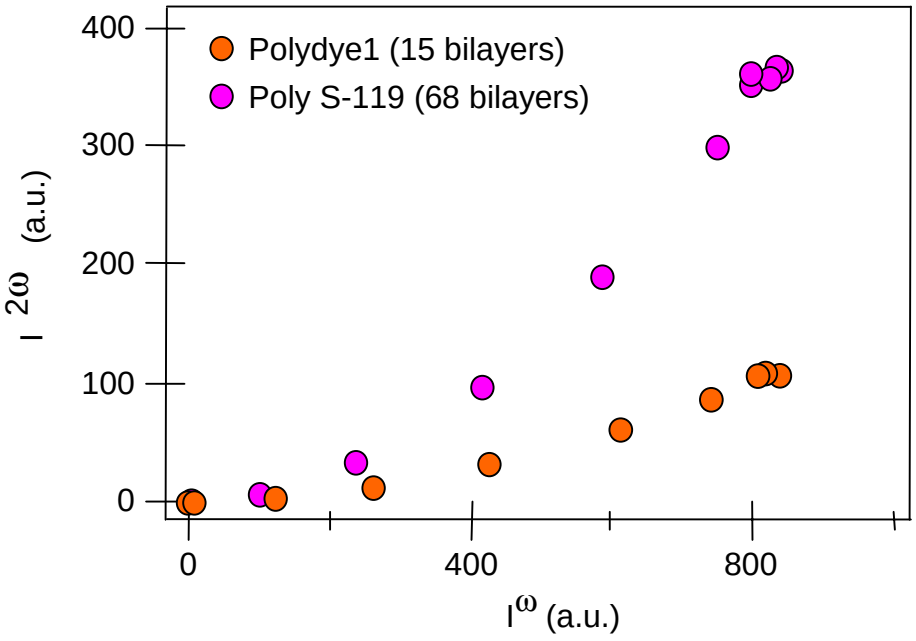

Figure 4-32. Comparison of second harmonic intensities observed for 15 bilayer Polydye1 (B) and 68 bilayer Poly S-119 ESA thin films.

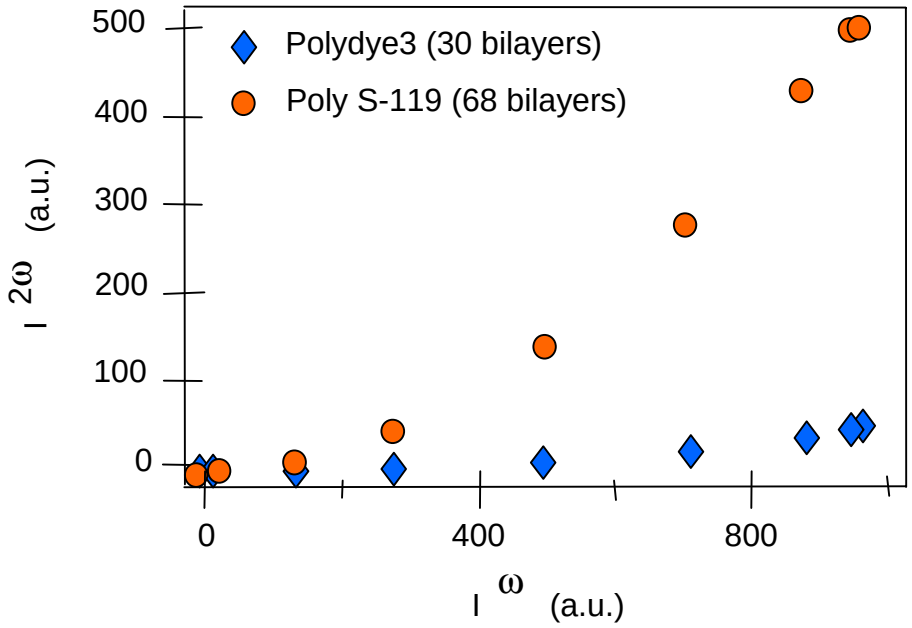

Figure 4-33. Comparison of second harmonic intensities observed for a 30 bilayer Polydye3 ESA thin film and a 68 bilayer Poly S-119 ESA thin film.

As mentioned in the previous section, the chromophore density in the second set of Polydye1 samples was decreased by a factor of 4.5, while the $\chi^{(2)}$ value was only decreased by half. The homogeneous film therefore made more efficient use of the chromophore when the reduced chromophore density is accounted for. The deposition process may possibly be modified to increase the chromophore density and dipole alignment while maintaining homogeneity. Concentration, dipping time, and solution pH should be considered first.

It is interesting to note at this point that polarization tests using the same Polydye and commercial polymer film samples described here have revealed that Polydye1 films exhibit the lowest chromophore tilt angle [26]. Due to the alternating cationic/anionic nature of the ESA process, the preferential polar axis in ESA films is expected to be normal to the substrate and film surface. In general, however, the NLO chromophores will not be aligned strictly perpendicular to the substrate; they will instead be distributed over a set of orientations that make an angle with respect to that normal. Comparison of the SHG intensity observed with s-polarized fundamental
to that observed with p-polarized fundamental provides the relative magnitudes of the $\chi^{(2)}_{zxx}$ and $\chi^{(2)}_{zzz}$ tensor components. This information, in turn, yields the average tilt angle ψ of the chromophores with respect to the film normal (ψ=0º corresponds to normal to the substrate) by the following relationship.

$$\frac{\chi^{(2)}_{zzz}}{\chi^{(2)}_{zxx}} = 2\cot^2\psi \qquad \textbf{(4.9)}$$

The dependence of the second harmonic intensity on the incident fundamental polarization is shown for the 68 bilayer Poly S-119 $\chi^{(2)}$ reference film and a 15 bilayer Polydye1 film in Figures 4-34 and 4-35, respectively. A polarizer angle of 0º corresponds to p-polarization while 90º corresponds to s-polarization. The results are summarized in Table 4-5, which lists the ratio of the second harmonic intensities for the two polarizations, the ratio of the $\chi^{(2)}$ tensor components, and the resulting average tilt angle for each sample.

Table 4-5. Ratios of the second harmonic intensities for p and s-polarizations, the $\chi^{(2)}$ tensor components, and the average tilt angle for four samples.

SAMPLE	NUMBER OF BILAYERS	$\frac{I_{2\omega}^{p\to p}}{I_{2\omega}^{s\to p}}$	$\frac{\chi_{zzz}^{(2)}}{\chi_{zxx}^{(2)}}$	ψ
Poly S-119	68	12.5	4.1	35º
Poly S-119	367	24.5	6.9	28º
PCBS	100	8.6	2.9	40º
Polydye 1	15	29.6	7.9	26º

The tilt angles measured ranged from 26 to 40º, indicating that there is a substantial variation of chromophore orientation away from the polar axis. The goal is to minimize the tilt angle as much as possible in order to maximize the $\chi_{zzz}^{(2)}$ tensor component. As stated above, the newly synthesized Polydye1 polymer had the smallest of the measured tilt angles. This indicates that the degree of ordering obtained in this polymer was better than that of the commercial polymers. As a useful reference point, the $\chi^{(2)}$ tensor ratio obtained in poled polymers is determined by the thermodynamics of the poling process to yield a value of 3.0, corresponding to a tilt angle of 39º.

Although one major advantage of the ESA process is that the noncentrosymmetric structures are formed without the additional poling step required by poled polymers, the effect of poling on ESA film behavior was briefly investigated. When a poling process was applied to these same Polydye ESA films, $\chi^{(2)}$ values as large as 85 pm/V, larger than even that of lithium niobate, were measured. This investigation concerned ESA films without additional processing, but considering the costly and complicated processes required to produce $LiNbO_3$ crystals, this concept warrants further study. Issues to consider include whether these poled ESA structures exhibit the same sort of decay as poled polymers or if they are more stable structures. These preliminary results also suggest that electric field assisted (EFA) ESA would produce favorable results for second order NLO applications.

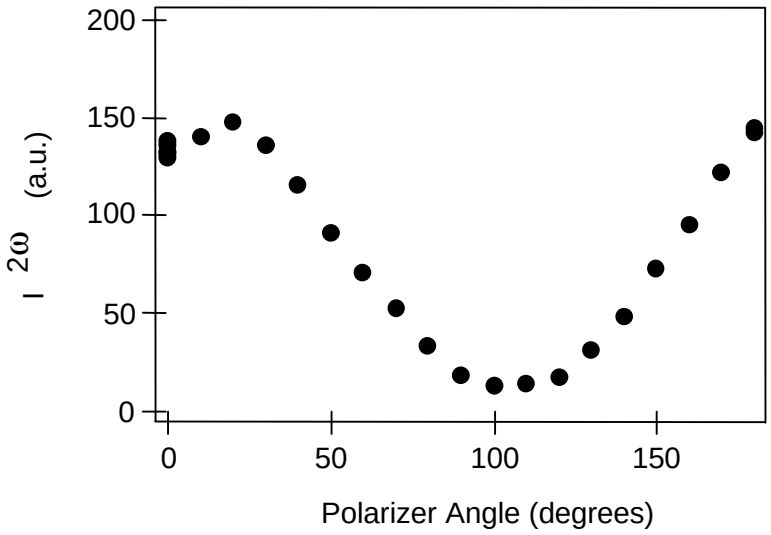

Figure 4-34. Dependence of SHG on fundamental polarization for 68 bilayer Poly S-119 reference ESA $\chi^{(2)}$ film.

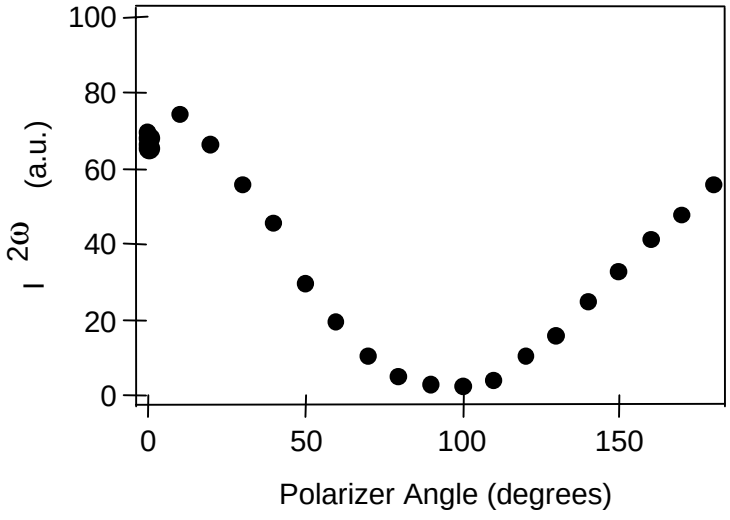

Figure 4-35. Dependence of SHG on fundamental polarization for 15 bilayer Polydye1 ESA film.

4.4 Thermal stability of ESA NLO thin films

Thermal stability is a necessary attribute for all but a limited number of second order nonlinear optical materials and devices. Poled polymers, for example, exhibit accelerated response decay as the temperature is raised [5, 27], limiting their commercial development. Although thermal SHG experiments themselves were not part of this dissertation work, the fabrication of the ESA films used in these experiments was. Discussion of the temperature dependent results are therefore included here for completeness, as thermal stability of the NLO characteristics of ESA films was an objective of this study.

The temperature dependence of the $\chi^{(2)}$ response in ESA films was examined by monitoring the second harmonic output of a 100 bilayer Poly S-119/PAH film as the temperature was raised to 150° C and maintained there for over 15 hours. The SHG experimental setup was as described in Section 4.2.2, modified to enclose the sample in a programmable heating cell [20]. The temperature was ramped from RT to 150° C over 3 hours, maintained at 150° C for 15 hours, and allowed to cool back to RT over 1.5 hours. As illustrated in Figure 4-36, the second harmonic intensity decreased to 75% of its initial value as the temperature was raised. More interestingly, the SHG output remained extremely stable as the temperature was maintained at 150° C (Fig. 4-37), and, in fact, increased as the sample was cooled back to room temperature (Fig 4-38.) The second harmonic intensity at each temperature exhibited excellent quadratic dependence on the fundamental intensity.

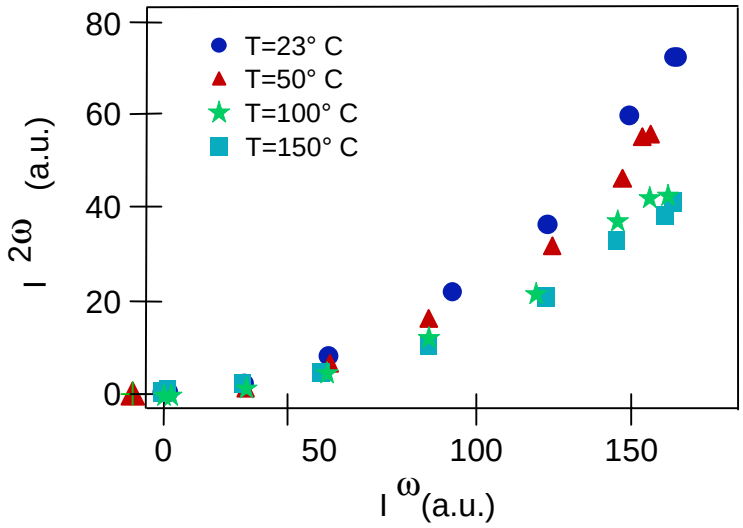

Figure 4-36. Second harmonic intensity as a function of incident fundamental intensity for Poly S-119/PAH ESA film as the temperature is increased from RT to 150° C.

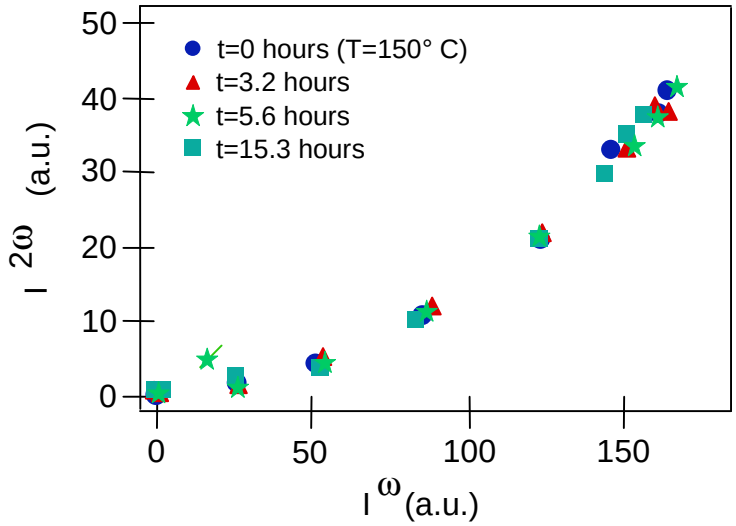

Figure 4-37. Second harmonic intensity as a function of incident fundamental intensity for Poly S-119/PAH ESA film as the temperature is maintained at 150° C for 15 hours.

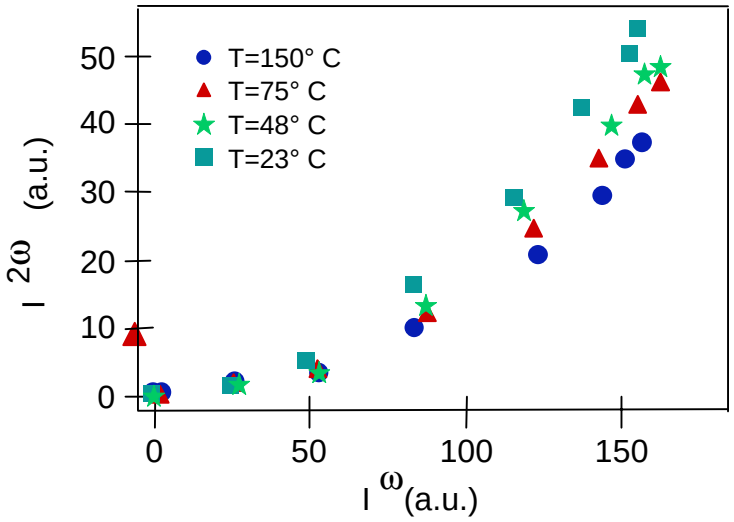

Figure 4-38. Second harmonic intensity as a function of incident fundamental intensity for Poly S-119/PAH ESA film as the temperature is cooled from 150° C to RT.

The data were fit to the expression $I^{2\omega}=A(I^{\omega})^2$ and the $\chi^{(2)}$ value determined using Eq. 4.8. However, thickness was not quantitatively evaluated during these tests, so it is more valid to compare second harmonic intensity, which was reduced by 25% of its initial value during the heating segment, remained constant while maintained at the elevated temperature, and increased to 91% of its initial value during the cooling segment. The SHG was not measured again after the sample remained at RT for an extended time period.

Decher and co-workers have reported, using small angle x-ray scattering, that the total thickness of an ESA film was reduced as the temperature is increased and restored to its initial value only after keeping it at RT and ambient environment for two weeks [24]. Independently, Y. Liu has measured the contact angle (CA) of ESA films as a function of temperature, reporting an increase in CA with an increase in temperature and restoration of the original CA only after overnight storage [28]. These results can be interpreted as an expulsion of water with the temperature increase, a reabsorption of some of the water as the film cools to RT, and complete reabsorption of the original water content as the film is stored for an extended time in the ambient environment.

For the experiment discussed here, results are found to be similar. As the temperature was increased, water was driven out, producing a compaction of the film accompanied by an increased chromophore tilt angle and therefore a reduced second harmonic output. The increase in SHG signal observed as the sample was cooled was due to reabsorption of some of the water and subsequent swelling of the film, resulting in a reduced average tilt angle. Since the second harmonic intensity measured immediately on return to RT was 9% less than the initial value, it can be assumed that film thickness and tilt angle are not completely restored, most likely due to incomplete water reabsorption. Initial SHG output could potentially be restored by storing the film overnight.

4.5 Summary

This chapter concerned the evaluation of noncentrosymmetric thin films fabricated using the ESA technique. Initial studies utilized commercially available nonlinear optical polymer dyes and produced $\chi^{(2)}$ values on the order of quartz. Several novel polymer dyes were then incorporated into ESA films, resulting in enhanced $\chi^{(2)}$ values. Second harmonic generation results were presented as the basis for film comparison. Finally, the temperature dependence of ESA $\chi^{(2)}$ films was examined.

4.6 References

1. See, for example, R.W. Boyd, *Nonlinear Optics*, Academic Press, Boston, (1992).
2. P. Thomas, "Inorganic nonlinear materials," *Physics World* **3** (3), 34-8 (1990).
3. D.S. Chemla and J. Zyss ed., *Nonlinear Optical Properties of Organic Molecules and Crystals*, Vol. 1, Academic Press, New York (1987).

4. C. Bosshard, K. Sutter, P. Prêtre, J. Hulliger, M. Flörsheimer, P. Kaatz, P. Günter, *Organic Nonlinear Optical Materials*, Gordon and Breach (1995).
5. H.S. Lackritz and J.M. Torkelson, "Polymer Physics of Poled Polymers for Second-Order Nonlinear Optics," in *Molecular Nonlinear Optics - Materials, Physics and Devices*, ed. J. Zyss, Academic Press, New York (1994).
6. I. Ledoux and J. Zyss, "Molecular Nonlinear Optics: Fundamentals and Applications," in *Novel Optical Materials and Applications*, ed. I.-C. Khoo, F. Simoni, C. Umeton, John Wiley & Sons, New York (1997).
7. V. Lemoine, J.P. Pocholle, P. le Barny, P. Robin, "Integrated Optics with Nonlinear Polymers," in *Molecular Nonlinear Optics - Materials, Physics and Devices*, Ed. J. Zyss, Academic Press, New York (1994).
8. P.N. Prasad and D.J. Williams, *Introduction to Nonlinear Optical Effects in Molecules and Polymers*, John Wiley & Sons, New York (1990).
9. C. Flytzanis, "Fundamentals of Nonlinear Optics," in *Nonlinear Optical Materials and Devices for Applications in Information Technology*, Ed. A Miller, K.R. Welford, B. Daino, Kluwer Academic Publishers, Boston (1993).
10. K.D. Singer, S.J. Lalama, and J.E. Sohn, *Appl. Phys. Lett.* **49**, 248 (1986).
11. K.D. Singer, "Molecular Polymeric Materials for Nonlinear Optics," in *Polymers for Lightwave and Integrated Optics: Technology and Applications*, L.A. Hornak, ed. (Marcel Dekker, New York, 1992) pp. 321-342.
12. C.P.J.M. Van der Vorst, W.H.G. Horsthuis, G.R. Mohlmann, "Nonlinear Optical Side-Chain Polymers and Electro-optic Test Devices," in *Polymers for Lightwave and Integrated Optics: Technology and Applications*, L.A. Hornak, ed., Marcel Dekker, New York, pp. 365-396 (1992).
13. K.D. Singer and J.H. Andrews, "Quadratic Nonlinear Optics in Poled Polymer Films: From Physics to Devices," in *Molecular Nonlinear Optics - Materials, Physics and Devices*, Ed. J. Zyss, Academic Press, New York (1994).
14. K.D. Singer and L.A. King, "Relaxation phenomena in polymer nonlinear optical materials," *J. Appl. Phys* **70**, 3251 (1991).
15. H.L. Hampsch, J. Yang, G.K. Wong and J.M. Torkelson, "Second harmonic generation in doped glassy polymer films as a function of physical ageing and dopant size," *Polym. Comm.* **30**, 40 (1989).
16. M. Eich, A. Sen, H. Looser, G.C. Bjorklund, J.D. Swalen, R. Twieg and D.Y. Yoon, "Corona poling and real-time second-harmonic generation study of a novel covalently functionalized amorphous nonlinear optical polymer," *J. Appl. Phys.* **66**, 2559 (1989).
17. I. Teraoka, D. Jungbauer, B. Reck, D.Y. Yoon, R. Twieg and C.G. Willson, "Stability of nonlinear optical characteristics and dielectric relaxations of poled polymers with main-chain chromophores," *J. Appl. Phys.* **69**, 2568 (1991).
18. G. Roberts ed., *Langmuir-Blodgett Films*, Plenum, New York (1990).
19. A. Ulman, *An Introduction to Ultrathin Organic Films*, Academic Press, San Diego, CA (1991).
20. C. Figura, D. Marciu, Y. Liu, Y.X. Wang, K. Lenahan, R.O. Claus and J.R. Heflin, "Thermal Stability of Ionically Self-Assembled Second Order Nonlinear Optical Thin Films," *Proc. Am. Chem. Soc.* (Boston), August 1998.

21. J.R. Heflin, Y. Liu and R.O. Claus, "Noncentrosymmetric Ionically Self-Assembled Thin Films for Second-Order Nonlinear Optics," *OSA Thin Films Conference*, Long Beach, CA, September 1997.
22. J. Schmitt, T. Grünewald, G. Decher, P.S. Pershan, K. Kjaer, and M. Lösche, "Internal Structure of Layer-by-Layer Adsorbed Polyelectrolyte Films: A Neutron and X-ray Reflectivity Study," *Macromolecules* **26**, 7058-63 (1993).
23. G. Decher, Y. Lvov, J. Schmitt, "Proof of multilayer structural organization in self-assembled polycation-polyanion molecular films," *Thin Solid Films 244*, 772 (1994).
24. Y. Lvov, G. Decher, and H. Möhwald, " Assembly, Structural Characterization, and Thermal Behavior of Layer-by-Layer Deposited Ultrathin Films of Poly(vinyl sulfate) and Poly (allylamine)," *Langmuir* **9**, 481-6 (1993).
25. M. Ferreira, J.H. Cheung, and M.F. Rubner, "Molecular self-assembly of conjugated polyions: a new process for fabricating multilayer thin film heterostructures," *Thin Solid Films* **244**, 806-9 (1994).
26. J. R. Heflin, Y. Liu, C. Figura, D. Marciu and R.O. Claus, *Proc. SPIE* **3147**, 10 (1997).
27. M.A. Hubbard, T.J. Marks, J. Yang and G.K. Wong, *Chem. Mater.* **1**, 167 (1989).
28. Y. Liu, *Characterization and Patterned Polymer Films from a Novel Self-Assembly Process*, Department of Chemistry, Ph.D. Dissertation, Virginia Tech, 1996.

CHAPTER 5

Conclusions and Recommendations

This dissertation demonstrated the feasibility of using electrostatic self-assembly to fabricate a wide range of optical thin films and components. The capability of nanoscale control over film optical and secondary properties allowed the fabrication of complicated refractive index profiles required for linear optical filtering applications. The inherent ordered nature of ESA films yielded extremely stable noncentrosymmetric thin films for second-order nonlinear optical applications. In addition, the effect of processing conditions on resulting film characteristics was investigated. This chapter delineates the significance and novel contributions of this dissertation and suggests future studies which may build on this work.

5.1 Significance of investigation

The advantages of molecular engineering and self-assembly are combined in electrostatic self-assembly, allowing the formation of multifunctional thin films, controlled on the nanometer scale. ESA can be adapted to incorporate a wide variety of molecules, as demonstrated by previous work with OLEDs [1-3], biosensing [4], catalysis [5,6], protective coatings [7] and magnetics [8], illustrating the great flexibility of this process. Not only does this dissertation research represent the first application of ESA to optical interference filters and NLO devices, the process evaluation contributes significantly to the development of ESA films for other applications. The capability of incorporating multiple layers and materials in a single film at the molecular, nanoscale level offers great potential for improved material and device characteristics, as well as nanostructures previously unattainable. The novel contributions of this dissertation extend the work of previous researchers by efforts focused on commercial optical applications of ESA films as follows.

- Demonstration of uniform ESA coatings on all surfaces of large and irregularly shaped substrates,

- Demonstration of ESA films greater than 2000 bilayers thick,
- Continued investigation of ESA processing parameters, including process automation,
- Nanoscale control of the refractive index profile of ESA films several microns thick using two distinct methods,
- Synthesis of optical interference filters (dielectric stack, Rugate, and AR) by ESA, and
- Incorporation of novel NLO polymers and demonstration of the resulting nonlinear optical behavior using second harmonic generation.

5.3 Future Research

It is evident that ESA is still in its infancy and work up to this point, including this dissertation, can be considered feasibility studies. The process itself is not thoroughly understood and much remains to be done to correlate variable deposition parameters and resulting film properties. For commercial manufacturing, the process must also be automated and optimized. This section proposes further investigations that will specifically extend the work described in this document.

5.2.1 Linear optical filtering applications

This dissertation demonstrated prototype optical interference filters synthesized using the ESA method and a number of optical materials characterized in the initial portion of the study. Continuation of this work will first and foremost require an expansion of the range of optical materials available for inclusion in filter designs. Both high and low index bilayer systems are required; the range available for the current study was 1.54 to 1.77. It is important to note that the properties of an ESA film are dependent not on a single molecular species, but on all polyanionic and polycationic species incorporated. For example, a high index cationic layer may be diluted by its opposing anionic layer. Each material must be carefully characterized, physically and optically, in combination with its appropriate counterion layer. As an example, the determination of a high index bilayer system with negligible absorption in the visible spectral range will allow the synthesis of AR filters at visible wavelengths. Accurate bilayer thicknesses are critical to avoid time-consuming iterative index profile designs. Methods to maintain consistent deposition parameters between batches must be developed before commercial application can be considered.

Once new material components are evaluated, more complicated index profile designs can be fabricated, allowing enhancements to the transmission spectra presented in this dissertation. For example, greater numbers of layers or periods will increase filter reflectance, and apodized profiles can reduce sidelobes. An example of a simple apodization of a dielectric stack profile is shown in Figure 5-1. The profile on the left represents a filter similar to those fabricated in this dissertation. Modifying the step heights in this way should not be difficult, but can almost entirely suppress the sideband ripples in the transmission band of the reflectance filters described in Chapter 3 [9]. At present, using the simple, unapodized dielectric stack and Rugate filter profiles that were demonstrated in this investigation, and simply altering the layer and period thicknesses can provide numerous reflectance wavelengths and multi-notch filters. A method for

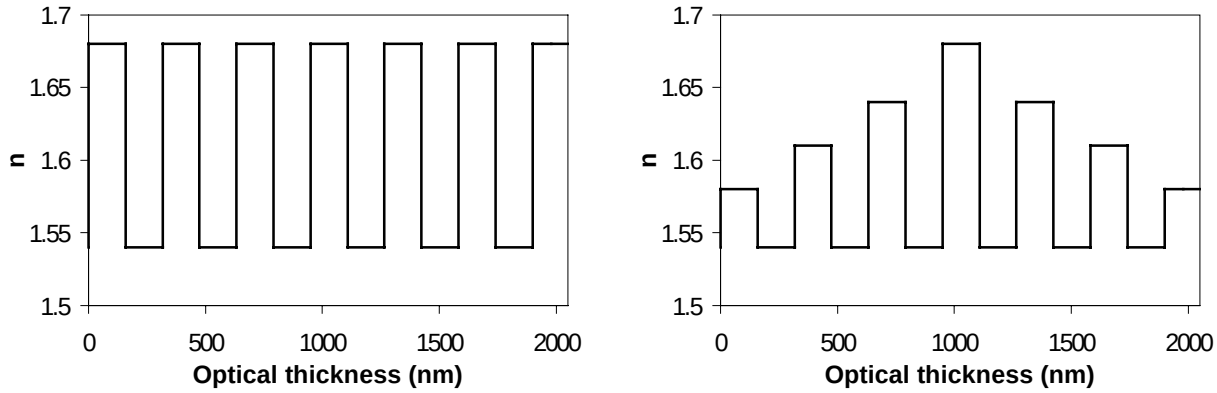

Figure 5-1. Unapodized (left) and apodized dielectric stack refractive index profiles.

index control and grading has been established by this dissertation research; all that is required for future designs is determination of the appropriate multilayer pattern and dipping order.

Another concept deserving attention is the incorporation of protective coatings into ESA optical components to provide the durability required by practical applications. ESA-fabricated hard coatings have been the focus of a separate study at the Fiber & Electro-Optics Research Center at Virginia Tech [7, 10] and the combination of optical polymers and hard coat into a single composite film has been demonstrated.

5.2.2 Second-order nonlinear optical applications

In this dissertation, a limited number of NLO materials were incorporated into ESA films and demonstrated. As with the linear optical applications, the range of materials utilized needs to be expanded and consideration given to alternate water-soluble, high-β molecules. With each new material, preliminary optical and structural characterization will be required. Process variations to enhance dipole alignment can also be considered. Poling of ESA NLO films was very briefly explored in this study. Numerous questions remain concerning this topic, primarily stability in comparison to standard poled polymers. The application of an electric field during film assembly, i.e. electric-field assisted ESA (EFA-ESA), also warrants investigation for enhanced dipole alignment.

Many more experiments are possible using the same SHG testing setup described in Chapter 4. The study of $\chi^{(2)}$ thermal stability can be extended in much greater depth. Well-behaved thermal characteristics are critical attributes for $\chi^{(2)}$ applications. The precise dependence of film thickness on temperature in combination with SHG is required for a full analysis. In addition, polarization studies, such as those described in Section 4.3, as a function of temperature will allow determination of the chromophore tilt angle with increased temperature, providing important insight into thermally induced ESA film structural behavior.

Although the NLO measuring stick used for this dissertation was SHG, the electro-optic properties of noncentrosymmetric ESA films offer a number of opportunities for commercial devices. The electro-optic coefficients of ESA films can be evaluated using a simple reflection technique [11]. An EO modulator in a waveguide configuration would be an excellent demonstrator article for this concept. The refractive index profile control required for the self-assembly of an optical waveguide was illustrated in Chapter 3 of this dissertation and a simple waveguide has been fabricated as part of a separate study. Coupling and absorption losses need to be evaluated. Further development of this simple, inexpensive technique for producing nonlinear optical thin films with long-term stability and low waveguide scattering losses will have an exceptional impact on optoelectronic applications utilizing modulators and switches.

5.3 References

1. M. Ferreira, J.H. Cheung and M.F. Rubner, "Molecular self-assembly of conjugated polyions: a new process for fabricating multilayer thin film heterostructures," *Thin Solid Films* **244**, 806 (1994).
2. A.C. Fou et al., "Fabrication and properties of light emitting diodes based on self-assembled multilayers of poly (p-phenylene vinylene)," *J. Appl. Phys.* **79**, 7501 (1996).
3. J.W. Baur et al., "Thin-film light emitting devices based on sequentially adsorbed multilayers of water-soluble poly (p-phenylene vinylene)," *Adv. Mater.* **10**, 1452 (1998).
4. G.B. Sukhorukov, H. Möhwald, G. Decher and Y. Lvov, "Assembly of polyelectrolyte films by consecutively alternating adsorption of polynucleotides and polycations," *Thin Solid Films* **284/285**, 220 (1996).
5. Y. Lvov et al., "Direct Electrochemistry of Myoglobin and Cytochrome $P450_{cam}$ in Alternate Layer-by-Layer Films with DNA and Other Polyions," *J. Am. Chem. Soc.* **120**, 4073 (1998).
6. Y. Liu, A. Wang and R. Claus, "Molecular Self-Assembly of TiO_2/Polymer Nanocomposite Films," *J. Phys. Chem. B* **101**, 1385 (1997).
7. A. Rosidian, *Nanocomposite of ZrO_2/Polymer Thin-Film Coatings by the Ionically Self-Assembled Monolayer Technique*, M.S. thesis, Materials Science Department, Virginia Tech, Blacksburg, VA, March 1998.
8. Y. Liu, A. Wang and R. Claus, "Layer-by-layer electrostatic self-assembly of nanoscale Fe_3O_4 particles and polyimide precursor on silicon and silica surfaces," *Appl. Phys. Lett.* **71**, October 1997.
9. J.A. Dobrowolski, "Usual and Unusual Applications of Optical Thin Films - An Introduction," in *Handbook of Optical Properties, Vol. I: Thin Films for Optical Coatings*, Ed. R.E. Hummel and K.H. Guenther, CRC Press: Boca Raton (1995).
10. A. Rosidian, Y. Liu and R. Claus, "Ionic Self-Assembly of Ultrahard ZrO_2/Polymer Nanocomposite Thin Films, *Adv. Mater* **10**, 1087 (1998).
11. C.C. Teng and T. Man, "Simple reflection technique for measuring the electro-optic coefficient of poled polymers," *Appl. Phys. Lett.* **56**, 1734 (1990).

Vita

Kristie Lenahan Cooper was born on October 28, 1971 in Bremerton, Washington. She graduated in honors from Virginia Polytechnic Institute & State University with a Bachelor of Science in Electrical Engineering in May 1994. Ms. Cooper continued her studies at Virginia Tech as a member of the Fiber & Electro-Optics Research Center, earning her Master of Science in Electrical Engineering degree in May 1996. Her M.S. thesis concerned adaptive composites for aerospace applications using fiber optic EFPI strain sensors. During both her undergraduate and graduate programs, Ms. Cooper worked at the Federal Aviation Administration Technical Center in Atlantic City, New Jersey. Her Ph.D. dissertation, completed in April 1999, focused on novel molecular assembly methods for the synthesis of optical thin films. Applications include second harmonic generation, electro-optic modulation and optical interference filtering techniques.